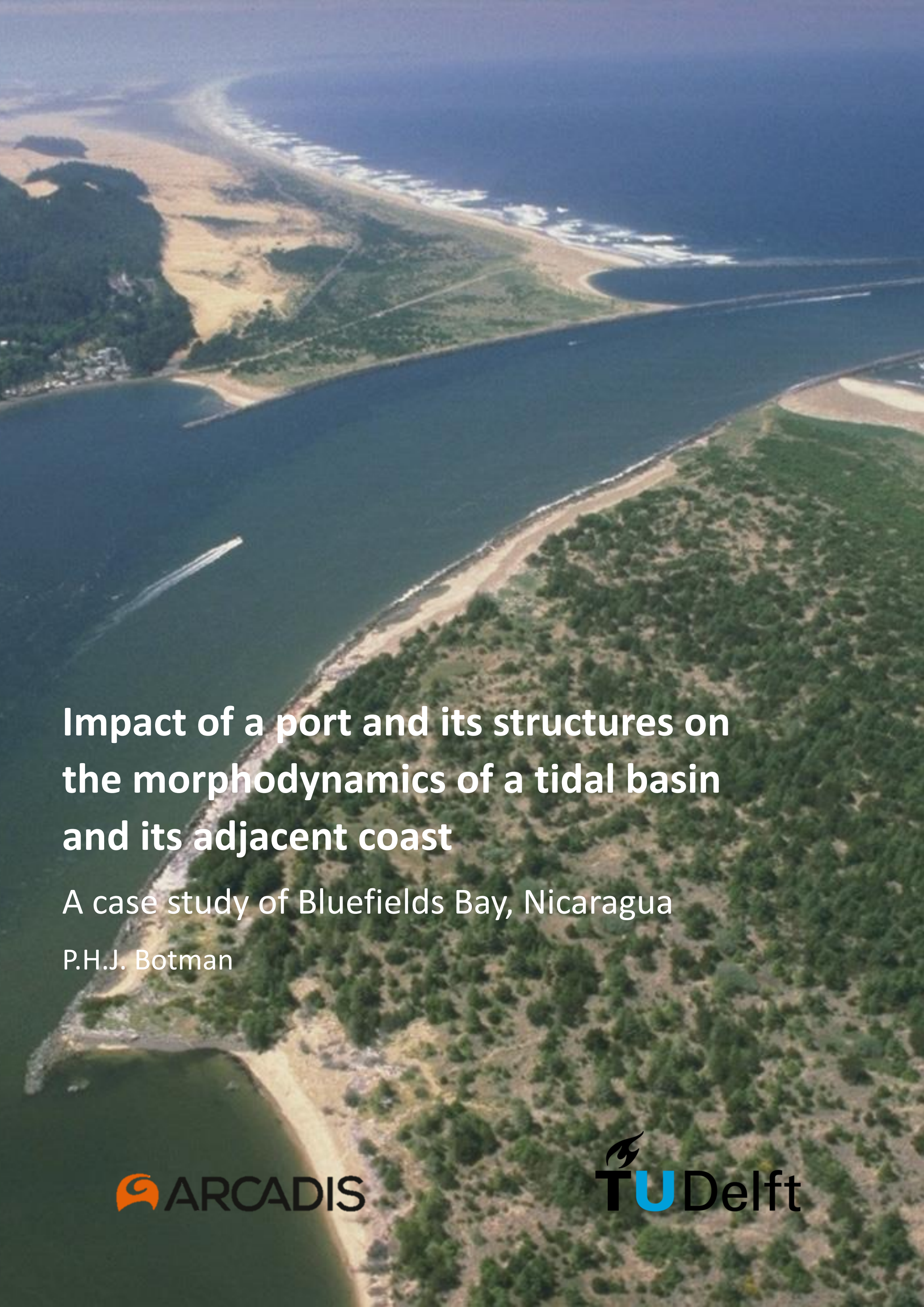

Impact of a port and its structures on the morphodynamics of a tidal basin and its adjacent coast

A case study of Bluefields Bay, Nicaragua

P.H.J. Botman

ARCADIS

TU Delft

Impact of a port and its structures on the morphodynamics of a tidal basin and its adjacent coast

A case study of Bluefields Bay, Nicaragua

by

P.H.J. (Paul) Botman

in partial fulfilment of the requirements for the degree of

Master of Science
in Civil Engineering

at the Delft University of Technology (TU Delft)
to be defended publicly on Tuesday, September 29, 2020 at 13:00.

An electronic version of this thesis is available at http://repository.tudelft.nl/.
Scource cover page: US Army Corps of Engineers (2020)

Student number:	4254295	
Chair Committee:	Prof. dr. ir. S.G.J. Aarninkhof,	Delft University of Technology
Committee members:	Ir. J. van Overeem,	Delft University of Technology / Aracids Nederland
	Dr. Ir. B. van Maren,	Delft University of Technology
	Ir. J. de Groot,	Arcadis Nederland

Preface

This thesis marks the final stage of the Master of Science program in Hydraulic Engineering at Delft University of Technology.
This thesis has been performed in collaboration with Arcadis Nederland, a renowned engineering company. I would like to thank Arcadis Nederland for offering the opportunity to perform my thesis at their company. I would like to thank the people there for showing their curiosity about my work and for their support when needed. The people and overall ambience made it pleasant to work on my thesis. I have enjoyed and learned a lot last year.
I would like to take this opportunity to express special gratitude to the people that have guided me through this thesis. To start, I would like to thank Jan van Overeem for his endless enthusiasm in the field of hydraulic engineering and in supervising students. I think I am his last student, so I hope it was pleasant for him as well. Moreover, I would like to express my gratitude to Jaap de Groot of Arcadis Nederland for supervising the relaxed way he did, and for keeping the research practical and clear. Also, I would like to thank my other committee member, Bas van Maren, for, although joining late in research, helped out a lot with his knowledge of the subject. Lastly, I would like to thank Stefan Aarninkhof for being the chair of the committee and for the opportunity to do this thesis.
In addition to my committee, I would like to thank staff members of Arcadis Nederland. In particular Jos van der Baan, who was not a part of the committee, but always available to support me with Delft3D. I would like to thank Jochem Roubos for explaining me the basics of Matlab. And of course, the other graduate students at Arcadis who not only helped me out with everyday thesis issues but also who made the process more fun.
Finally, I would like to thank my mom and dad for supporting me throughout my entire student life. This achievement would not have been possible without your love and support.

Paul Botman
Rotterdam, September 2020

Summary

To improve the socioeconomic situation in the Republic of Nicaragua, the government has decided to strengthen the country's transport infrastructure by building a port on the Caribbean coast. The future port will be in Bluefields Bay, which can be characterised as a lagoon-shaped estuary. The inner basin is connected to the sea by two tidal inlets, located north and south of a barrier island. This study assesses the hydrodynamics and morphodynamics of the area; in addition, it analyses the influence of the port structures on these natural processes. A qualitative analysis of the hydrodynamics and sediment transport in the area is conducted, and sedimentation rates in the navigation channel and the erosion rates of the coast are calculated. The area is analysed with the help of a conceptual model that is supported by the process-based model Delft3D. Large parts of the area consist of shallow depths of around 1.5 m below mean sea level (MSL). The bed of these shallow parts consists mainly of mud. In those areas with a depth of more than 5 m below MSL, which are the river channel and the tidal channels at the inlets, the flow velocity increases, and a more substantial fraction of sand can be observed. In the data analysis, distinct wet and dry seasons can be observed; these seasons change the hydrodynamic influences over the course of the year. The river discharge increases by a factor of 10 during the wet season. In addition, the river delivers large quantities of mud, particularly during the wet period. When the tidal flow enters the lagoon, it influences sediment transport. As the dominant hydrodynamics change throughout the year, the sediment fluxes change with them. Beyond the hydrodynamics within the lagoon, the adjacent coast is under the influence of a swell wave climate. As the waves mainly come from the east-northeast at a height of 1 m, a moderate southward longshore transport is initiated year-round.

The Delft3D model is used to analyse the hydrodynamics and sediment transport of the area in more detail. The model is used to analyse the flow magnitudes and directions. This approach allows the dominant hydrodynamic components to be identified. The most relevant hydrodynamic components are considered in the Delft3D model. These include tide, river discharge, waves, and wind. The 2D mode is sufficient to model these hydraulic components. Because of the hydrodynamic climate changes that occur throughout the year due to changes in the meteorological climate, the simulation period is one representative year. The model is calibrated and validated by means of phenomenological calibration and expert judgement, as field data is scarce.

The results of the system analysis and numerical model show that the Rio Escondido discharges a large amount of sediment into the tidal basin during the wet period, namely 2.5 to 3.44 million t/yr. It is, however, the tide that initiates the most sediment transport. During the dry season, the lagoon is flood dominant, importing mud from the adjacent coast. This mud is deposited near the inlets and in the shallower area. In the wet period, the river discharge counteracts the tidal flow preventing mud from entering the tidal basin. Most of the mud originating from the river is transported directly to the northern inlet through the river channel during this period. Also, the imported mud from the dry period is exported in the wet period, as the southward directed residual currents have increased. A fraction of this mud moves southward along the tidal basin to the south and is exported by the southern inlet. Based on historic coastal development, it is concluded that the coastal area is in a dynamic equilibrium. Due to a moderate wave climate, a small longshore southward transport of 150,000 m^3/yr is initiated.

The study implements two different port layouts. Both alternatives have the port at the same location; it is only the trajectory of the navigation channel that differs. The navigation channel of Alternative 1A goes through the northern tidal inlet, which has a depth of 5 m. When the channel enters the lagoon, it bends to the west and crosses shallow areas of 1 m. The depth and width of the channel are 15 m and 123 m, respectively. The navigation channel of Alternative 1B creates a new gap through the barrier island. Thereafter, it crosses the same shallow area as Alternative 1A. Because Alternative 1B crosses the barrier island, it has a shorter trajectory to the port. When the alternatives are constructed in the area, the hydrodynamic climate changes. The impact on the hydrodynamics of the area is less for Alternative 1A than for Alternative 1B. The channel's route of Alternative 1A is in the natural trajectory of the tidal flow. As a new opening is created for Alternative 1B, the hydrodynamics are changed more extreme. The tidal wave has a new entrance through which it flows into the lagoon.

In both situations, the tidal wave follows the path with the least resistance, which is the newly dredged channel. The volume of mud that the tidal flow imports in the dry season is now deposited directly in the dredged channel. Because the channel trajectories are to the west and south, the tidal flow has a less strong current to the north. Around the channel the flow velocities and thus bed shear stresses have increased, suspending sediment locally. The discharge of the Rio Escondido enters the lagoon from the north, and

it encounters less resistance from the tidal wave in both alternatives. The river discharge becomes more dominant in the northern area. These changed hydrodynamics initiate erosion and sedimentation patterns which change the tidal basin bathymetry. The ebb directed current is strengthened due to the greater influence of the Rio Escondido, and the northern area changes from being a flood to an ebb dominant area. Although the northern area turns to ebb dominance, mud does not leave the basin in greater quantities. The residual currents transport a large fraction of the mud to the navigation channels, where the flow velocity decreases substantially. The tidal flow is not able to carry the mud in the channels, and the mud is thus deposited. A low export of mud is the result. The southern inlet does not export any mud after the implementation of the port layouts. The southward directed residual current has decreased in velocity. This decrease in velocity is because the river discharge follows the dredged channel to the northern inlet and thus does not reach the southern inlet. Additionally, the decrease in sediment export by the southern inlets is because the large sediment flume that goes southward in the basin for the existing situation is accumulated in the channel.

The channels in the inner basin tend to refill over a period of more than 10 years, which is a low rate. For both layouts, the most substantial part of the channel is in the areas with mild sediment transport mechanisms. The tide transports most of the mud to the port and channel. The tidal amplitude only has a range of 0.6 m. When considering the relatively large area of the basin and the low tidal amplitude, the force of the tide is considered mild. Although Alternative 1B imports more mud for annual period, the sedimentation in the inner channel and port are smaller for Alternative 1B than Alternative 1A, 0.94 Mm^3/yr and 1.23 m^3/yr respectively. A large quantity of the imported mud in the dry period is flushed out in the wet period for Alternative 1B because the channel trajectory is relatively short.

The sedimentation of sand and mud in the outer channel for Alternative 1A and 1B is 1.08 m^3/yr and 2.05 m^3/yr, respectively. Both alternatives catch all of the longshore transport. However, the sedimentation of sand for Alternative 1B is greater for the outer channel, because it catches more locally induced sediment transport. This higher quantity of local sediment is because the outer channel is located over a larger stretch in the breaker zone of the area. When a channel is dredged through this active morphodynamic environment, the dynamic equilibrium is restored at a faster rate. The outer channels tend to refill over a period of 9 to 6 years for Alternatives 1A and 1B, respectively.

Contents

1 Introduction

In this chapter the context of this research is introduced. The background is presented in Section 1.1, and in Section 1.2 the problem statement is given. The objective resulting from the problem statement is explained in Section 1.3. Finally, the approach of the research is elaborated upon in Section 1.4.

1.1 Background

To improve the country's socioeconomic situation, the government of the Republic of Nicaragua has decided to strengthen the transport infrastructure by building a port on the Caribbean coast. The location for this port will be in Bluefields Bay. Figure 1.1 shows the area of interest. Bluefields Bay has high ecological value, constitutes the main access route for commerce in the city of Bluefields, and supports a hectic artisanal fishing activity. The area is characterised as a lagoon-shaped estuary. Multiple rivers, namely the Rio Escondido, Rio Kukra, Rio Docuno, Rio Torsuan, and Caño Negro, flow into the basin. The basin is protected against wave influences by a barrier island that creates a northern and a southern entrance to the basin.

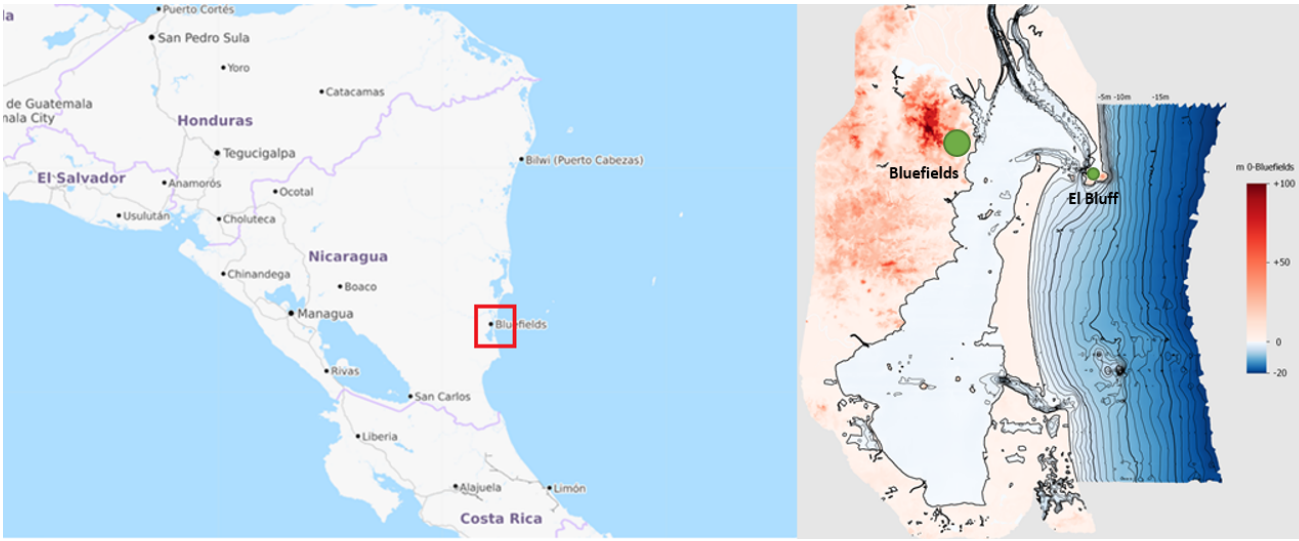

Figure 1.1: Area of interest

Various port locations are being considered, as presented in Figure 1.2. In this study two alternatives are analysed. In Figure 1.2 both the alternatives have their port at Location 1. Alternative 1A enters the lagoon through the northern tidal inlet and Alternative 1B enters the lagoon through a newly created opening in the barrier island. Different factors play a role in defining the preferred site. The most important factors for this study are dredging costs, environmental aspects, other maintenance and construction costs, and social impact.

Dredging costs depend on capital and maintenance dredging. Capital dredging is the amount of money required to construct the navigational channel. Maintenance dredging is the amount of money required to maintain the navigation channel during usage to guarantee sufficient sailing depth. A balance between these two is pivotal in the choice between the alternative port layouts. Capital dredging costs can be high if the channel is dredged over a long trajectory. However, a longer trajectory may be beneficial in keeping the maintenance costs low if the sediment supply deposited in the channel is lower.

The environmental aspects are another notable concern for this project, as this is a protected environment. When constructing a port and its structures, impact on the environment should not be too high. Changes in hydrodynamics and morphodynamics affect flow, erosion, and sedimentation patterns. These changes alter the environment in terms of the exchange of water and sediment with the adjacent coast. Further, the local population conducts fishing activities throughout the basin, and these activities ought not to be disturbed too much.

Other construction costs not only depend on the port itself but on the infrastructure over land and water from and to the port. New infrastructure may be required to reach the port in certain locations.

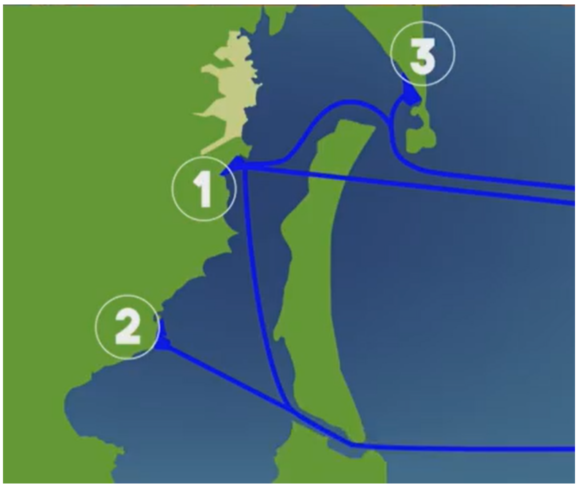

Figure 1.2: Possible port locations

The area is under the influence of complex hydrodynamics, which in their turn influence the morphodynamics. The rivers, predominantly the Rio Escondido, discharge a large amount of sediment into the tidal basin, while the tide, entering the basin through the two tidal inlets, also influences sediment transport. The tide and the river discharges have complex interactions. The seasonal variability that influences the magnitude of the discharges is substantial because hydraulic processes in the estuaries vary during the year. At the adjacent coast, other coastal dynamics such as waves influence the morphodynamics. These waves create sediment transport that deposits in the lagoon entrances and on the adjacent coast.
These dynamics and processes can be disturbed by human interventions, such as dredging a navigation channel or constructing a groyne. When this occurs the hydrodynamics and morphodynamics alter, meaning new sedimentation erosion patterns in the area are formed. These features and the ways they influence each other must be analysed thoroughly before the decision of a port location is made.
This research concentrates on the potential interactions of the new port with the hydrodynamics and morphodynamics of the area. The area considered for study is the entire Bluefields Bay and the adjacent coastline.

1.2 Problem statement

Earlier studies lack a detailed description of the hydrodynamic influence on sediment transport in the Bluefields Bay area, and thus, substantiation of the port location is incomplete. An analysis of these processes, in a considered spatial and temporal scale, is required.
The biggest forcers of sediment transport in coastal dynamics are river discharges, waves, and tides. All these hydraulic processes occur in the study area, and the interactions between these processes are complicated. The morphodynamics of the area depend on which hydrodynamic process dominates, something that is currently unknown.
The river discharge is the biggest supplier of sediment, which consists mainly of mud. The way the sediment of the river is spread over the tidal basin is unknown. When the tide enters the basin through the inlet, the tidal amplitude deforms and becomes asymmetric. The tidal asymmetries influence the direction and quantity of sediment transport. Finally, the waves initiate longshore transport at the coast, and wind-induced waves initiate this within the tidal basin. The quantities of sediment that each of these hydrodynamic processes can transport are also unknown.
The sediment in the area is a mix of gravel, sand, silt, and mud, and each of its components are transported differently. Sediment fractions are divided into cohesive and non-cohesive sediment. Cohesive sediment and fine non-cohesive sediment move mainly as suspended sediment, while the heavier fractions of non-cohesive sediment transports as bedload transport. When these fractions mix, they influence each other's transport.
The influence of human interventions on the environment is unknown. If port structures are located outside the basin, erosion on the adjacent coast may occur. In addition to this, the variations caused by a port in the basin's hydrodynamics and morphodynamics are not known. When a tidal basin is forced out of its morphodynamic equilibrium, nature reacts to restore its balance. However, when the morphodynamic equilibrium of the system in the basin is unbalanced too far, the hydrodynamics and morphodynamics will

no longer return to their previous state.
The location of the port and its navigation channels will uniquely determine these processes. Each potential location would induce different changes in hydrodynamics and force different changes in morphodynamics. The amount of sediment that is transported into the navigation channels would differ. The erosion and sedimentation quantities on other places on the coast would differ. A study of these changes is necessary.

1.3 Objective

This research explores the potential interactions between the port and the hydrodynamics and morphodynamics of the area. A conceptual model was used to analyse the area before and after the potential constructions of the port and its structures. This conceptual model was supported by a numerical model that had to be computationally efficient but detailed enough to make useful predictions and comparisons. The analysis of the sediment transport in the area detailed the processes behind the sediment transport. The capacity of the hydraulic factors to transport sediment fractions was examined. As stated, the area consists of a broad range of different sediment fractions. Thus, the sedimentation and erosion of each fraction separately and jointly in the channel and area were analysed.
The main research question of this thesis is:

How would the potential locations of a newly constructed port and its channel affect the hydrodynamics and morphodynamics in Bluefields Bay and its adjacent coast, and how would the sediment transport in Bluefields Bay and its adjacent coast affect the potential locations of a port and its channel?

Different sub-questions were created to answer the main research question:

1. What transport processes of sand and mud occur under the influence of the hydrodynamics of the tidal basin, discharging rivers, and adjacent coast?
2. How can an efficient numerical model compute the dominant transport processes of sand and mud in the area of interest?
3. What are the dominant hydrodynamics and dominant transport patterns of sand and mud transport in the area of interest?
4. What would be the dominant hydrodynamics in the area of interest after the potential constructions of the port and its structures?
5. What would be the dominant sand and mud transport patterns in the area of interest after the potential constructions of the port and its structures?

1.4 Approach

This thesis centres around a case study that seeks a deeper understanding of the influence of the hydrodynamics and sediment transport processes in the area of interest. The way the construction of a port and its structures would influence these processes is also examined. The approach of the research is stepwise and is presented in Table 1.1.

Steps	Description	Chapter
1	Literature study	A
2	System analysis and data analysis	2
3	Conceptual model	2.5
4	Model setup	3
5	Model calibration and validation	3.5
6	Results analysis	4
7	Discussion	5
8	Conclusions and recommendations	6

Table 1.1: Steps of the research

First a literature study was done to gain an understanding of hydrodynamics and their influence on morphology. This literature study is presented in Appendix A.

Next an analysis of the area, based upon the literature study and applicable data, was done to identify which hydrodynamic and morphodynamic processes are of relevance. A clear picture of the magnitudes of the hydraulic boundary conditions is given. This system analysis is shown in Chapter 2.
After this a conceptual model of the sediment transport was developed. This conceptual model describes the hydrodynamic system and addresses which processes were considered for further study. It was the basis for the interpretation of the study area and, eventually, the setting up of the numerical model and the analyses of the results. Thus, it is the basis of the answers to the first and second research questions, which focus on the sediment transport processes. This conceptual model is presented in Section 2.5.
The literature study clarified which numerical models could be used for computation of the morphodynamics. A validated hydrodynamic Delft3D model of the area is available, and thus it was chosen to use this model. The capabilities of the Delft3D model were studied. This study gave insight into what processes of the conceptual model could be transformed into a numerical model. The efficiency of the model must be considered when deciding which natural processes are modelled. After these steps the Delft3D-module was constructed and simulated the morphodynamics of the present sediment transport in the area, answering the third research question. The model setup and validation are presented in Chapter 3.
Research questions 4 and 5 are answered with the conceptual model and the support of the numerical model. The existing hydrodynamic situation was studied with both models. Then the existing morphodynamics were analysed. After this the different port layouts were included, and the changes in the hydrodynamics were examined. Sedimentation and erosion rates were computed as a next step. The elaboration of the potential port's impact was done through analysing the hydrodynamic and morphodynamic results and comparing them with the knowledge from the conceptual model and the literature study. This delivered how the different port locations would influence the morphodynamics and which port location would have the most sedimentation. The analysis of these results is shown in Chapter 4.
The research and results are discussed in Chapter 5, and the conclusion and recommendations are presented in Chapter 6.

2 System analysis

The physical processes of the Bluefields Bay area are described in this chapter. The main characteristics of the area are elaborated upon in Section 2.1. From this information the dominant physical processes are identified. In Section 2.2, the past morphological development is examined. This provides a basis for understanding current and future development. The available data about the current environment is analysed in Section 2.3 and 2.4. Finally, the conceptual model based on the system analysis is described in Section 2.5.

2.1 Area characteristics

Figure 2.1 presents the geographical area of interest. Bluefields Bay is on the east shore of Nicaragua. The water area of this bay is about 176 km^2. Its length from north to south is 30 km, with an average width of 6 km (Brenes et al., 2007b). Due to the wave-shaped barrier island and a spit that developed at the eastern shore, wave penetration into the basin is negligible and therefore excluded. Bluefields Bay is characterised as a lagoon-shaped estuary. This classification is based on Table A.1. The lagoon connects with the Caribbean Sea through two tidal inlets, namely El Bluff and Honesound. Multiple rivers have openings in the basin, namely the Rio Escondido, Rio Kukra, Rio Docuno, Rio Torsuani and Caño Negro. The most significant fresh water runoff from the rivers is in the northern part of the basin, where the Rio Escondido has its entrance. In the southern part of the basin, the fresh water runoff is much less. In the wet season, the northern part of the bay is characterised as an estuary due to the high fresh water runoff. The fresh water in its turn dilutes the saline water.
The morphology of the area inside the lagoon is shaped by fluvial sediment. This sediment is delivered through the Rio Escondido. In the lagoon and estuary, the processes are tide-dominated. At the adjacent coast, the inlets to the basin and shoreline are influenced by waves and tides. The shoreline is smooth, with a spit developed in the past. This indicates a wave-dominant delta. The coarser sediment fractions settle here, while more land-inward the finer sediment fractions are dominant (Bosboom and Stive, 2015).

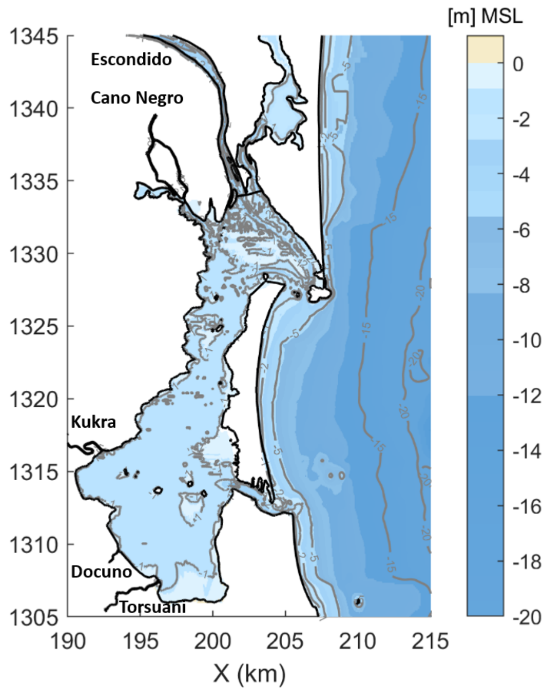

Figure 2.1: Bathymetry of the area

Bathymetry

The bathymetry of the area indicates the dominant hydrodynamics. The dominance of tides, river discharges, or waves leaves different structures in the bathymetry. There are two channels at the northern in-

let. One is the channel through which the flow of the Rio Escondido is connected to the Caribbean Sea. An extra ebb-tidal channel runs directly to the west.
The Rio Escondido has created a deep channel in the northern part of the basin. This channel has a depth of around 3 to 4.5 m below mean sea level (MSL) along its route. The chart datum (0–Bluefields) is 0.6 m below MSL. Around the tidal inlets, flood and ebb channels are present. The tide follows the river channel partly, as its depth offers less friction. Some small, braided flood channels originate out of the main river channel. These braided channels indicate the tidal influences of the morphodynamics (Van Veen et al., 2015). The southern tidal inlet has a depth of about 9 m. However, no channels with substantial depth originate from this inlet. This lack of different depths in the area is partly because the depth measurements are not of high resolution.
The main part of the bay consists of shallow depths that range between 0.5 and 1.5 m. These depths are within the influence of wind-induced waves on sediment suspension (Fagherazzi and Wiberg, 2009). From 1328 km on the y-axis, the depth seems to be constant, which indicates the wind-induced waves are the dominant process for morphodynamics.
Outside the basin the shore has a flat slope, creating dissipative conditions. Around the northern tidal inlet, the slope is around 0.002, and at the midpoint of the barrier island, the slope is 0.0035. These slopes correspond with dissipative beaches, which are the result of high energy waves that start breaking far offshore. They are the result of a storm wave climate (Wright and Short, 1984).

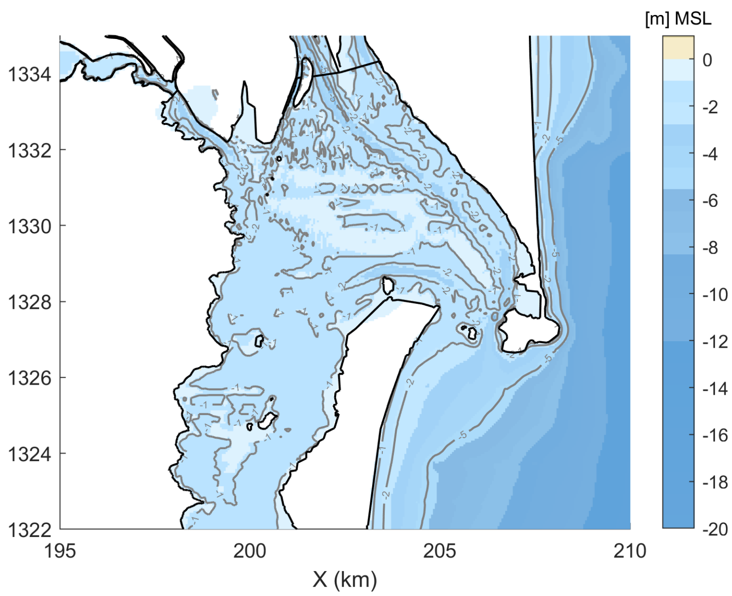

Figure 2.2: Bathymetry area of interest

2.2 Past morphological development

In this section the past morphological development of the area is examined. This can be used to clarify the present morphodynamics of the area.

2.2.1 Coast

Figure 2.3 shows satellite images from the past 47 years. The left picture was taken in 1970, and the right picture was taken in 2017. The shape of the coast has not changed over the last 47 years. This indicates that the coastline is in morphological equilibrium, meaning that erosion and sedimentation due to longshore transport and sediment leaving the inner tidal basin are of low quantities.

Figure 2.3: Bluefields Bay in 1970 (left) and 2017 (right) (Google Earth, 2020))

The coast is currently connected to the inner basin through two openings. In the past there were three openings, as presented in Figure 2.4. An opening north of El Bluff was created on several occasions by hurricanes (Alkyon, 2004). In 1974 and 1976, openings occurred but were closed as a result of longshore transport. The construction of a port was ongoing there in 1988 when a hurricane destroyed it and created a gap. Because of the breakwater that originated from the never-finished port, this gap did not close as quickly as it naturally would. The breakwater blocked the sediment flow going southward, and the gap kept growing. The left picture shows this opening in 2007. Eventually, the gap was too large to close by itself, and thus it was closed artificially. The right picture shows the recent situation.

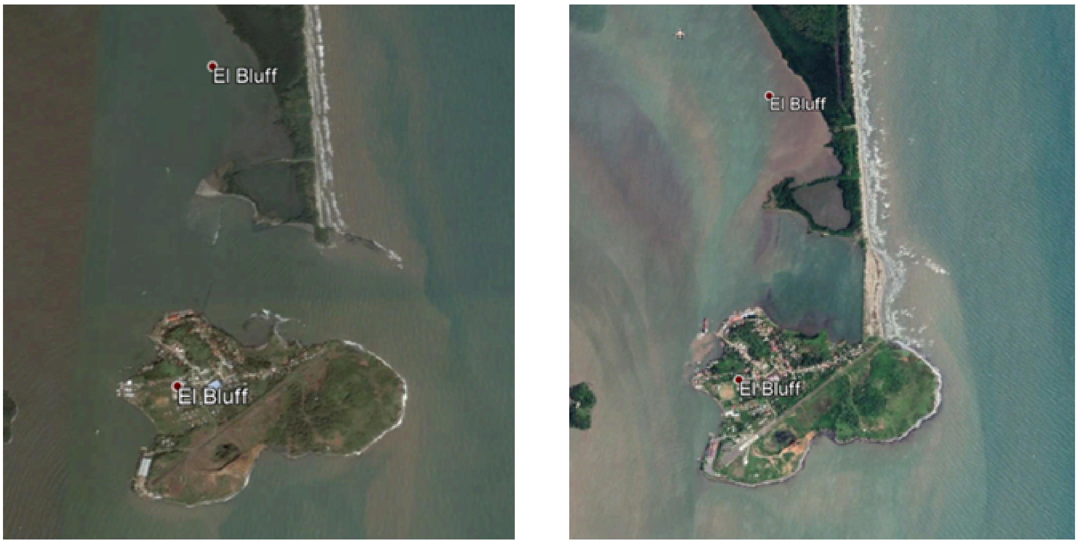

Figure 2.4: Gap at El Bluff in 2007 (left) and 2017 (right) (Google Earth, 2020)

2.2.2 Inner tidal basin

The morphological development of the tidal basin can be investigated by comparing depth measurements from the year 2019 with depth measurements from the past, as shown in Figure 2.5. The 2019 depth measurements are the green dots. The actual depth measurements from this year are shown in Figure B.5. In a previous study by Alkyon (2004), depth measurements were done from 2001 to 2004. These measurements were executed in the main channel connecting the Rio Escondido's mouth and the northern tidal inlet. The location of the measurements is presented in Figure B.4. This shows that the depth has not varied much between the 1000 and 8000 m point since 2004. The changes between 2000 and 2004 in those figures are probably due to fluctuating river discharges. When comparing the depth from 2001 to 2004 with the depth from 2019, the changes are not substantial. Because the changes are small, the inner tidal basin is assumed to be in morphodynamic balance.

There is also no historical information on the bathymetry for the area. No changes, such as land reclamation or dredging were found in the past for the shallower areas. It is assumed that the shallower parts are in morphodynamic equilibrium.

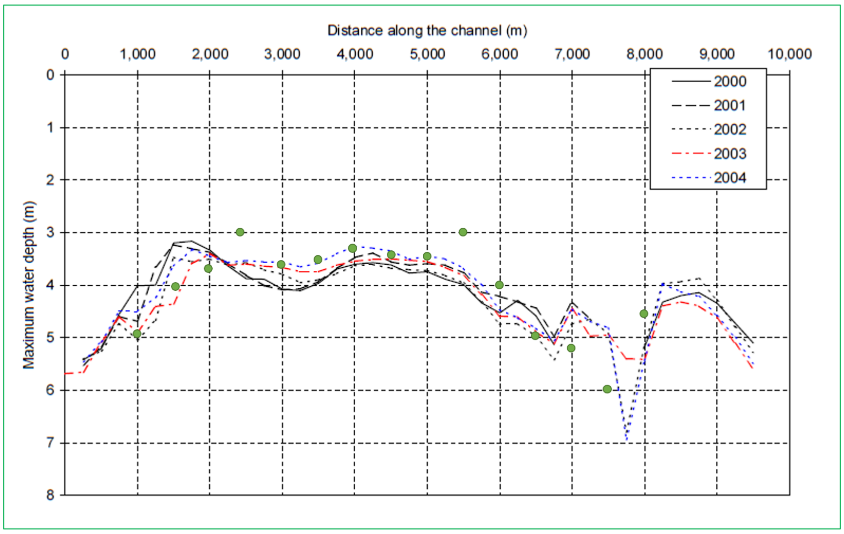

Figure 2.5: Measured depth from 2000 to 2004 (Alkyon, 2004), with measurements from 2019 notated by green dots

2.3 Meteorology and hydrodynamics

The tidal basin and its adjacent coast are subject to the dynamics of tides, waves, and currents. This section details further the dominant magnitudes and directions of these dynamics. The most important physical processes that influence the morphodynamics of the area are examined.
As stated in A.3.1, the hydraulic boundary conditions identify the kind of tidal basin because they determine the sediment transport in the area, which in its turn influences the hydrodynamics (Van der Wegen and Roelvink, 2012). If the hydraulic conditions are identified and compared with each other, predictions about the sediment transport can be made. The hydrodynamics responsible for the currents that move the sediment include the astronomical tide, meteorological tide, river discharges, and waves.

2.3.1 Meteorology

Meteorological characteristics play an essential role in the hydrodynamics of an area and are therefore essential to study. The study area has a monsoon climate with an average annual rainfall of about 4400 mm/yr. June and August are the wettest months, and the driest months are February through April.
Trade winds dominate the wind climate in front of Bluefields Bay, creating swell waves throughout the year. A CFSR node in front of Bluefields Bay was analysed. The average wind speed is below 9 m/s 95% of the time. The dominant directions are from the northeast and east-northeast. Two periods of more intense winds were found during the winter and summer solstices. During the hurricane season, from June through November, wind speeds can reach more than 100 km/h.
In the area seawater warms up every three to seven years. This warming up of the water is called the El Niño phenomenon and initiates droughts in parts of the country while passing hurricanes produce strong winds, cyclonic swells, and heavy rains. Tropical depressions from El Niño have a significant impact on the meteorology of Bluefields Bay.

2.3.2 Rivers

Different rivers deliver fresh water to the basin through several beddings. The data on the discharges is limited. The river discharges were estimated using a runoff model, specifically the logistic equilibrium model (Álvarez Díaz et al., 2015). The outcomes include extreme peak flows and tropical cyclones. Table 2.1 gives the results of the 10th percentile, 50th percentile, and 90th percentile flow regime. The river has the highest discharges in the wet season, May through December, and the lowest discharges in the dry season, January through April. The Rio Escondido has the largest discharge and therefore the most substantial influence on the hydrodynamics of the area.

River	Medium discharge	Q10 (m^3/s)	Q50 (m^3/s)	Q90 (m^3/s)
Caño Negro	86.83	8.30	63.23	196.51
Kukra	51.32	5.14	32.11	114.36
Docuno	5.43	0.61	3.20	11.99
Torsuan	12.59	1.43	7.44	27.76
Escondido	410.30	38.31	299.81	940.35

Table 2.1: Percentiles of the river discharges

Figure 2.6 shows the discharge of the Rio Escondido throughout the year 2001. During the wet period, the discharge rises above 1000 m^3/s, whereas during the dry period, the discharge does not reach 100 m^3/s. This difference in discharge has a huge influence on the sediment transport per period, as the amount of sediment transported is nonlinear dependent on the quantity of water flux carrying it. More about this is explained in Section 3.4.2.

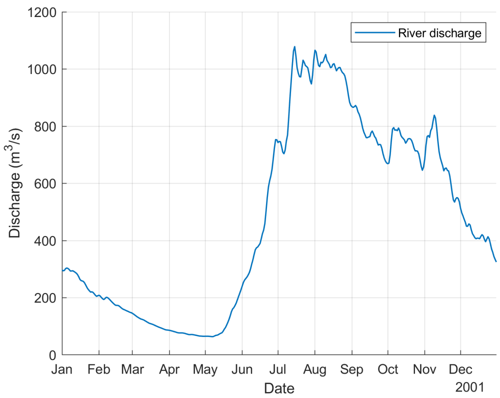

Figure 2.6: Discharge of the Rio Escondido in 2001

2.3.3 Tides

The tidal range in the area is between 0.2 and 0.6 m, which characterises it as a microtidal regime. The tidal signal has a highly irregular shape and the character of a mixed type that is predominantly semidiurnal (Mangor, 2004).

Measurements with an ADCP were done at the tidal inlets in March. The tide is ebb dominant at the northern inlet, which is clarified by the exiting of the discharge of the Rio Escondido through the inlets. Velocities of around 1 m/s are reached during spring tide. This velocity is near the velocity of 0.9 m/s, which is considered the speed of an inlet cross-section in equilibrium (Escoffier, 1940).

2.3.4 Waves

Measurements of wave heights were taken at a depth of 15 m in front of the barrier island. The wave height is moderate, with persistent and long wave periods. The significant wave height does not exceed 1.5 m 90% of the time. This relative low height is partly because the shallow continental platform induces wave dissipation through friction with the bottom. As the waves are uniform in form and direction, they qualify as swell waves. Swell waves are typical for the trade winds that generate the wave climate in the area (Schwartz, 2005). The only variation they have around the mean is due to tropical storms. The storms are, however, too seasonal to dominate the long-term wave climate. Instead, they initiate the extreme wave heights. The extreme wave heights coincide with the subtropical anticyclonic and cyclonic activity, where the hurricane season lasts from June through November. The wave directions predominate from the northeast and east-northeast as caused by the trade winds from that direction.

2.3.5 Currents

The ocean current dominates near the coast. It flows from the Caribbean Sea to the coast of Nicaragua, where it splits in a northern and a southern direction through trade winds and quasi-geostrophic adjustment due to fresh water contribution. At Bluefields Bay the largescale currents run from north to south. These have strong baroclinic structures and the frictional effects of northeast winds, which have a width of 10 – 30 km. The winds are dominant, and they are highest in the months August through October and lowest in February through July. The longshore current has a velocity of between 0.1 0.5 m/s. How this fluctuates through the year can be seen in Figure B.2. The strong currents coincide with the stronger winds in the months of August through October.
In the lagoon the tide and rivers initiate a circulation current. Figure B.3 shows the movement of the current due to the fresh water of rivers and the tidal flow. The fresh water flow of the rivers moves by way of the edge of the basin to the southern inlet (Brenes et al., 2007a). The seawater moves into the basin through both inlets, where it creates saline fronts with the fresh water discharges. These currents have a velocity magnitude of 0.36 m/s for the surface and 0.20 m/s for the bottom (Brenes and Castillo, 1999).

2.3.6 Salinity intrusion

Marine water enters the bay through the northern inlet, producing a saline front when meeting the fresh water flow from the northern rivers. When the marine water enters through the southern inlet, it flows to the west, generating two saline fronts when converging with the fresh water flows coming from the northern part of the lagoon and from the southern rivers. This general pattern of surface circulation intensifies during winter due to the increase of the river discharges (Brenes et al., 2007b).
In Appendix A.1 it is explained that the estuary should have significant water depth for horizontal stratification due to salinity intrusion. Figure B.1 shows the salinity distributions in October and March. The river discharge is small in March, and the salinity intrusion reaches therefore far into the lagoon. The horizontal stratification it therefore not that substantial in this period. In October, which is in the wet period, the river discharges increase substantial, and the salinity intrusion is pushed back. The horizontal stratification increases substantially in this period. When the horizontal stratification is substantial, gravitational circulation is induced. The effect of horizontal stratification intensifies when the water depth is large. The channel depth, which is 4.5 m, and the depth of the lagoon, which is 1.5 m, is too shallow for large sediment fluxes due to gravitational circulation.

2.4 Sediment

In this section the sediment of the area is analysed. The transportation of cohesive and non-cohesive sediment is explained in Appendix A.2. When these two types of sediment interact, the transportation is influenced.

2.4.1 Sediment fractions

Bed samples of the area were taken in March 2019. Figure 2.7 B shows the different sediment fractions per location in the tidal basin. For each sample the percentage of gravel, sand, and mud is determined. The highest mud percentages are in the southern shallower areas with low flow velocities. In the places with higher flow velocities, both at the river mouth of the Rio Escondido and around the tidal inlets, the highest sand content is observed. In the southern part, the flow velocities are lower than in the northern part. The mud in the southern area has time to consolidate, as this fraction is not moved frequently. The sample tests at the coast show that the bed composition is a combination of mud and sand. The mud is mainly from the Rio Escondido. The beach is dissipative, which suggests that the average sediment is fine sand (Bosboom and Stive, 2015).

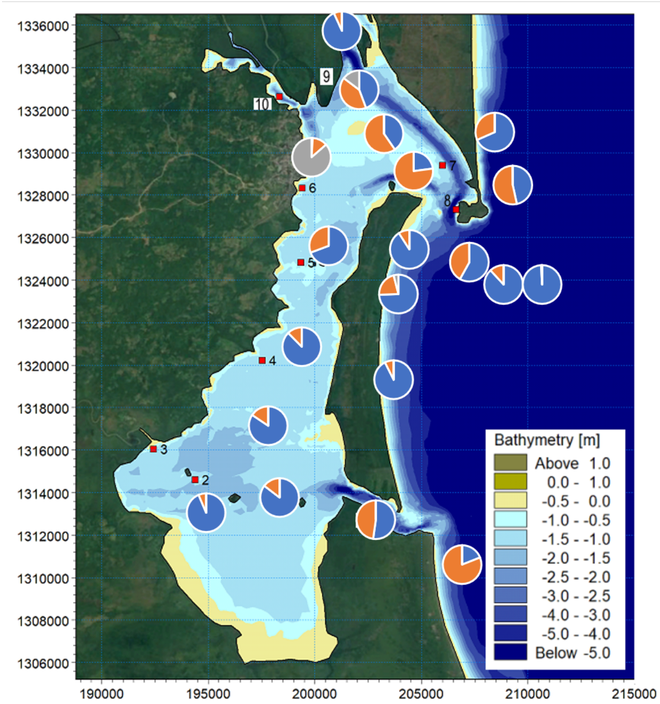

Figure 2.7: Sediment fractions, with blue being mud, orange being sand, and grey being gravel

Location	Rio Escondido	Rio Kukra	Rio Cano negro	Northern inlet	Southern inlet
1m below surface (mg/l)	15.34	6.37	16.09	29.17	19.91
Mid depth (mg/l)	27.06	13.22	16.86	31.74	21.39
1m above bed (mg/l)	36.30	15.17	18.60	34.99	27.11

Table 2.2: Suspension sediment concentrations

2.5 Conceptual model

The conceptual model of the area's hydrodynamics is presented in this section. It is based on the information presented in Section 2.3. The model addresses those natural processes that are accounted for and those which are neglected. A visualisation is made of these choices. The dominant forcing processes and the seasonal variation of these processes are elaborated on. Moreover, the model was used to identify the critical processes that were considered in the numerical model. It supports the decisions on critical parameters in the numerical model. The eventual results of the numerical model were substantiated with the conceptual model and were used as validation. Here first the conceptual model of the existing situation is described. Subsequently the models with the port alternatives are highlighted.

2.5.1 Existing situation

Figure 2.8a shows the sediment fluxes in the area of interest. In the existing situation, there are two large sediment fluxes entering the area. These are the fluvial sediment entering through the Rio Escondido and the longshore transport of sand. Both fluxes are indicated with yellow arrows. The longshore transport depends predominately on the hydraulic processes at the coast, which are the waves and tide. The microtidal range has a maximum of 0.6 m, while the significant wave height is 1 m. According to Figure A.3, the area is wave-dominant. The wave-dominance is substantiated, as the coastline is smooth and has not changed over the last 47 years. These waves initiate the sediment transport at the coast and the tidal inlet. The direction of the longshore transport is dependent on the angle of incidence for waves in the breaker zone, according to Appendix A.3. The predominating waves are from the northeast and east-northeast, and thus, the direction of the longshore transport is southward during the year. The swell climate with seasonal tropical storms causes a shallow littoral drift zone. The shallow zone is due to the moderate height and long

periods, thus creating a moderate steepness. Coarse sand is moved onshore by the swell waves, and finer sediments are transported the other way around. As the coast is in morphodynamic equilibrium, the fluvial sediment is transported away from the coast.
The swell waves tend to be plunging breakers; however, in Section 2.1 the slope of the bathymetry is one of a dissipative beach. An explanation for the dissipative beach is that Bluefields Bay is in a tropical cyclone area of influence. In a tropical cyclone area, cyclones have a high impact on the coastal profile. However, these storms occur in low frequency, and the normal wave climate (Mangor, 2004) foremost determines the coastal profile. It is possible that the bathymetry measurements were done after a storm, therefore explaining the dissipative beach.

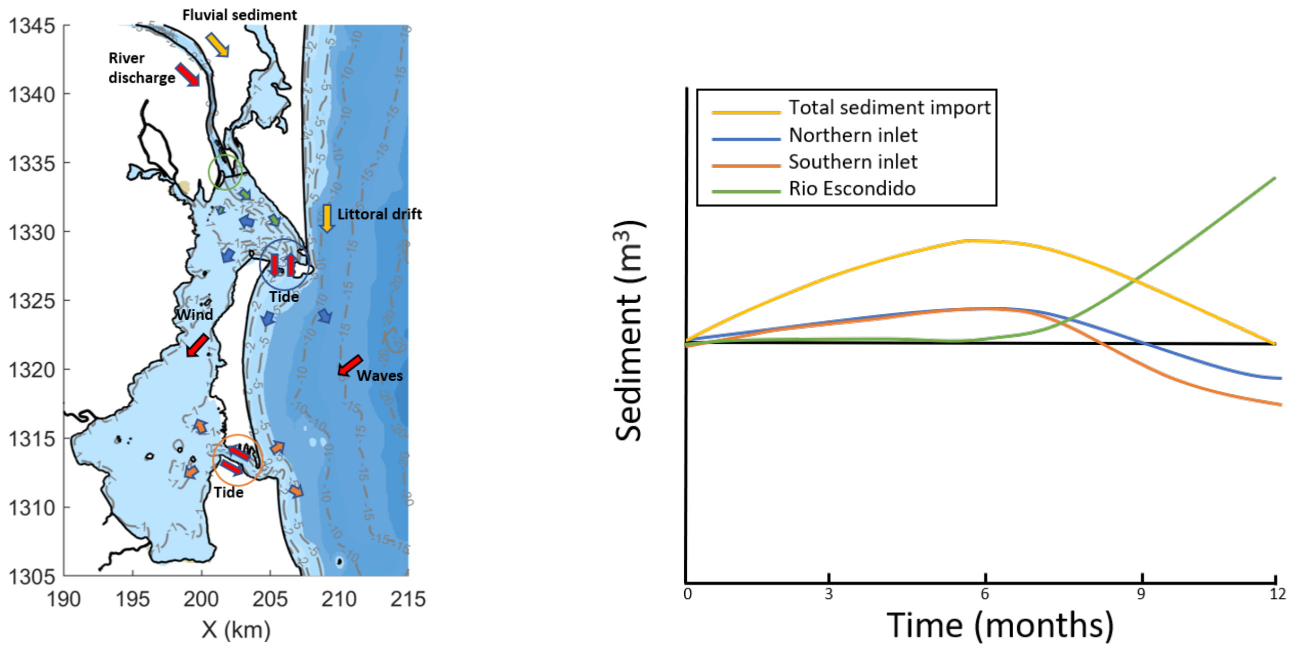

(a) Hydrodynamic forcing components and the initiated sediment transport

(b) Sediment balance

Figure 2.8: Hydrodynamic forcing and the area's sediment balance

The tidal basin is in the shelter of the barrier island, making the influence of waves minimal. This area can be characterised as a tidal lagoon with substantial fresh water runoff in wet months. In the tidal lagoon, the main processes that dominate are the fresh water discharges from the river, namely the Rio Escondido, and the tidal flow in the tidal inlets. The largest sediment flux that enters the lagoon is the fluvial sediment from the Rio Escondido. Figure 2.6 shows that the river discharge fluctuates from small quantities between March and May to large quantities between July and November.
During the wet period the largest part of the fluvial sediment, which is mainly mud, enters the lagoon. The river discharge increases and has a strong influence on the hydrodynamics and morphodynamics. The flow direction in the northern part of the lagoon will be constant in the ebb direction. The interaction with the tide is still present, but the tidal flow only strengthens or weakens the total flow velocity. Most of the mud follows the river flow through the river channel to the northern tidal inlet. This route is indicated with the green arrows in Figure 2.8a. When the discharge is substantial enough, fresh water from the Rio Escondido circulates over the tidal flats to the south of the basin, according to Section 2.3.5. A small part of the mud will flow to the south over the shallow areas. A small green arrow indicates this in the figure.
A substantial part of the basin is around 1 m below MSL without channels in the bathymetry. The absence of channels indicates that for this part of the basin, the wind-induced waves are the dominant factor. Wind-induced waves have a more substantial effect on bringing sediment into suspension in shallow areas. Waves induce higher bed-shear stresses in shallow areas than in deep areas. These waves create a more smoothed bathymetry. As the wind has a direction from the northeast and the basin has a width of 6 km and a length of 30 km, the fetch is long enough to initiate wind-induced waves. Because these wind-induced waves keep the sediment in suspension in the shallow areas, the strengthened southward current due to the river discharge transports a part of the sediment to the southern inlet. This sediment will exit at this inlet in the wet period.

During the dry period, the river runoff is small. Based on the bathymetry, the tides and the wind-induced waves are the dominant factors in sediment transport in the dry season. In the northern part of the lagoon, small flood channels indicate the tidal flow influences the morphodynamics. In Figure 2.8a, the sediment transport due to the tidal flow is indicated with the green and orange arrows around the inlet. The tidal basin has large storage capacities and shallow channels, indicating a net flood dominant transport of fine sediment (Bosboom and Stive, 2015). The blue and orange arrows are directed in the direction of these shallow areas. During the dry period, the lagoon imports sediment due to the flood dominance. The river discharge is too low to initiate a constant ebb directed flow. The sediment fractions reaching the shallower parts of the area are the finer sediment fractions. Only suspended sediment can reach the shallower areas because the flow velocities are low in this part of the lagoon. In the channels the flow velocity is higher than in the flat area, giving fine sediment less time to settle. The sediment of the bed composition in the channels is a coarser fraction, mainly sand.
Figure 2.8b shows the conceptual model of the sediment balance. Time is represented on the x-axis and is an annual total. The y-axis is the quantity of the mud fluxes. A positive gradient is in the direction of the lagoon. This means during ebb the line of the Rio Escondido is positive, while for the tidal inlet, the lines are negative. In Section 2.2 it is stated the basin is in dynamic equilibrium, meaning the total net import of the basin is zero. The coloured lines in Figure 2.8b correspond to the coloured arrows in 2.8a. The tidal basin is flood-dominant in the dry period, importing sediment in the first half-year. As the river discharges increase in the wet period, the tidal basin is forced into ebb-dominance, exporting sediment.

2.5.2 Possible port structures

The possible layouts of the port are shown in 2.9. In Appendix C the dimensions of the navigational channels and the quantity of capital dredging required are presented. The navigation channels are 15 m deep and 123 m wide. If the port and its structures are constructed, the hydrodynamics and morphodynamics seen in the conceptual model will change. In Appendix A.3.2 the dynamic equilibrium of the morphodynamics is explained. This equilibrium is disrupted by altering the area's dimensions in the Equations A.7, A.8, A.9, and A.10. The forcing factors of the hydrodynamics, namely waves, tidal prism, and river discharge, do not change. The morphodynamic system will be forced back into dynamic equilibrium. However, it takes many years to restore a morphodynamic equilibrium. The empirical relations indicate the dimensions of the parameters for the dynamic equilibrium. The equations show which elements will change in the long-term development of morphology to restore balance. The initial sediment transport patterns due to the hydrodynamic processes that restore the dynamic equilibrium are the focus of this research. This study concentrates on the initial changes in the hydrodynamics and sediment transport patterns. The morphodynamic development over multiple years is predicted with these initial changes.

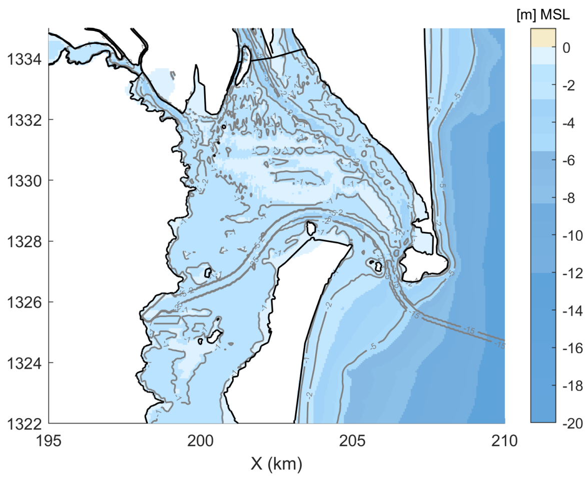

(a) Alternative 1A

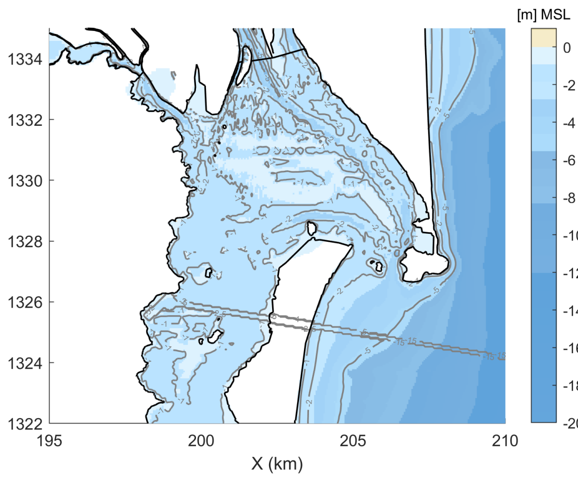

(b) Alternative 1B

Figure 2.9: Port alternatives

For the potential locations of the port and its navigation channel, different sedimentation processes would be of influence. The navigation channel of Alternative 1A would have an entrance through the northern

tidal inlet. The port itself and a part of the connected navigation channel would be in the shallower part of the lagoon. These areas have a morphodynamic equilibrium. As Equation A.10 shows, the total equilibrium channel volume below MSL is dependent on the tidal prism. The tidal prism would not change with the dredging of a channel. As the tidal prism would not change, the total equilibrium volume of the channel would not be impacted. The dredged volume would disrupt the balance, and sedimentation would reset it. The shallower area that would be crossed by the dredged channel at the land-inward part of the basin consists of fines. The currents in this area are low. When these fines would reach the channel and port, the flow velocity would decrease due to the more considerable depth. Because of the lower flow velocities, the bed shear stresses would be too low to keep the sediment in movement. During the dry period, the lagoon imports mud through the northern tidal inlet. The tidal flow is responsible for this import. This flow follows the path with the least resistance, which is the deepened channel. A large part of the imported mud would transport through the channel and would deposit once the flow velocity decreases. In the wet period, the river discharge forces the northern part of the area in ebb dominance. The lagoon only imports mud from the Rio Escondido. Small currents from this discharge would transport this mud to the channel.
The salinity intrusion in the dry period is substantial and is less so in the wet period, according to Section 2.3.6. When the newly dredged channel of 15 m would cross depths from 1 to 5 m, the increase in gravitational circulation inside the channel would be substantial. A constant land-inward directed near-bed flow would be initiated. This would mean that the import through the inlets would increase, and more mud would transport to the port and land-inward channel.
Furthermore, the dredged channel would cross deeper parts in the northern tidal inlet. The dynamic equilibrium of Equation A.9 is disturbed when the cross-section of the inlet is altered. The tidal prism would not change, but the cross-sectional area would be enlarged; because of the enlarged cross-section, the flow velocity would decrease. Sediment passing would have a higher chance of depositing here, as the flow would not have the capacity to carry all the sediment. The inlet would be pushed back into equilibrium by sedimentation. Fluvial sediment and coarser fractions from the longshore transport pass through the tidal inlet. The depth would enlarge from 4 to 16.9 m, increasing the cross-section substantially. The flow velocity might decrease to such an extent that the fluvial sediment could deposit. If this occurs either the erosion shear stress must be small, or the deposited sediment in the inlet consists mainly of sand fractions from longshore transport.
At the coastline the dredged channel would be in the influence sphere of the littoral drift. The dredged channel further from the shore would trap the sediment that originates from north of the split. When the dredged channel would capture the sediment from the littoral drift, the downstream coast would have a shortage in the sediment supply. Erosion would occur in the downstream area. A rule of thumb for dredging maintenance is the volume of cut method (Van Rijn, 2006). For this method different cases were studied, and a proportionality equation was found. The proportionality equation is between the volume of material that is removed and the amount of material deposition. Equation 2.1 gives this proportionality. For silty/sandy nearshore conditions, it is about 10% to 15% per year, and for silty/sandy offshore conditions, it is about 5% to 10% per year. For muddy land-inward conditions, the deposition consists of 25% to 75% of the capital dredged volume. These ranges of percentages are based on the sedimentation rates in different case studies. These percentages are from analysed case studied by Van Rijn (2006). Van Rijn (2006) observed the different hydrodynamic conditions and sediment properties in the case studies. For averaged hydrodynamic conditions, and neglecting extremes, the sedimentation rates should be between these ratios.

$$V_d = \gamma * V_{cut} \tag{2.1}$$

V_d	=	Sedimentation volume	$[m^3]$
γ	=	Proportionality factor	$[-]$
V_{cut}	=	Dredged volume	$[m^3]$

The sedimentation described above would mainly depend on the large sediment fluxes that enter the area, namely mud from the Rio Escondido and sand from the longshore transport. The channel would also alter the hydrodynamics locally. The flow directly around the channel would be higher because the tidal flow would have a higher velocity in this area. The tidal flow would have a less hard time reaching the shallower areas, as it would follow the channel to these areas. Higher bed-shear stresses due to this flow would suspend sediment locally. A large part of the sedimentation in the channel is because it would attract mud and sand from the direct surroundings.

The equations for the morphodynamic equilibrium are also valid for Alternative 1B, meaning the sedimentation that would occur has a similar clarification. The difference is that a more substantial part of the navigation channel for layout 1B would be located further away from the fluvial sediment input, namely the Rio Escondido. This fluvial sediment would have more difficulty reaching the channel and depositing here. The morphodynamic equilibrium would take a longer time to restore, meaning every year the sedimentation would be less than for Alternative 1A. Both port layouts would be exposed to encounter sedimentation by the tidal motion through the inlets. However, with Alternative 1B, a new entrance through the barrier island would be constructed. Due to the new opening, the hydrodynamic forcing conditions of the area would change. The tidal flow would have a new opening to flow through. Whether this new opening would remain open due to the tidal flow is dependent on the flow velocity. It is possible that the new opening would initiate such a flow force, and the flow velocity would be high enough to keep the opening due to natural processes. Because of the new opening, the flow velocity due to tide in the northern inlet would decrease. Due to the lower flow velocity in Equation A.9, a smaller cross-sectional area would be needed for the dynamic equilibrium. Sedimentation in the northern inlet would occur.
Finally, the external channel of 1B would have a longer trajectory in the breaker zone than that of Alternative 1A due to the dissipative beach around it. The seabed is dynamic and more active around a longer stretch around the outer channel of Alternative 1B. Locally sediment transport would restore the morphodynamic equilibrium at a faster rate. Both alternatives are likely to catch all of the longshore transport.

3 Approach and Model setup

The previous chapter presents a conceptual model of the area. This chapter explains the numerical model that supports the conceptual model. A numerical model is used to test the claims of the conceptual model. A numerical model either supports or challenges a conceptual model. For this complex system, a process-based model was used. This chapter elaborates the numerical model Delft3D. First, the type of model is explained. Then, the simulation approach to testing the conceptual model is given. Next, the main model setup and the input data are presented. Subsequently, the model calibration is explained through sensitivity analysis and model validation.

3.1 Type model

A multidimensional hydrodynamic and morphodynamic model, Delft3D, was used to assess the relevant processes of the area. This process-based model is an approach to reality executed to explicitly represent all the essential physical processes acting on sediment in the coastal environment. It translates empirical observations into mathematical formulations relating observed sediment transport to intrinsic properties such as sediment grain size and forcing processes like tide, waves, and wind (Lesser et al., 2004). This numerical model presents the sediment transport processes in sufficient detail while remaining computationally efficient. This idealised model represents best a fundamental understanding of the morphodynamic system. An extensive range of morphological dynamics is essential for the area. The modules of Delft3D-FLOW and Delft3D-WAVE are coupled to present the hydrodynamic processes. These modules combined solve sediment transport under the influence of waves and currents. The modules consist of a 2D or 3D hydrodynamic model. With the combined effort of the Delft3D-FLOW and the Delft3D-WAVE modules, the software is capable of modelling waves, tides, currents, and their additional sediment transport. The model gives insight into water levels, depth-averaged velocities, and bed-shear stress (Lesser et al., 2004). The calculations can be complicated by adding other processes, like salinity (Deltares, 2014).

3.2 Model approach

In this section, the approach to determining the existing and future morphodynamic behaviour of the area is presented. The aim of the morphodynamic study is to determine the sedimentation in the potential future access channels and to determine the impact of the potential channels on the estuary and the adjacent coastlines.

First the model must represent the existing situation as accurately as possible. As explained in Section 2.2, the sediment transport of the area is assumed to be in dynamic equilibrium. There are no large sink and source holes, which means that all the sediment from the rivers and coastal zone that enters the area also leaves the area.

The 2D model was chosen, as the important hydrodynamic components in the area can be modelled sufficiently in this way. The hydrodynamic components that influence sediment transport are explained in the conceptual model in Section 2.8. A 3D model would require enormous computational effort because the simulation time should be at least one year and because the area requires a large computational grid. The added value of the 3D model to the results would be small. The choice of whether to model in 2D or 3D is further elaborated upon in the discussion in Chapter 5.

The sediment transport results of the model must show a dynamic equilibrium eventually. The conceptual model from Section 2.5 explains that the initial sediment transport processes were analysed in the existing situation and in the situations after constructing the ports. For the initial transport patterns a simulation period of a year is sufficient. Morphodynamic development usually takes years or decades. The long-term morphodynamic development was not taken into consideration in the model, and thus the model did not account for bed-level updates.

In a numerical model that is in morphodynamic equilibrium, the erosion and deposition patterns are the same for successive simulations. In this model, the dynamic equilibrium for mud can be determined with a mud balance: The amount of mud that enters the system and leaves it must be repetitive for successive years. A time span of a year was chosen because the area shows an annual wet and dry period. The processes during these periods differ so much that both must be considered in the simulation of the morphodynamic equilibrium. The spin-up time needed to reach equilibrium for mud consisted of more than one model year. The model had to be restarted after a simulation period of a year in order for the mud balance

to show the same results in successive years. The model equilibrium also holds for the sand fraction of the longshore transport. The longshore transport must show the same transport rates through different transects on the shore in the successive years.
When the system is modelled in a dynamic equilibrium, the sediment transport depends on flow, which is initiated by the hydraulic processes. This dependence means the amount of sediment the flow can transport is present in the entire area. By creating a bed composition with sediment for the initial conditions, the full capacity of sediment transport due to flow was applied over the entire model grid. The flow was than able to transport sediment from and to the same places in each simulation, as there is never a shortage of sediment at a particular area in the model grid. When the model showed the same results of the sediment fluxes for successive simulations, it was in dynamic equilibrium.
The model was calibrated through phenomenological calibration, as field data is scarce. Calibration through knowledge of the physical processes is called phenomenological calibration. The only data available for sediment is measurements of sediment concentrations. No hydraulic data accompanies these measurements, making it hard to use the data as validation of the model. For the calibration of the mud parameters of the model, use was made of a mud balance. Aside from the mud balance, the deposition pattern of the mud was compared with the results of the conceptual model and the bed samples to validate the model. The longshore transport was validated by comparing the quantities with analytical calculations of a bulk longshore transport formula.
The Delft3D-FLOW module gives computational results of the flow velocities, the flow directions, the bed-shear stresses, and the tidal asymmetries. These are the primary hydrodynamic forcing for the bottom and suspended sediment transport in the tidal basin, as Appendix A.2 explains. These processes were used to describe the sediment transport patterns inside the tidal basin. The Delft3D-WAVE module gives computational results of the significant wave height, the angle of wave incidence, and the wave dissipation. These wave characteristics have the most substantial influence on longshore transport. The stability of the adjacent coast was analysed using the results of these processes. The transport of the cohesive fractions entering and leaving the tidal basin through the inlets is also influenced partly by the waves. The dynamics of the sediment transport around the tidal inlets is influenced by the river discharges, the tidal currents, and the currents due to waves. All these processes were included in the model simultaneously to achieve realistic results.
Once the results of the Delft3D model showed that the system was in a dynamic equilibrium, the existing situation was analysed with the model. The hydrodynamic processes and the sediment transport were described for the existing situation by means of the processes mentioned above. Next to these processes, the deposition and erosion patterns were analysed. When a clear picture was gained of the existing situation from the model, the alternative situations with the geometry of the access channel and port were included in the model. The impact the alternatives have on the hydrodynamic processes was analysed to assess the possible variations in sediment transport in the area. Subsequently the results of the model for these alternatives were compared to decide upon the optimal location of the port and access channel. The outcome of the model is only an approximation of reality, and the comparison was thus relative. The comparative study could indicate the preferred option for the location of the port between Alternative 1A and 1B. The sedimentation numbers were analysed meticulously, however, precise numbers of sediment transport are hard to produce for the stage of the project. Nonetheless, approximate numbers, including a range of accuracy, can be given regarding the sedimentation and erosion volumes. The focus of the model results was on the sedimentation of the navigation channel and erosion of the adjacent coast. In this way, the impact of the channel on the environment could be determined.

3.3 Model setup

The data and characteristics applied to the model are presented in this section. The model is setup based on the data collected in Chapter 2. Choices in the model setup are also dependent on missing data. In this study data about sediment properties such as size, suspension quantities are unknown. A sensitivity analysis is done to deal with unknown data. Based on the conceptual model and the data collection, choices are made regarding what is conceivable to simulate and study. The study concentrates on sediment transport before and after human intervention. A validated hydrodynamic model will be the primary driver of sediment transport. Since few field data on sediment have been collected, a strategy must be developed to simulate the sediment realistically. Hydraulic boundary conditions used in the model based on the observed data are waves, tides, and river discharges. The data of the sediment must still be translated into input parameters. There are no measurements of the input of sediment into the system by river discharge. Because the sedimentation processes of mud can differ a great deal per area, a proper analysis of the input parame-

ters of this sediment fraction is executed.
Few representative sediment fractions must be selected to gain a computationally efficient model.Based on the different samples described in Section 2.4, the bed is assumed to be well mixed. The mud of the Rio Escondido covers the bed composition with a small layer. The bed composition, composed of two layers, must be developed. The erosion of cohesive and non-cohesive soil occurs through various processes. When different kinds of soils are mixed, they influence each other's mobility. Larger grains become more mobile, and smaller grains, less so. The sediment transport module consists of a suspended sediment transport formula and a bedload transport formula. For the suspended sediment transport, the advection-diffusion equation is solved and, subsequently, for the bedload transport, the bedload equations are solved (Lesser, 2009). These equations are further elaborated in Section 3.4.3.

Physical processes

The water flow and sediment transport in Bluefields Bay and its adjacent coast is mainly by tidal conditions, waves, and river discharges, as explained in Chapter 2. The hydraulic physical processes that the model includes at the boundaries are river discharges, tide, and waves. For the river discharges, the Rio Escondido, Docuno, Torsuan, Kukra, and the Cano Negro are modelled. The tidal constituents are computed to simulate the tide in the area. Waves are also computed to simulate the longshore current that is initiated by them. Moreover, the wind processes are modelled, as they influence the wave-induced waves in the tidal basin.
The sediment transport is divided into processes for cohesive fractions and non-cohesive fractions. For non-cohesive transport, the Van Rijn formulations are used (Van Rijn et al., 2003). For the cohesive mud fraction, the Partheniades' (Partheniades, 1965) and Krone's (Krone, 1965) equation for erosion and deposition are applied.

Computational grid

Figure 3.1 shows the computational grid that covers the entire bay and the coastal area with the adjacent coast. The grid extends 36 km northward from the northern inlet, 23 km southward from the southern inlet, and 37 km offshore to the east. The rivers are also included in the length of known bathymetry data. The computational grid resolution is approximately 50 m in the area of interest, coming up to about 800 m at open sea. The grid cells for the Rio Escondido are curvilinear. The model consists of 243,361 grid cells. Figure 3.1b shows the area of interest with higher-resolution grid cells.

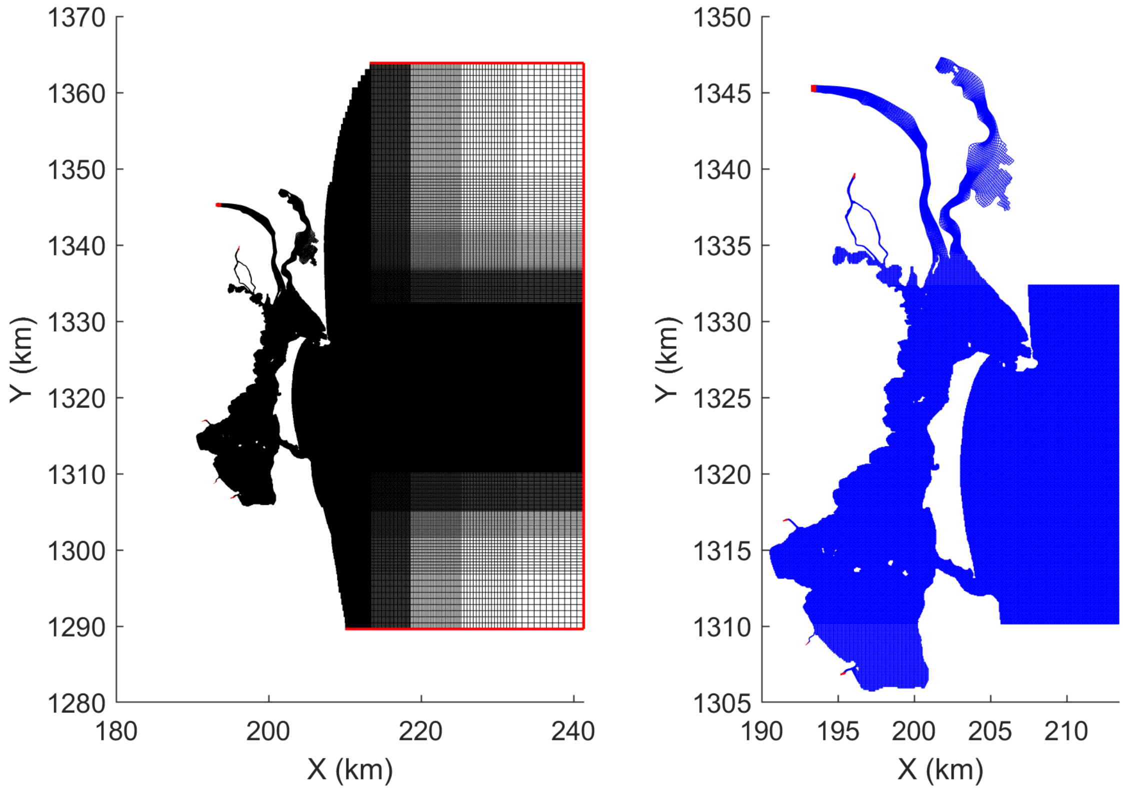

(a) Entire area

(b) Area of interest

Figure 3.1: Computational grid of the entire area and area of interest

Boundary conditions

There are eight open boundaries in the model. These boundaries are depicted in red in Figure 3.1. Five are upstream boundaries of the rivers, shown more clearly in Figure 3.1b. The time series of the river discharges originating from the river boundaries fluctuate heavily over the year, with a wet season and a dry season. The three other boundaries are offshore, which have tide and waves as a boundary condition. The northern and southern boundaries of the ocean are Neumann conditions, indicating no gradients in surface elevation and velocity in the along- shore direction.

Bathymetry

Bathymetry measurements were equipped for the area of interest represented in Figure 3.1b. The most detailed measurements are derived inside the lagoon, the two inlets, and partly offshore. For the offshore measurements, which are not of interest, ETOPO is used with a resolution of 1 min. Although the Rio Escondido is not part of the area of interest, it has a significant influence on the morphodynamics of the area. Field measurements were only done at the mouth of the river. For the upstream part, old marine charts from EPN from 2004 are the only source of information on the bathymetry and are therefore used as input.

Simulation period

The area has a clear dry and wet season. The fluvial sediment input is of only substantial quantity during the wet period, as shown in Section 3.4.2. In the dry period, other hydrodynamic processes are dominant in sediment transport. The wave conditions during storm seasons fluctuate during the year, as shown in Section 2.3.4. The simulation's timeline was thus set to one year, since the hydraulic forcings change during this period. The simulation takes 12.5 days to run.

3.4 Input data

This section explains how the available analysed data in Chapter 2 is schematized into model input parameters. The parameters to model the hydrodynamics, sediment, and morphodynamics are presented, as this study concentrates on these processes. The main model settings of Delft3D are set to their defaults. These settings are presented in Table D.1 of Appendix D.

3.4.1 Hydrodynamic input

In this work, the K-media classification technique (Hastie et al., 2008) is used to obtain conditions that represent hydrodynamic behaviour corresponding to the last 20 years. These conditions are translated in hydraulic input parameters. The data of the physical hydrodynamic conditions, presented in Section 2.3, are reduced to several sea, wind, and flow states. The probabilities of each process, in combination with other processes, is calculated, and a yearly appearance of combined hydrodynamic processes is presented for each process. This technique is preferred when analysing the average conditions. The hydraulic data of the year 2001 emerged as the most representative year and is used in this study.

Tide

The parameters representing the tide have a meteorological and astronomical component. The meteorological component is derived from the Global Tide and Surge Reanalysis (GTSR) database. This database is derived from worldwide meteorological tide analysis and extreme sea levels using hydrodynamic models (Muis et al., 2016). The database has a daily time series of meteorological and astronomical tides.
For the astronomical tide, the data from the global model TPXO global tide model, developed by Egbert and Svetlana (2002), is used. The database, which results from the model, offers four biannual harmonic components (M2, S2, N2, and K2), four daily components (K1, O1, P1, and Q1), two long periods (MF and MM), and three non-linear components (M4, MS4, and MN4). The resolution is 0.25 in the latitude and longitude.

Waves

The model settings to represent waves at the offshore boundaries comprise an hourly time series obtained from the Global Ocean Waves (GOW) dataset. The dataset presents time series of wavelengths, wave periods, peak frequencies, directions, and directional dispersion. The data has the parameterisation of physical processes as wave development and dissipations through the wind, non-linear interactions, white capping, and bottom friction. No interactions of wave currents are considered. More information can be found in Perez et al. (2017). The resolution is 0.25° in latitude and longitude. Besides the waves that are a boundary condition, local waves are also generated inside the basin by wind.

River discharges

Several rivers deliver fresh water to the basin through their beddings. The data on the discharges are limited. The river discharges are calculated using a run-off model, namely the logistic equilibrium model of Álvarez Díaz et al. (2015). The outcomes include extreme peak flows and tropical cyclones. Table 2.1 gives the results of the low, averaged, and extreme flow regimes. The river has the highest discharges in the rainy season, May through December, and the minimum discharge in the dry season, January through April. For each day in the model, a discharge quantity is given.

Wind

The wind data input comprises hourly time series gathered from the climate forecast system reanalysis (CFSR) (Saha et al., 2014). The dataset presents time series of wind speed and direction. The time series is reduced from a combination of atmosphere, ocean, land, and ice on the sea surface. The wind data indicates s local wind-induced waves inside the basin have a substantial influence on the bathymetry there.

3.4.2 Sediment input

Section 2.4 presents the known data of the sediment fractions. The data is composed of bed samples and suspended concentrations. As parameters in the model, this data is reduced to three different components. These components are a fluvial sediment fraction that enters the model through the boundary of the Rio

Escondido and two sediment components present in the bed composition in the model. Only three fractions are used to keep the model computationally efficient. Tables D.2, D.3, and D.4, as well as Appendix D.2, present the parameter settings of the fractions.

Fluvial sediment

The sediment fraction that enters the model through the boundary set on the Rio Escondido is mud, modelled as a cohesive fraction. The fraction size is based on the most upstream sediment bed sample of the Rio Escondido. The variable parameters that influence the transport of the cohesive fractions are fall velocity, critical erosion shear stress, and the erosion parameter. In Section 3.5.1, a sensitivity analysis is done to calibrate the input parameters for this fraction, as these are unknown from the data analysis in Section 2.4. For the tidal basin, the fluvial sediment is the most important sediment fraction transported. A large part of the basin of the Rio Escondido is deforested, especially along the banks of the river. This deforestation results in high erosion rates and large volumes of soil that are washed away by rivers every year (Alkyon, 2004). These flows will contribute to sediment entry into the basin. No data is available for sediment quantities except for LIVSET (1963), where the sediment load was estimated to be between the 3.9 to 5.36 million tons per year in 1963. However, river discharges have decreased since then, meaning the sediment transport has also decreased. For high suspended sediment, other factors than discharge are of importance, such as land use in the form of deforestation (Alkyon, 2004). The relation between suspended sediment load and water discharge is non-linear. Transport becomes even more non-linear when bedload transport is considered. Alkyon (2004) estimated sediment transport in 2004 based on the known river discharges around that time. An estimation of between the 2.5 to 3.44 million tons was made. Because new field measurements are scarce, an approach for sediment input is applied linking the flow of sediment directly to the discharge with Equation 3.1 (Jiménez Van Patten, 1975; Lewis Jr and Saunders III, 1985).

$$Q_{solid} = a \cdot Q_{liquid}^{b} \tag{3.1}$$

Q_{solid}	$=$	Solid flow	$[t/day]$
Q_{liquid}	$=$	Liquid flow	$[m^3/s]$
a	$=$	constant	$[-]$
b	$=$	constant	$[-]$

The constants a and b were found by studying tropical rivers with the same characteristics. Table 3.1 displays the potential sediment transport of the Rio Escondido. The average concentration of mud in the Rio Escondido is 0.143 kg/m^3. The total sediment load of 2.6 million tons is between the upper and lower boundaries found by Alkyon (2004). As the tidal basin is assumed to be in balance, the sediment should be transported out of the system.

	Q (m^3 /s)	Sediment load (t/day)	Sediment concentration (kg/m^3)
Dry season (March)	190	769	0.047
Wet season (October)	950	19226	0.234
Average	578	7139	0.143
Total ($t/year$)		2,605,701	

Table 3.1: Sediment transport capacity of the Rio Escondido

Bed composition

The bed composition consists of a combination of mud and sand. The sediment size for mud is larger in the bed composition in the tidal basin than sediment originating from the boundary at the Rio Escondido. Moreover, the sediment fraction is assumed consolidated, as it has been present for an extended period. As a result, the critical erosion shear stress is greater. In this model, the critical erosion shear stress for the fraction of the bed composition is 0.5 N/m^2.

The transport and sedimentation of sand is mostly of importance at the adjacent coast, as explained in Section 3.4.2. The non-cohesive fraction for the entire basin represents the fraction found at the adjacent coast, to keep the number of fractions in the model small. The sand is classified as a fine sand fraction in this area. According to the Wentworth classification, sediment size of 200 μm corresponds to this classification (Wentworth, 1922).

The erosion rate of the separate sediment fractions is affected if the bed is composed of multiple sediment types and sizes. The preference is for a well-mixed bed as fractions in the bed composition are measured (as demonstrated in Section 2.4.). The smaller sediment fractions hide between the larger fractions. Erosion of the smaller sediment fractions decreases so that an underestimation may occur. The erosion rate is proportional to the bed composition. The alternative is that the cohesive fraction covers the other fraction, and its erosions rate is not hindered. Constructing the bed composition is a part of the model calibration, as further explained in Section 3.5.

3.4.3 Sediment transport

In this section, the equations the Delft3D model uses to compute sediment transport are explained. With these equations, insight is obtained into what the critical input parameters of the sediment fraction are that influence the results of the computations. For more in-depth explanations of default settings and other unchanged parameters, one should consult the manual for Delft3D (Deltares, 2014).

Cohesive suspended transport

The transport of suspended sediment in a 2D-model is calculated by solving the depth-averaged model presented by Equation 3.2. The flow velocities are the results of hydrodynamic calculations, and the eddy diffusivities are input parameters. The vertical profiles of velocity, sediment concentrations, and turbulent mixing are not computed in a depth-averaged model. To calculate the bed shear stress and depth-integrated sediment transport, an assumption is made regarding the logarithmic velocity profile (Lesser et al., 2004).

$$\frac{[h\overline{c}]}{\delta t} + \frac{\delta[h\overline{U}\overline{c}]}{\delta x} + \frac{\delta[h\overline{V}\overline{c}]}{\delta y} = h[\frac{\delta}{\delta x}(D_H\frac{\delta\overline{c}}{\delta x}) + \frac{\delta}{\delta y}(D_H\frac{\delta\overline{c}}{\delta y})] + hS \tag{3.2}$$

$\overline{c}$	$=$	Depth-averaged sediment concentration	$[kg/m^3]$
h	$=$	Depth	$[m]$
$\overline{U}$	$=$	Depth-averaged velocity	$[m/s]$
$\overline{V}$	$=$	Depth-averaged velocity	$[m/s]$
S	$=$	Sediment source	$[kg/m^3]$

The exchange between the bed and material in suspension is calculated by the difference between deposition (D) and erosion (E). In the Delft3D model, the equations for deposition and erosion of the cohesive fraction are the Partheniades– Krone formulation shown in Equations 3.3 and 3.4. The erosion parameter (M), critical erosion shear stress ($_cr, w$), and fall velocity (w_s) are the parameters of the cohesive sediment component in the model. Fall velocity is chosen based on a representative sediment size. As Section 3.4.2 has explained, the fall velocity and critical erosion shear stress are unknown for the fluvial sediment entering the boundary of the Rio Escondido. A sensitivity analysis is done for these parameters. The erosion parameter is determined by a sensitivity analysis with the bed composition.

$$E = M * S * (\tau_{cw}, \tau_{cr,e}) \tag{3.3}$$

E	$=$	Erosion flux	$[kg/m^2s]$
M	$=$	Erosion parameter	$[kg/m^2s]$
S	$=$	Erosion step function	$[-]$
τ_{cw}	$=$	Maximum bed shear stress due to current and waves	$[N/m^2]$
$\tau_{cr,e}$	$=$	Critical erosion shear stress	$[N/m^2]$

$$D = w_s * c_b * S * (\tau_{cw}, \tau_{cr,d}) \tag{3.4}$$

D	$=$	Deposition flux	$[kg/m^2s]$
w_s	$=$	Fall velocity	$[m/s]$
c_b	$=$	average sediment concentration in the near bottom computational layer	$[kg/m^3]$
S	$=$	Deposition step function	$[-]$
τ_{cw}	$=$	Maximum bed shear stress due to current and waves	$[N/m^2]$
$\tau_{cr,d}$	$=$	Critical deposition shear stress	$[N/m^2]$

The parameters of the equations above and the suspended load transport for non-cohesive fractions are further explained in Appendix D.1.1.

Non-cohesive bedload transport

For the non-cohesive sediment transport, the method developed by Van Rijn et al. (2003) is used, presented in Equation 3.5. In this equation, the bedload transport (S_b) depends on specific weight (ρ_s), fall velocity (w_s), sediment size (D_{50}), sediment mobility number due to waves and currents (M), and excess sediment mobility number (M_e). The only input parameter that can be adjusted for the non-cohesive sediment component is the sediment size (D_{50}). The sediment size for the non-cohesive fraction is 200 μm (as explained in Section 3.4.2). How the parameters in Equation 3.5 are computed is further explained in Appendix D.1.2.

$$S_b = 0.006 * \rho_s * w_s * D_{50} * M^{0.5} * M_e^{0.7} \tag{3.5}$$

S_b	=	Bedload transport	$[kg/m^2s]$
ρ_s	=	Sediment density	$[kg/m^3]$
w_s	=	Fall velocity	$[m/s]$
D_{50}	=	Median sediment diameter	$[m]$
M	=	Sediment mobility number due to waves and currents	$[-]$
M_e	=	Excess sediment mobility number	$[-]$

3.5 Model calibration

This section explains how the model is calibrated through phenomenological calibration and sensitivity analysis. Calibration and validation are generally difficult in sediment transport modelling. As datasets about the sediment in the area are small, other strategies are used. In this case, the knowledge of the physical processes and the conceptual model is used. Calibration through knowledge of the physical processes is called phenomenological calibration. Calibration is an iterative process of executing sensitivity analysis and qualitatively assessing the physical processes of the model.
Because the system is in dynamic equilibrium, the model is calibrated by concentrating on the sediment fluxes. The total import of the sediment must be near zero for the inner basin. For the longshore transport, movement through a transect must be about the same amount as the transport through the previous one. When the transport is constant, no sedimentation or erosion takes place on the coast. A sensitivity analysis is done with the parameters described in Section 3.4.3 to achieve this constant transport.
After the sensitivity analysis has achieved the desired goal, the model is validated through phenomenological validation for the mud transport and through a comparison between analytical results and computational results for the longshore transport.

3.5.1 Sensitivity analysis

A sensitivity analysis splits and allocates the uncertainty in the output of the numerical model to sources in the uncertainty in input parameters. This model requires a sensitivity analysis of the parameters of the sediment fractions, as there are only indications of the sediment properties. As the model does not precisely reproduce the reality, this calibration, through sensitivity analysis, is qualitative and meant to validate the essential processes. For this study, this is mainly the quantity of sediment transport due to hydrodynamic processes.

Mud from the Rio Escondido

The system is assumed to be in balance, as analysed in Section 2.2, meaning that for annual period, the model must have a minimum amount of sedimentation in the Rio Escondido and the lagoon. The amount of sedimentation in the lagoon is calculated by computing the sediment fluxes and making a sediment balance. Cross-sections are placed at the entrance and exit of the Rio Escondido and the tidal inlets. These cross-sections compute the cumulative sediment transport of a fraction. The sum through these cross-sections must be as close to zero as possible. Figure 3.2 depicts the cross-sections and the accompanying sketch of expected sediment fluxes resulting from the conceptual model. In Figure 3.8b, a positive sediment flux is directed inward to the tidal basin.

In the conceptual model, the tidal basin is flood dominant in the dry period, and thus it imports sediment. The blue and red lines, belonging to the two inlets, therefore have a positive sediment flux in the dry period (January– June). When the river discharge starts increasing in the wet period, the circulation in the lagoon changes. The lagoon is pushed into ebb dominance, and a stronger southward directed current is initiated. The sediment that is transported into the basin by the Rio Escondido is transported out of the basin through the northern and southern inlet. Furthermore, the sediment that is imported in the dry period is exported in the wet months. The desired total net sediment import is zero.

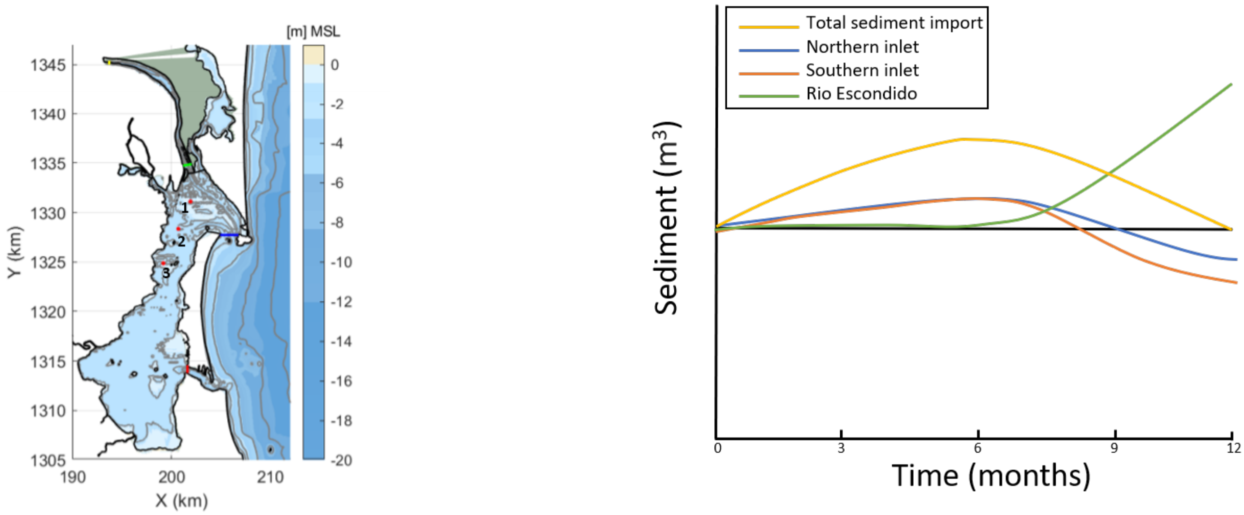

(a) Cross-sections inlets (b) Sediment balance

Figure 3.2: Silt transport fluxes through different cross-sections

Section 3.4.3 explains that the parameters which can be changed for a cohesive fraction are the erosion parameter, critical erosion shear stress, and fall velocity. A sensitivity analysis is done for these parameters to reach a model that produces the sediment fluxes shown in Figure 3.8b. The details of this sensitivity analysis are found in Appendix D.3.

From the sensitivity analysis, the parameter of the fall velocity did not have any influence, as Appendix D.3.2 shows. A fraction diameter of 12 μm was therefore chosen. For the sensitivity analysis with only a mud fraction from the river, a critical erosion shear stress of 0.05 N/m^2 is found. However, the mentioned parameters are found without a bed composition. The erosion parameter of the mud fraction is calibrated with a bed composition. The results of the runs with a bed composition are depicted in Figure D.3 (in Appendix D.3.3). In both the results, the basin exports mud in the dry period. Aside from this export, the basin starts to import sediment in the wet season. This co-occurrence is physically impossible according to the conceptual model. The error in the output is due to the sand in the bed composition. The critical erosion shear stress for the mud fraction has become too high.

A sand fraction is neglected for the sediment transport in the inner basin, as the resulting critical erosion shear stresses are too high. Since sand is of importance for the longshore transport, it is considered when modelling the processes at the adjacent coast. In the further study, the inner basin and longshore transport are modelled separately.

By adjusting the parameters, the results of the sediment fluxes of mud are shown in Figure 3.3. In these model results, only two cohesive fractions are present. These fractions are the mud fraction entering through the river boundary and the mud fraction that serves as the bed composition. The parameters for mud fraction in the bottom are presented in Table D.3 of Appendix D.2. In Table D.2 of Appendix D.2, the final settings are presented for the mud fraction entering through the river. The main difference between these two mud fractions is the difference in critical erosion shear stress.

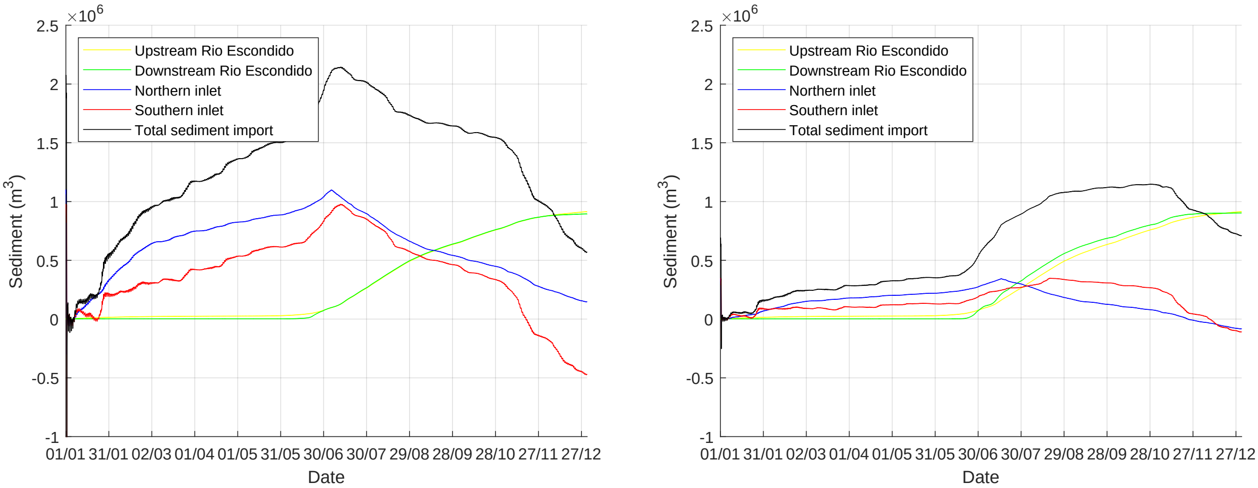

(a) Critical erosion shear stress of 0.05 N/m^2 (b) Critical erosion shear stress of 0.10 N/m^2

Figure 3.3: Sediment fluxes for a different critical erosion shear stress

The difference between the two model results in Figure 3.3 is the critical erosion shear stress for the mud fraction entering the river boundary. In the dry months (January–June), there is a net import through the inlets. This import is the case for both the model results. In Figure 3.3a, the peak of the import for both the inlets is too high. More sediment enters the basin through the inlet than through the Rio Escondido, which is unlikely. In Figure 3.4, the sedimentation concentrations are shown for the stations in Figure 3.2a. The suspended sediment concentrations for Figure 3.4a of about 1.5 kg/m^3 for the spring tide are too high, even when a storm is considered. In the Wadden Sea, the sediment in suspension is 0.2 kg/m^3 during a storm. The bed composition of the Wadden Sea also consists mainly of silt (De Vries et al., 2018). Storms are not considered in the model. For a critical erosion shear stress of 0.10 N/m^2, the suspended sediment concentrations in Figure 3.4b are about 0.5 kg/m^3 for a spring tide. This concentration remains quite high, but is more realistic.

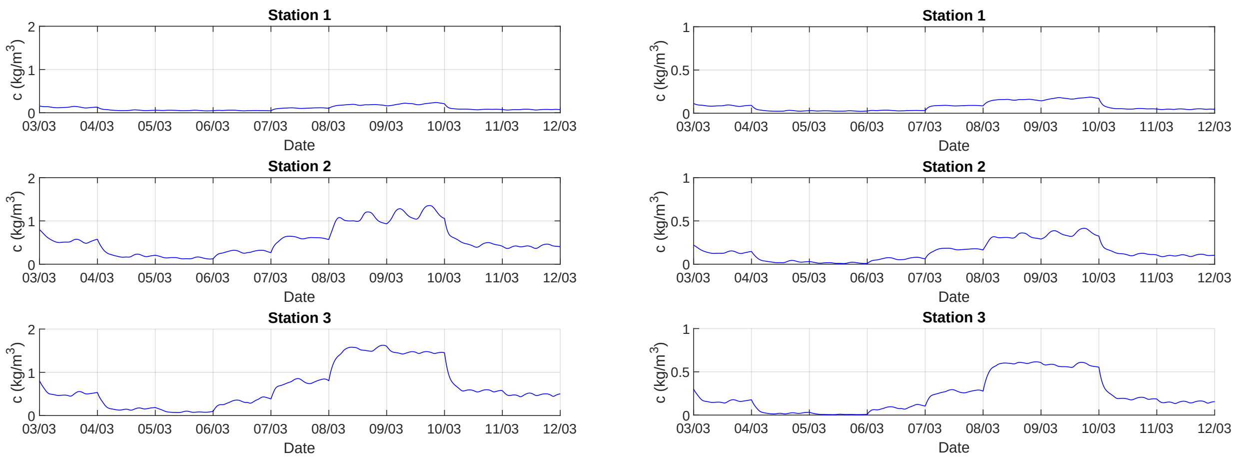

(a) Critical erosion shear stress of 0.05 N/m^2 (b) Critical erosion shear stress of 0.10 N/m^2

Figure 3.4: Suspended sediment concentrations throughout the basin

The total net import of sediment for a critical erosion shear stress of 0.05 N/m^2 corresponds more to the conceptual sediment balance of Figure 3.8b than a critical erosion shear stress of 0.10 N/m^2: in particular, the fact the total import through the river is washed out through the inlets during the wet period. However, unrealistically high sedimentation rates are expected in the navigation channel when using these model settings. When a large portion of the sediment goes southward, it is trapped when the navigational channel is constructed. High sedimentation numbers are expected in the channel. Moreover, the high concentrations imported in the dry season are trapped by the future port in the model. A critical erosion shear stress of 0.10 N/m^2 was adopted for the model. This choice is mostly due to the more realistic numbers of net import during the dry season. Although the suspended sediment concentrations remain too high, only a small calibration factor must be used for the dry period when using these settings. However, a large portion of the sediment of the Rio Escondido is deposited in the basin in the wet months. It seems only half of the sediment that is transported to the lagoon through the river in the wet season also leaves the basin. A large calibration factor must be used for the final results when these deposition rates are considered. The mud with a higher critical erosion shear stress originating from the bed composition is not notably moved. Figure D.4 in Appendix D.3.4 shows that the cumulative transport through the cross-sections is close to zero. The mud with a higher critical erosion shear stress is further neglected in the sediment fluxes.

Sand from the longshore transport

A sensitivity analysis is also performed for the longshore transport of sand on the adjacent coast. To eventually calibrate the longshore transport, analytical computations with bulk transport formulas are made. Appendix D.4 shows and explains the executed calculations with these bulk transport formulas. The longshore transport computations from the Delft3D model are assumed to approach the quantities of the analytical calculations.
The calculated longshore transport in Appendix D.4 results from the application of the numerical model UNIBEST. UNIBEST uses bulk transport formulas and a uniform coast to calculate longshore transport. In this UNIBEST model, Van Rijn (1993) transport formula is used. The results show a transport quantity of about 500,000 m^3/yr for a fraction size of 200 μm at the island's midpoint. Bulk transport formulas calculate the full potential of sediment transport, possibly overestimating transport in its process (Bosboom and Stive, 2015). Furthermore, UNIBEST is programmed to compute based upon a uniform coast. The barrier island is clearly not uniform, as Figure 3.5 shows. In a comparison of the Delft3D and UNIBEST models, a point must be selected on the coast where the x-axis is perpendicular to shore: the island midpoint, which is the black transect in the figure. The transects perpendicular to the coast in Figure 3.5 measure the longshore transport of the coast in the Delft3D model.

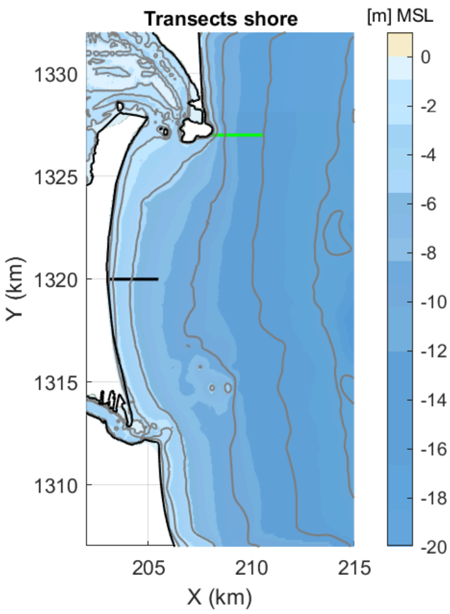

Figure 3.5: Transects along the shore

Figure 3.6 shows the results of the cumulative amount of suspended sediment transport through the transects. Sediment size is the only variable parameter when modelling a non-cohesive fraction. The data study showed a sediment size of 200 μm. The total yearly longshore transport computed by the Delft3D model is deficient compared to the results of bulk transport formulas. Figure 3.6a shows the cumulative transport with a wave-related transport vector magnitude factor of 0.25. A wave-related transport vector of 0.25 is the default option of Delft3D. The result is a total transport of about 50,000 m^3/yr for the island midpoint, which a factor of 10 lower than the total transport of 500,000 m^3/yr of the analytical calculations.
The sensitivity analysis for the non-cohesive fraction is done by changing the wave-related transport vector

magnitude factor. Figure 3.6b shows the cumulative transport with a wave-related transport vector magnitude factor of 1. The result is a total transport of about 110,000 m^3/yr for the island midpoint. This result remains low compared to the UNIBEST model. However, further increasing the wave-related transport vector magnitude factor would not be acceptable according to best practices for modelling. Because the Delft3D model uses more processes to compute the longshore transport, it is considered to be more precise than the UNIBEST model A wave-related transport vector magnitude factor of 1 is used further in the study. Because 110,000m^3/yr is low quantity even for mild wave conditions a calibration factor is advised for design safety reasons. The used calibration factor is explained in Section 3.5.2.

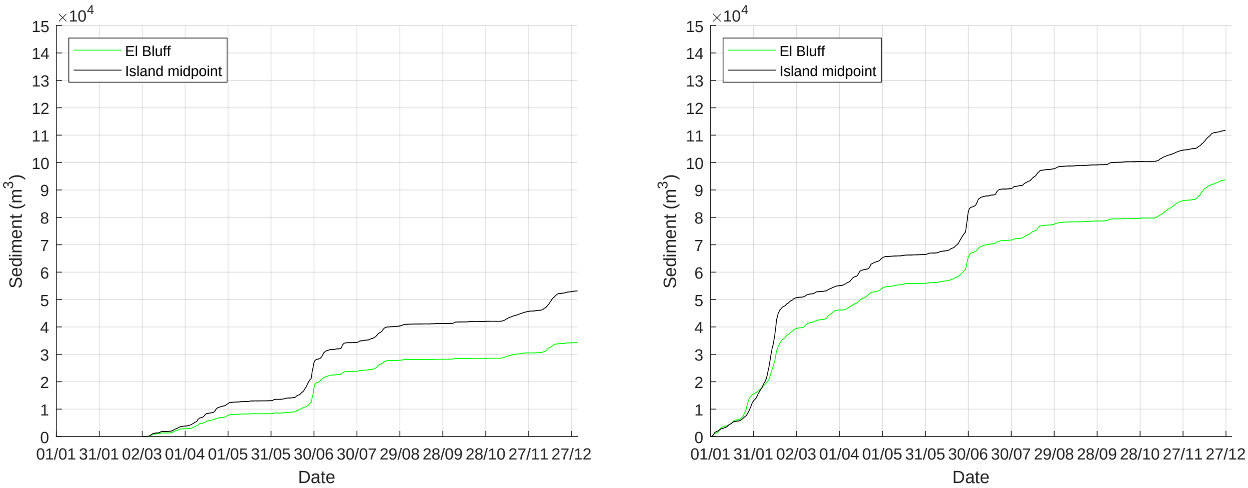

(a) Wave transport coefficient of 0.25

(b) Wave transport coefficient of 1

Figure 3.6: Cumulative amount of sediment going through the transects as computed by Delft3D

3.5.2 Calibration factors for the results

The model is not able to produce the sediment balance from Figure 3.8b. The eventual results of the model must be considered cautiously. The model calibration showed different deviations for the dry and wet period. Some calibration factors must be applied to the final model results to make up for these deviations.
It is impossible to combine the model results of the longshore transport and the mud transport in the inner basin in one simulation. The model results yield outcomes that are not physically plausible. The longshore transport at the adjacent coast is therefore simulated separately from the mud transport in the inner basin. Further study includes a littoral drift model and a mud model. The results of these models are combined for analysis. Crucially, the sedimentation results from the littoral drift model for the mud in the inner basin are not used. Figure 3.7 shows a flow-chart of the two used models. The littoral drift model focuses on the adjacent coast and the mud model focusses on the mud transport in the inner basin and adjacent coast. The similarity between the models is in the used hydraulic processes. Both models consider all the hydraulic components. Deviations in the two models are in the area of interest, sediment input and calibration factors. There is a difference in the bed composition for both models. In the mud model no sand is implemented in the bed composition. The calibration phase of the model showed the critical erosion shear stress for the fluvial mud becomes too high when sand is added to the bed. The mud is not able to move anymore. It is therefore chosen to only use a mud fraction in the bed composition that has a critical erosion shear stress of 0.5 N/m^2 in the mud model. Besides this cohesive component, the mud fraction that enters through the boundary of the Rio Escondido is present in the model.
For the littoral drift model a sand fraction of 200 μm is implemented in the bed composition at the adjacent coast. The bed composition in this area is made of 100% sand. Besides this sand fraction the mud fraction originating from the Rio Escondido is present in the model. With the longshore transport this mud fraction is suspended and is able to move. The results of this model concentrate only on the adjacent coast.

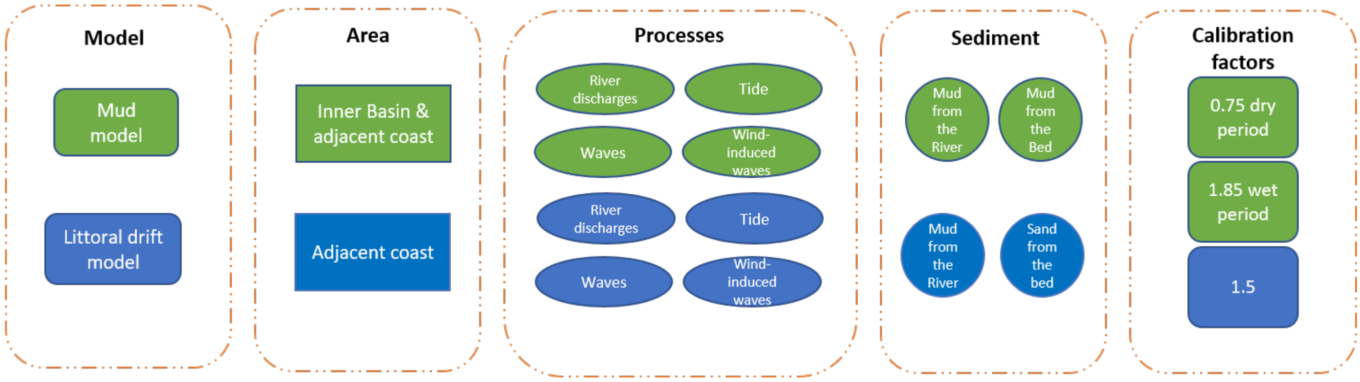

Figure 3.7: Models used

The calibration factors needed and used for the results of the model are further explained here. The credibility of the model used in this study is elaborated in the discussion in Chapter 5. Figure 3.8b shows the mud balance, that is aimed at with the calibration factors. This mud balance is made of the result of Figure 3.8a multiplied with the calibration factors. It must be noted that the sediment in the transport fluxes have a specific density of 2650 kg/m^3. The quantities of the sediment (in m^3) in the transport fluxes are, therefore, smaller than the eventual sedimentation volume in the port and channel. The volume of the sedimentation in the alternatives is computed with a dry bulk density, which has a larger value than the specific density.
During the dry season, the import of mud in the tidal basin is overestimated in the inner basin model. The suspended sediment concentrations show values of up to 0.5 kg/m^3 in the shallower areas during spring tide. As stated, these concentrations are higher than those in the Wadden Sea in The Netherlands during a storm. Due to these high concentrations, large fluxes of mud are expected in the direction of the navigation channel. The deposition rates in the channel are expected to be too high because of these fluxes. To compensate for the high deposition rates, and by keeping design safety in mind, a compensation factor of 0.75 is used for the results of sedimentation in the channel. A total import for both inlets of 0.25 Mm^3 is found in the dry season.
The model does not export enough mud during the wet season in the inner basin model. The amount of deposition of the fluvial mud in the lagoon is too high. As it is assumed that the basin is a dynamic equilibrium, the mud must entirely leave the basin. When the deposition on the river banks is too high, the mud cannot reach the tidal inlet nor the eventually constructed navigation channel. The transport gradient between river inlet and exit in the wet season is too small. The results of the sedimentation in the channel are underestimated in this way. In Figure 3.8a, the net import has a surplus of 672,000 m^3, without using calibration factors. In order to export all the mud that is imported in the dry season and received in the wet season by the river, the two inlets must export 1,572,000 m^3 during the wet period. The model results show an export of 852,000 m^3 at both the inlets. This means the inlets have to export 720,000 m^3 more for a net import of 0 m^3. A calibration factor of 1.85 is used on the model results in the wet season to reach this number.

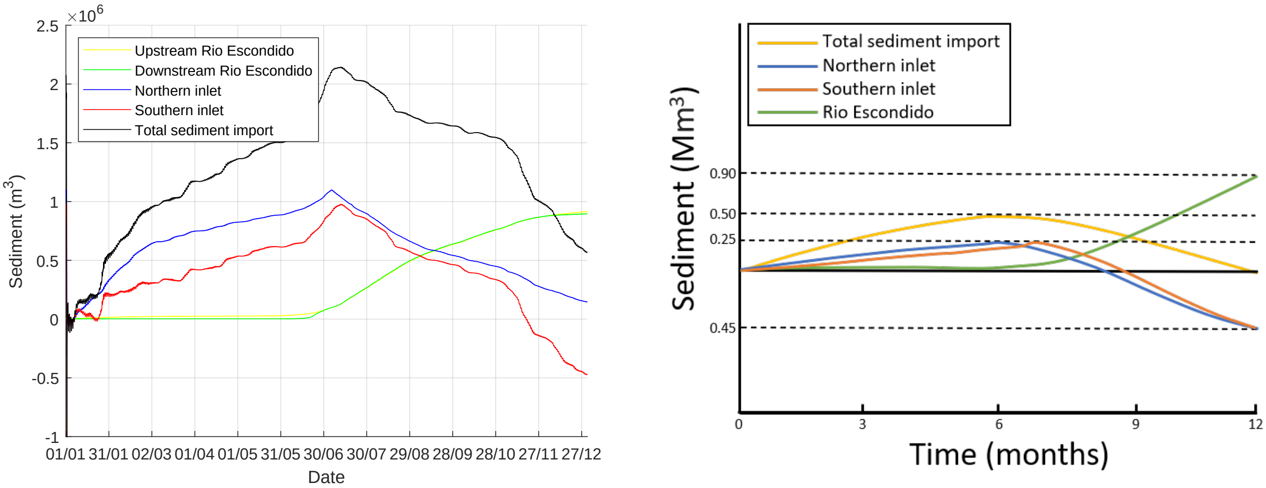

(a) Sediment balance from the model (b) Sediment balance multiplied by the calibration factors

Figure 3.8: Sediment balance from the model and multiplied by the calibration factors

For the longshore transport, the difference between the analytical calculations and Delft3D is a factor of 5. The bulk transport formulas of the analytical results overestimated the transport quantities, as evidenced by the mean significant wave height being about 1 m in the area. A wave climate of 1 m is considered mild. A transport quantity of 500,000 m^3/yr resulting from these calculations is therefore too high. Based on expert judgement and safety reasons, a compensation factor of 1.5 is used for the 100,000 m^3/yr from the Delft3D results. This safety factor is used for uncertainties in the magnitude of the littoral drift and the impact of the erosion and sedimentation that result from the Delft3D computations.

3.6 Model validation

In this section, the validation of the sediment transport of the model is explained. An accurate representation of the hydrodynamics is essential for sediment transport. A validated model of hydrodynamics is used. Validation of the morphodynamics is complicated, especially if the data is scarce.
Validation of the morphodynamic module is done by phenomenological calibration. The deposition pattern of mud from the Delft3D model is compared with the mud content of the bed samples. Moreover, the deposition pattern is elaborated with knowledge of the conceptual model.
The reliability of the longshore transport is validated by comparing the results of the Delft3D model with the results of the numerical model. The validation compares the reaction of the sediment on the wave input for both models, as both models use the same wave data.

3.6.1 Sediment deposition

As field data is scarce to validate the morphodynamic module, a comparison is made between the processes that result from the model with the processes that result from observations in the area. The deposition in the model is compared with the bed samples from the area for the mud fraction. Figure 3.9a shows the measured surface bed samples. The mud fractions (represented by the grey pies) have high percentages in the shallower areas. The shallower area is found in the southern part of the tidal basin. Around the river channel in the tidal basin, the mud content percentages are lower, as the flow velocities there are too high. The high mud percentages outside the tidal basin are noticeable.
Figure 3.9b shows the deposition in the model. The deposition takes place in the shallower areas, especially on the riverbank. The area's depth is much lower here, and the flow velocity decreases. The flow velocity is not high enough to transport the sediment any longer and deposits it. As bed-level updates are turned off in the model, the sediment continues to deposit here. The sediment will be pushed more equally further southward if the bed level elevates.
High deposits rates are seen in the shallow areas located in the southern half of the basin. Mud is transported southward in the model, which coincides with Figure 3.9a. The percentage of mud is the highest here in Figure 3.9a. The sediment does concentrate on specific places. If the model takes bed-level updates into account, it is assumed the mud is more dispersed in these places.

At the southern inlet, many depositions of mud take place at the inner side of the basin in Figure 3.9b. This deposition decreases through the opening in the direction of the sea. In the measurement in Figure 3.9a, the same decrease in mud fraction are observed.

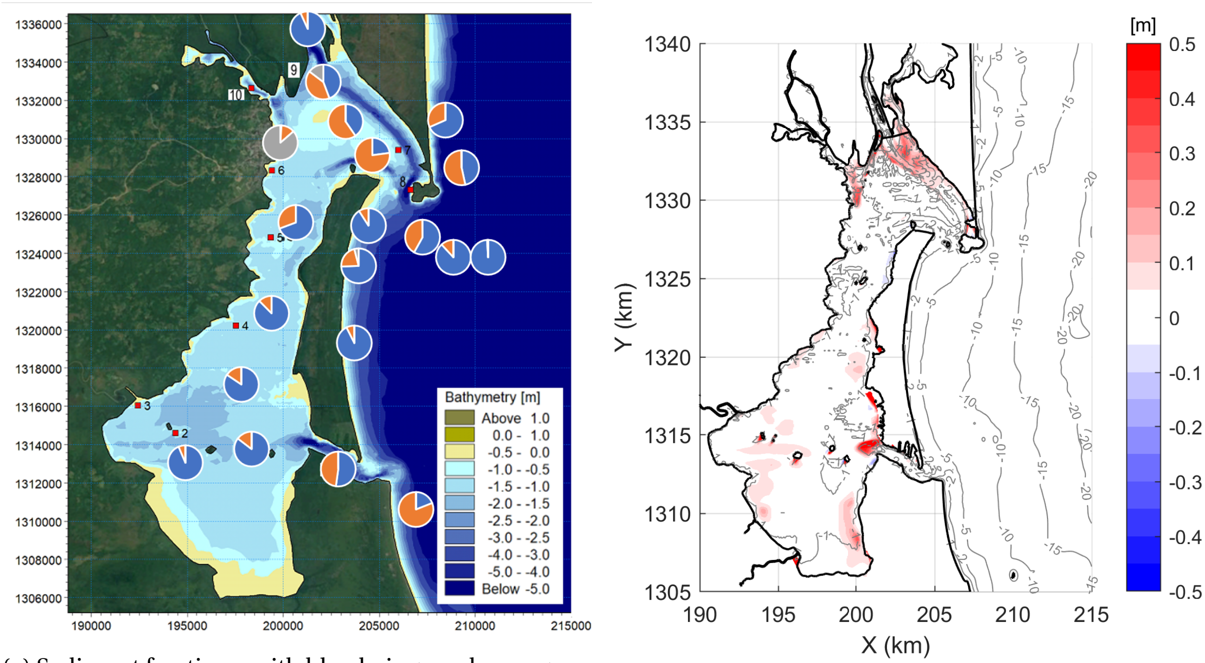

(a) Sediment fractions, with blue being mud, orange being sand, and grey being gravel

(b) Deposition of mud for the existing situation

Figure 3.9: Comparison of the deposition of the mud with the mud fractions found in Bluefields Bay

3.6.2 Longshore transport

The Delft3D model result for the longshore transport is validated through comparison with the analytical results from the UNIBEST model in Appendix D.4. In addition, the transport results are validated through analysis assisted by the wave climate (the wave climate is analysed in the system analysis in Section 2.3.4). Figure 3.10 depicts the instantaneous longshore transport quantities for the midpoint of the island, which is the island midpoint in Figure 3.5. It appears that the periods from January to March and June to July have higher sediment transport rates. During the periods of May and September through November, hardly any sediment transportation occurs. The seasonal significant wave height is low for the last-mentioned periods. These low transport quantities correspond with the transport formula D.14 in Appendix D, as the longshore transport in this equation depends on the significant wave height at breaking point and angle of incidence. Additionally, in the periods with higher sediment transportation, the extreme significant wave heights above the 90th percentile appear to be more substantial in contributing to higher sediment transport.

Figure 3.10b shows the instantaneous longshore transport for the UNIBEST model. Section 3.5.1 demonstrates that the total transport quantities have a difference of factor of 5 with the Delft3D model during the calibration of the model. However, in Figures 3.10a and 3.10b, the same transportation pattern results from the Delft3D model as well the UNIBEST model. The two models react in the same way to the wave climate, in terms of direction and moments of transport initiation. Although the UNIBEST model tends to overestimate longshore transport, it remains acceptable to make a fair first estimation. The transport patterns from Delft3D are the same as the analytical model, so the process-based model is trusted.

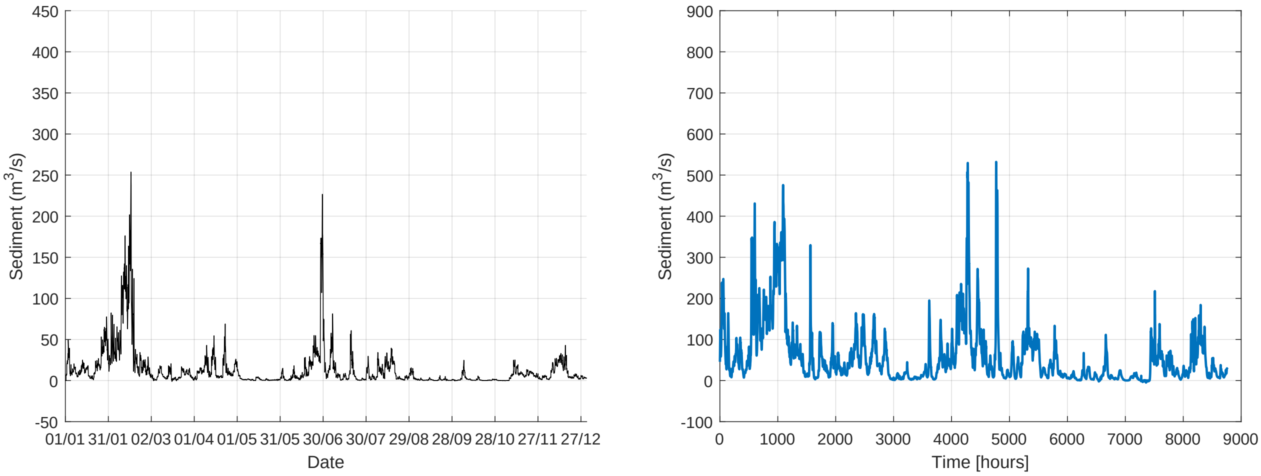

(a) Delt3D results

(b) UNIBEST results

Figure 3.10: Comparison between the instantaneous longshore transport through the island midpoint

4 Results

This chapter presents the results of the numerical model. The results are analysed and substantiated by the conceptual model. The processes described in the conceptual model are quantified using the results of the numerical model.
First, the results of the hydrodynamic model of the existing situation are analysed. The dominant processes for the dry and wet season are earmarked by analysing the residual currents and bed shear stresses. Subsequently, the results of the morphodynamic model are elaborated in order to obtain sediment transport patterns for the existing situation. Next, the influence on the hydrodynamics after implementing the alternatives in the model is studied. The change in influence is studied by comparing the new residual currents and bed shear stresses with the existing situation. Additional the changes in the sediment fluxes are elaborated. A sediment balance is made of the existing situation and the situation with the ports. Finally, the quantitative results of the sediment deposition in the channels are presented, along with those for coastal erosion.

4.1 Hydrodynamic model

This section offers an analysis of the hydrodynamic results of the Delft3D-FLOW and Delft3D-WAVE module. The flow fields of the area give the primary direction of sediment transport. With the help of these flow fields, the dominant hydrodynamic processes are identified. The flow velocity suggests the quantity of movement of the sediment while bed shear stresses indicate whether sediment is moving at all.
For the longshore transport, the movement of the sediment is subject to the significant wave height and angle of incidence. The magnitude and direction of the waves indicate the direction of the transport, while wave dissipation initiates sediment movement.
Since March is one of the driest months, it represents the dry season. Figure 2.6 shows that the discharge is only slightly greater in March than in April and May. However, the scarce field data presented in Chapter 2 were obtained in March. Therefore, March is chosen for the comparisons of the model results with the data. July is the wettest month, as Figure 2.6 shows, so this month is selected to represent the wet season.

4.1.1 Inner tidal basin

According to the conceptual model, the river discharges, tide, and wind-induced waves are the dominant hydrodynamics in the inner tidal basin. In the wet months, the river discharges and the tide are the main forcings of the currents. In the dry months, the tide is the primary hydraulic forcing, as the river discharge is very low. Wind-induced waves have a substantial influence on bed shear stresses in the area. In Appendix E.1, the mean velocities and directions for the dry and wet period in the entire basin are shown.

Residual currents

Residual currents are of importance for the direction of movement of suspended sediment in a tidal basin. The direction and speed of the residual currents are studied by taking the average current over a spring tide in the dry and wet season. Section A.1 states that residual currents are the leading indicators of suspended transport.
Figure 4.1 shows the residual currents of a spring tidal cycle during the dry and wet season. Note that the choice was made to display a difference at maximum velocity in the figures shown, since the two periods differ substantively in flow velocity. For the dry season, the maximum residual current is 0.1 m/s, and for the wet season, this current is 0.2 m/s. In Appendix E.2, the flood and ebb current are shown separately for the dry and wet season.

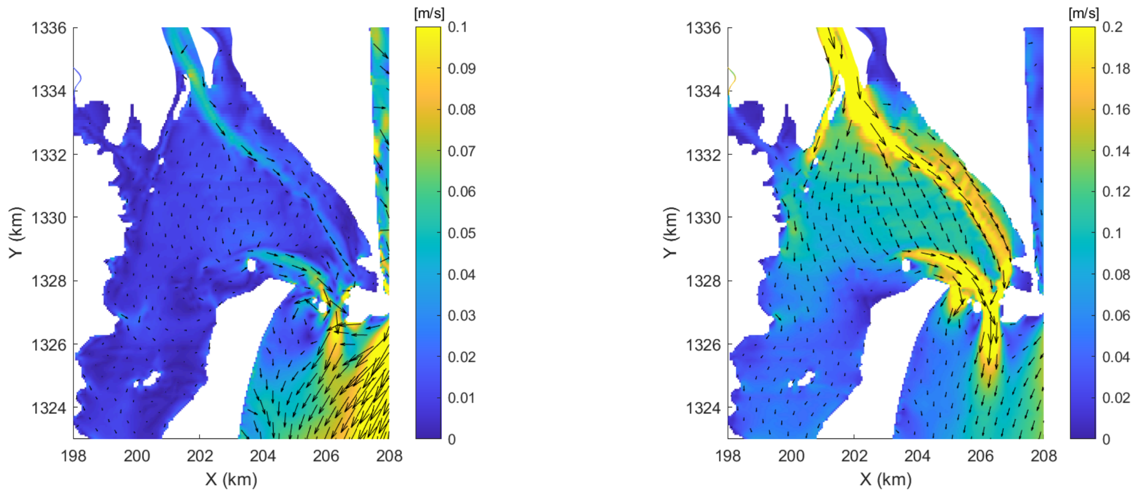

(a) Dry period

(b) Wet period

Figure 4.1: Residual currents

In the conceptual model, the tidal basin is classified as flood dominant in the dry period. In Figure 4.1a, a residual current with a direction going out of the basin is observed in the ebb-tidal channel. Around the ebb-tidal channel, especially south the 1328 km line, the currents have a flood dominant direction in the shallower areas. The flood dominant currents have a direction away from the inlet. This current direction indicates flood dominance, and the tidal lagoon imports fines for this area. This direction is a result of tidal wave deformation due to changes in bathymetry and cross-sectional area of the flow.
In Figure E.2, it is observed for the area above the 1329 km line that during flood, the flow is directed eastward, while during ebb, it is westward. The resulting residual current is southward in Figure 4.1b. North of 1329 km, the fines are transported southward to the southern tidal inlet. Some of this movement is directed to the ebb channel, while some is directed to the shallower part, south of the 1328 km line. In the dry season, the Rio Escondido adds minimal sediment to the system. The combination of low sediment input and low residual current speeds of 0.02 m/s indicate the fluvial sediment transport is low at this time of year. Equation 3.2 shows that suspended sediment transport is a function of sediment concentration and flow velocity. The eventual net import of the total system is flood dominant during the dry period, as a large part of the lagoon is flood dominant. However, these currents are small, as the lagoon is in dynamic equilibrium.
According to the conceptual model, the river discharge substantially influences the currents in the wet season, with minimal influence in the dry season. Figure 4.1b, presenting the wet season, shows a residual current larger than 0.2 m/s in the river channel. In Figure 4.1a, presenting the dry season, the residual currents are on average 0.05 m/s in the river channel. For the wet season, the river discharge is high enough to substantially influence the circulation in the entire tidal basin. The residual current is directed more towards the ebb channel, transporting sediment from the river directly out of the basin. South of the 1328 km line is a stronger current, flowing southward. Sediment is transported in higher concentrations and further southward in the wet season than in the dry season. In the wet season, flow velocity increases to 0.1 m/s heading southward.
In Figure E.3, it is observed that the tidal current does not really change direction during the wet season when it is compared with the dry season in Figure E.2. It is, however, less strong and reaches less far in the tidal basin. The force of the tidal wave has decreased, as it has more resistance over the river discharge in the tidal inlet. The areas with ebb dominant residual current directions south of the 1328 km line are forced into a flood dominant direction, which is southward, in the wet season. This change of direction is due to river discharge. The tidal current is dampened because of the river discharge, making the ebb current in this area weaker.
Figure E.4 shows the existing residual currents at the southern inlet. No large flow channels in the bathymetry are observed. During the dry season, the residual currents are circulating over the shallower area, as Figure E.4a shows. As a large part of these currents are directed in the flood direction, mud is imported in this area. Figure E.4b shows the residual currents are in the ebb direction during the wet season. The river discharge of the Rio Escondido flows to the south, and the Rio Kukra starts to discharge more fresh water into the lagoon. The residual currents are all directed in the ebb direction, and mud is exported during this pe-

riod.
Figure 4.1 shows the currents as a function of space. As stated in Appendix A.1, the horizontal and vertical tidal asymmetry influence sediment transport. Vertical asymmetry is largely examined through the magnitude of the velocity during ebb and flood. Horizontal asymmetry is analysed through looking at the slack duration between ebb and flood. By studying the area's currents as a function of time, more insight is gained into the asymmetry of the tide. In this study, a comparison is made between two port alternatives and the amount of sedimentation in their respective structures. Metering points are built in the numerical model to monitor the sediment transport in the direction of these port layouts. The metering stations are situated in the tidal inlets and on the shallower areas at the location of future navigation channels. The locations are shown in Figure 4.2.

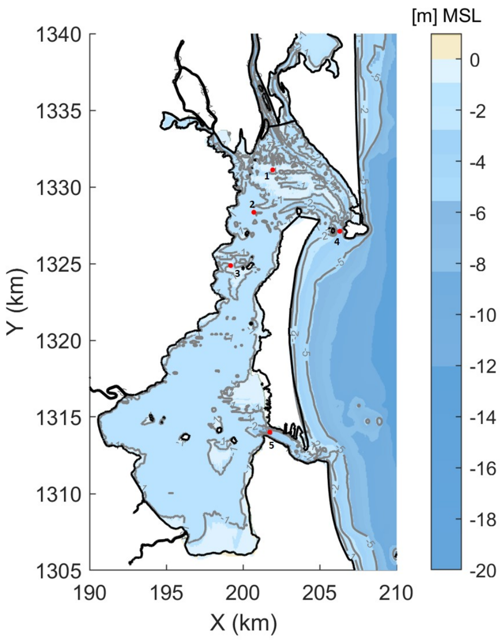

Figure 4.2: Location of measuring stations

Figure 4.3 displays flow velocity in the northern tidal inlet and water levels during the dry and wet seasons. The area has a mixed semidiurnal tide cycle. When the tide has a low volume, the flood has a higher flow speed. During the tide with a high volume, the ebb has a higher speed. During the smaller tidal cycle, there is flood dominance, while during the bigger tidal cycle, there is ebb dominance.
Figure 4.3b shows that in the wet season, the flow velocity is substantially greater during ebb than during flood, due to river discharge. The current in the ebb direction is enlarged, while the flood current is opposed.

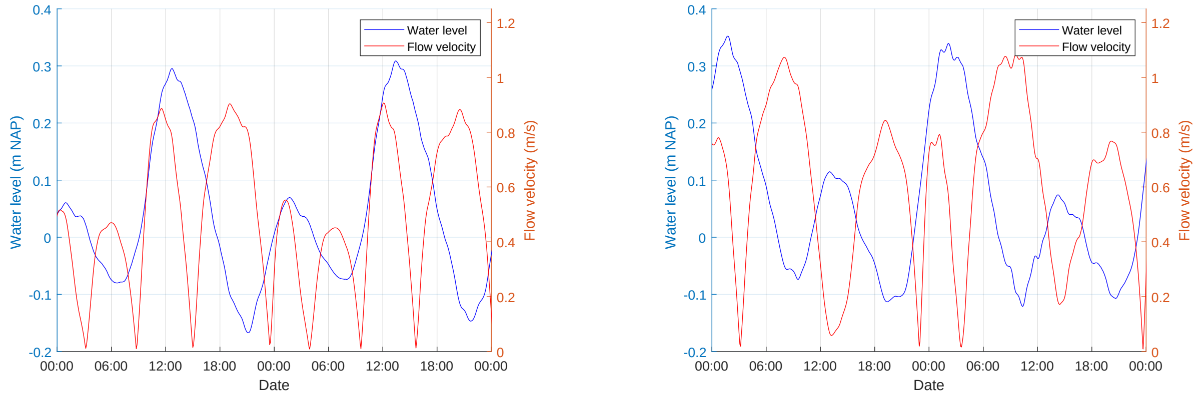

(a) Dry period (b) Wet period

Figure 4.3: Flow velocity and water level at the northern tidal inlet

In Figure E.5, the water levels and flow velocities are shown for the southern tidal inlet. In the wet period, the same sort of pattern is found as for the northern inlet. During the tide with a small volume, the inlet is ebb dominant, while during the more substantial tide it is flood dominant.
Figure 4.4 displays the flow velocities and water level for Stations 1, 2, and 3 in Figure 4.2. For Station 1, the flow velocity drops to 0 m/s at certain times. No constant flow due to a river discharge is observed. Therefore, it is concluded that the tidal current is the dominant factor. However, the fluctuations in flow speed are smaller than for Stations 2 and 3. The tidal wave has less influence in Station 1 than Stations 2 and 3, as it mainly heads west and subsequently southward, following the tidal channel.
In the wet season, a constant flow velocity through Station 1 occurs. This constant flow means the river discharge is large enough to force a constant current. The fluctuation due to the tide is small, indicating the river discharge is the dominant factor in this area during the wet season.
For Station 2, a slightly flood dominant current is found during the dry period, as the flow speed for flood is higher than for ebb during the dry period. In the wet period, a constant current is found. However, due to the tide, fluctuations in speed are found. The flow velocities for flood are higher than for ebb, indicating flood dominance.
A flood dominant current is also found for similar reasons at station number 3. However, in the wet period, the velocity drops to zero for station number 3. This low velocity means the current due to the river does not consistently influence the area, and the tide comprises the dominant hydraulic forcing.

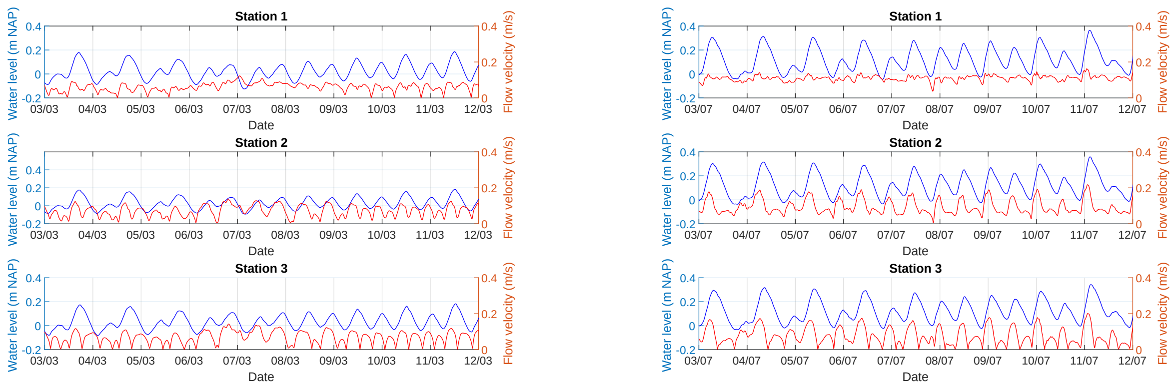

(a) Dry period (b) Wet period

Figure 4.4: Flow velocities and water levels at the stations

Bed shear stresses

Sediment is put into motion if bed shear stresses are substantial enough, as is explained in Appendix A.2. Figure 4.5 shows the 90th percentile of the maximum bed shear stresses that occur in the area over a spring tide. By selecting the 90th percentile, extreme maximum outliers are excluded.

In the conceptual model, the bed shear stresses in the lagoon are dominated by wind-induced waves and the tide during the dry period. Wind-induced waves initiate bed shear stresses in the areas with shallow depths. Freshly deposited mud has an erosion shear stress between the 0.1 N/m^2 and 0.5 N/m^2 (Winterwerp and Van Kesteren, 2004). In the dry period, the shallow parts of the lagoon have bed shear stresses from 0.2 N/m^2 to 0.35 N/m^2. In channels with more depth, the shear stress is low, as the depth is too substantial for waves to initiate bed shear stresses. The low level of river discharge cannot initiate the movement of mud. The fluvial sediment supply is low in the dry period. However, sediment is deposited on the riverbanks during the wet period. The bed shear stresses on the riverbanks are high enough to transport these deposits partly during the dry period. The tidal current initiates high bed shear stresses in the tidal inlet and the nearby channels. Sediment is suspended here. However, the tidal current induces less substantial bed shear stresses on the shallower areas located more land-inward.
During the wet period, the bed-shear stresses are substantial in the deeper areas of the northern part of the lagoon. In this period the river brings a high amount of sediment to the lagoon. In the river channel, the bed-shear stresses are substantial enough to keep the sediment moving. When the river reaches the basin, the bed-shear stresses in the channel decrease and much of the fluvial sediment deposits on the riverbanks. However, the flow velocity remains substantial enough to transport a large portion of fluvial sediment away from the riverbanks before it can settle. Lower bed-shear stresses at the shallower parts in the basin during the wet period are a result of increased water levels in this period of the year due to the higher river discharges. A larger quantity of water enters the lagoon through the rivers, increasing the water level. Besides, the flood wave enters the lagoon with a higher resistance of the river discharge than in the dry period, having less of an influence on bed shear stresses during flood.

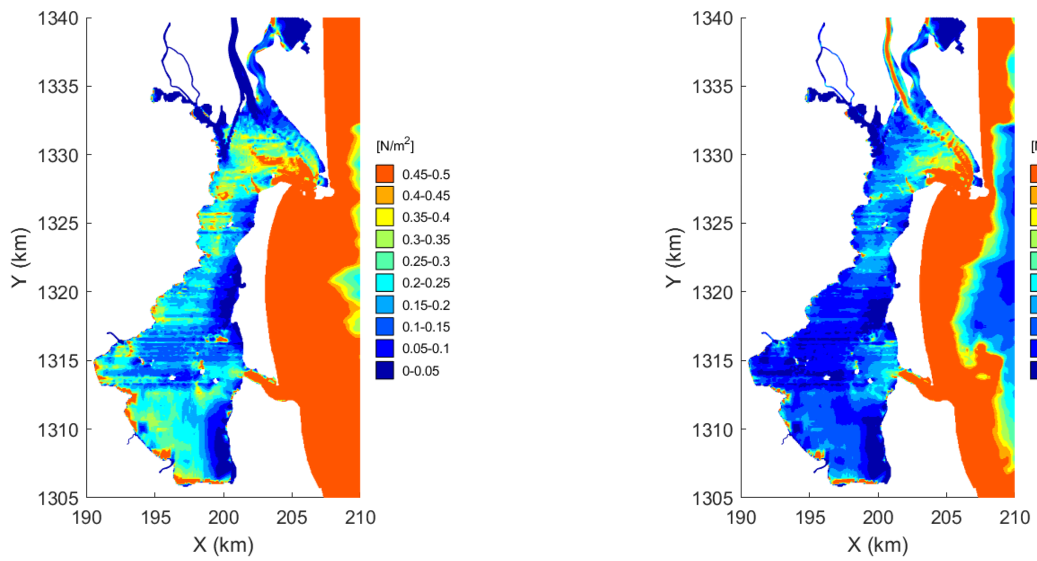

(a) Dry period

(b) Wet period

Figure 4.5: The 90th percentile of the bed shear stresses

Figure 4.5 shows the bed shear stresses as a function of space. The 90th percentile shows bed shears stresses that are exceeded 10% of the time. Figure 4.6 shows the bed shear stresses for a neap and spring tide in both the dry and wet period. The same stations from Figure 4.2 are used. The bed shear stresses, as a function of time, tell how often the bed shear stresses reach certain heights during a tidal cycle. The time series show that the bed shear stresses are affected by the tide. The fluctuations in the bed shear stress are tide-induced. For Station 3, the tide has more effect, as the bed shear stresses are more substantial and fluctuate more than in Station 1. The higher peak values at Stations 2 and 3 are because the flood directed flow has a higher velocity than for Station 1. The friction term is quadratically dependent on the flow velocity (Battjes and Labeur, 2017).
Only the sediment with low critical erosion shear stress stays in motion. This fact, in combination with the flow velocities reaching only about 0.1 m/s (in Figure 4.3), means that the sediment transport is low during the dry months. In the wet season, flow velocities are higher. At Station 1, the river discharge induces a constant bed shear stress in the wet period, keeping the sediment in constant movement. Higher veloci-

ties, in combination with higher sediment concentrations due to bed shear stress, indicate a higher level of sediment transport.
The mud has time to consolidate when there is a specific time between crossing the threshold twice. When mud is consolidated, the critical erosion shear stress for movement rises to 0.5 N/m^2. This study, however, does not focus on this rise.

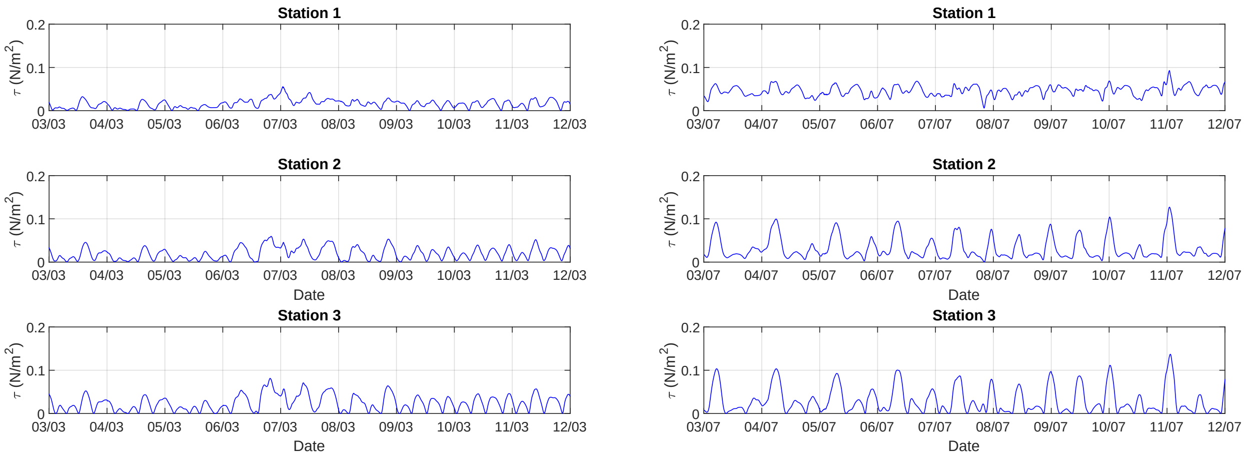

(a) Dry period (b) Wet period

Figure 4.6: Bed shear stresses during neap and spring tide

4.1.2 Adjacent coast

According to the conceptual model, waves are the dominant hydraulic force inducing sediment transport at the adjacent coast. Appendix A.4 explains that the direction and magnitude of the transport depend on the significant wave height and angle of incidence. In the Delft3D model, the longshore current is also considered. The longshore current is partly induced by the waves and partly by the tide. Since the coast is wave dominant, the current is mainly controlled by waves. The width of the zone of wave dissipation indicates sediment movement, as wave breaking induces turbulence.

Wavefield

The significant wave height is not substantial, as analysed in the conceptual model. The significant wave height is about 1 m during the year, getting as high as 2.5 m to 3 m in extreme conditions. October and November have the highest wave heights due to the hurricane season.
Figure 4.7a presents the mean significant wave height and angle of incidence for March. The average angle of incidence is from the east-north-east, inducing a small southward directed current. Near the northern entrance, wave height diminishes due to refraction. The shore in front of the barrier island is more dissipative than north of El Bluff, influencing waves through friction further from shore. This earlier friction makes waves break sooner, explaining the lesser significance of wave height in front of the island compared to north of the tidal inlet.
Figure 4.7b shows the mean longshore current. The current from north of El Bluff goes mostly to sea. This current indicates that a large part of the sediment transported from the north goes directly to the sea and does not reach the coast of the barrier island.

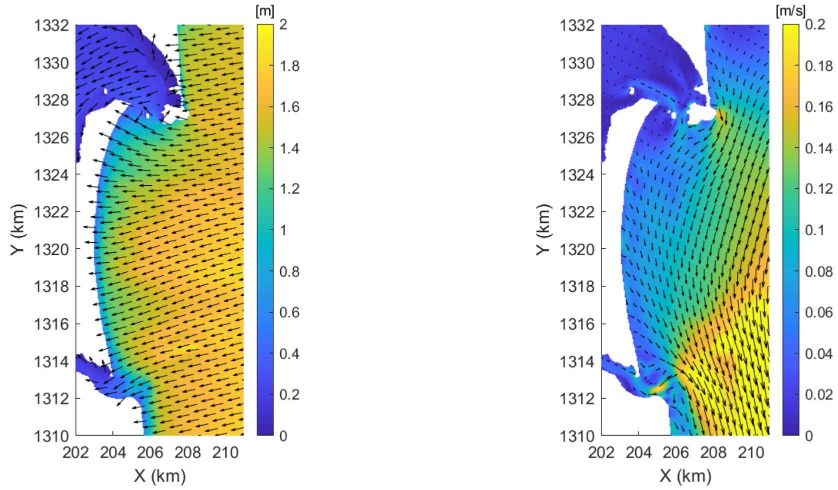

(a) Wave height and angle of incidence

(b) Longshore current

Figure 4.7: Mean wave height, angle of incidence, and current in March

Figure 4.8 shows the mean significant wave height and angle of incidence for July and its accompanying longshore current. The results show that the mean significant wave height is higher in March than in July. The figure shows that the mean significant wave height at a depth of 15 m for March is slightly lower than 1 m, while for July it is slightly above 1 m. However, in March, more extreme conditions occur. These extreme conditions increase the mean wave height in Delft3D. A difference in the angle of incidence is not visible. The difference in wave height in the model means larger transport quantities for March compared to July. The longshore current does not differ from the longshore current in March. Only near the tidal inlets do the currents increase, since the river discharge exits the tidal basin at these points. The southward-directed longshore current increases at the northern inlet. At the southern inlet, the circulation currents reach further north, meaning the sediment is pushed further offshore. These circulation currents are due to the interaction between waves currents and the exiting currents from the basin.

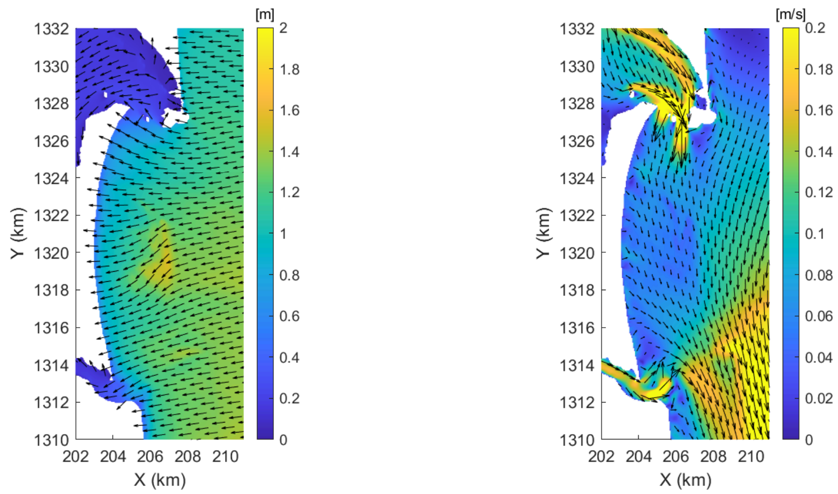

(a) Wave height and angle of incidence

(b) Longshore current

Figure 4.8: Mean wave height, angle of incidence and current in July

Wave dissipation

Appendix A.1 explains that the movement of sand at the coast is due to wave dissipation. Figure 4.9 shows the wave dissipation at the adjacent coast in the dry and wet period. In March, the wave dissipation is more substantial than the wave dissipation in July. The wave dissipation starts further offshore in front of the barrier island. According to the conceptual model in Section 2.5, the swell wave climate creates a shallow littoral drift zone. A shallow zone of wave dissipation is seen on the coast north or northern inlet. Section 2.1 has stated that the coastal state in front of the island is that of a dissipative beach. Wave dissipation starts further from shore, declaring the wider stretch in front of the island in Figure 4.9. In the zone with a smaller dissipation zone, waves break in shorter stretches. The waves induce greater forces and move more sediment in the area with this shorter stretch than they do in an area in front of the barrier island.

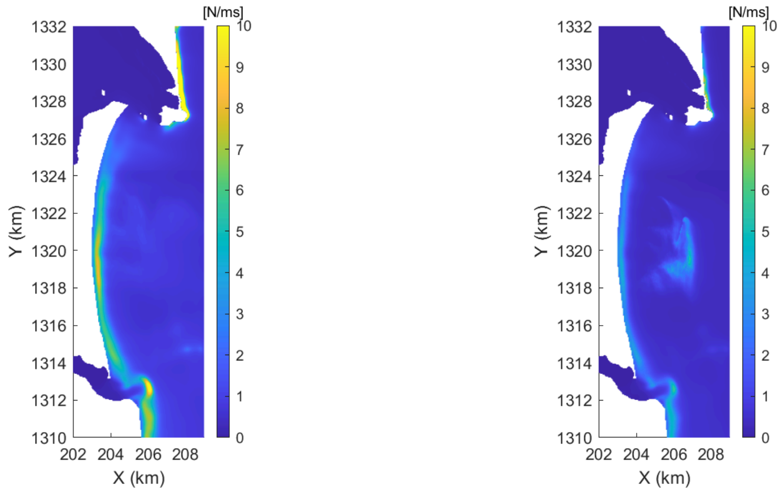

(a) March (b) July

Figure 4.9: Mean wave dissipation

4.2 Morphodynamic model

In this section, the results of the morphodynamic model for the existing situation are presented. As the mud fraction and sand fraction are two different input parameters in the model, each is analysed separately. Mud transport is analysed through the sediment balance. The sediment balance is created to understand the substantial sediment fluxes in the area. Aside from the transport fluxes, sediment concentrations are analysed to examine at which locations the most extensive sediment transport arises.
For sand transport, longshore transport and cross-shore transport are analysed. The gradients in longshore transport indicate erosion and sedimentation in specific areas.

4.2.1 Distribution of mud in the system

The mud transport inside the tidal basin depends on different hydraulic forcings, as analysed in the conceptual model and the hydrodynamic results. During the dry period, mud transport is influenced by tidal currents. The hydraulic results show that the tidal basin is flood dominant. This flood dominance is explained by the small channels and a large storage area. In the wet period, the river increases substantially, changing the currents in the basin.
Figure 4.10a shows the cumulative transport of mud through differently placed cross-sections in the tidal basin. The cross-sections are depicted in Figure 3.2a. For the dry period, the sediment transport in the rivers is low. Due to this low sediment transport, the cumulative transport through the cross-sections of the river is close to zero. From January to May there is a net import of suspended sediment through both the northern inlet and southern inlet. This direction of transport coincides with the conceptual model of flood dominance. For the tidal basin to import sediment through the inlets means mud remains present at the adjacent coast. This mud originates from the year before. The waves do not transport all the mud away from the system.
In the wet period, the river discharge increases substantially. The amount of sediment the river transports to the lagoon is increasing, as Figure 4.10a shows. The hydrodynamic results show that the currents in the direction of the south increase, and flood dominance in this area are enhanced. Sediment that enters through the northern inlet in the dry period are eventually transported southward with the current to be exported again through the southern inlet. The export does begin to occur after substantial time in the wet period since it needs time to reach the southern inlet.
Although the shallower areas remain flood dominant in the wet period, there is net export of mud at the

northern inlet. This exported mud does not originate from the shallower areas. The mud is mainly from the Rio Escondido and is transported through the river channel and exported directly. The other reason for a net export of mud is that at the opening there is constant outward-directed flow, meaning mud has more difficulty entering the inlet.
The black line represents the total import of the cross-sections. The northern and southern tidal inlets have a small net export of mud at the end of the year. The total import starts to decrease in November when the export of the inlets are larger than the import at the river. The export of mud remains insufficient to reach a net import of zero. The reason for this insufficiency is explained in Section 3.5.1.

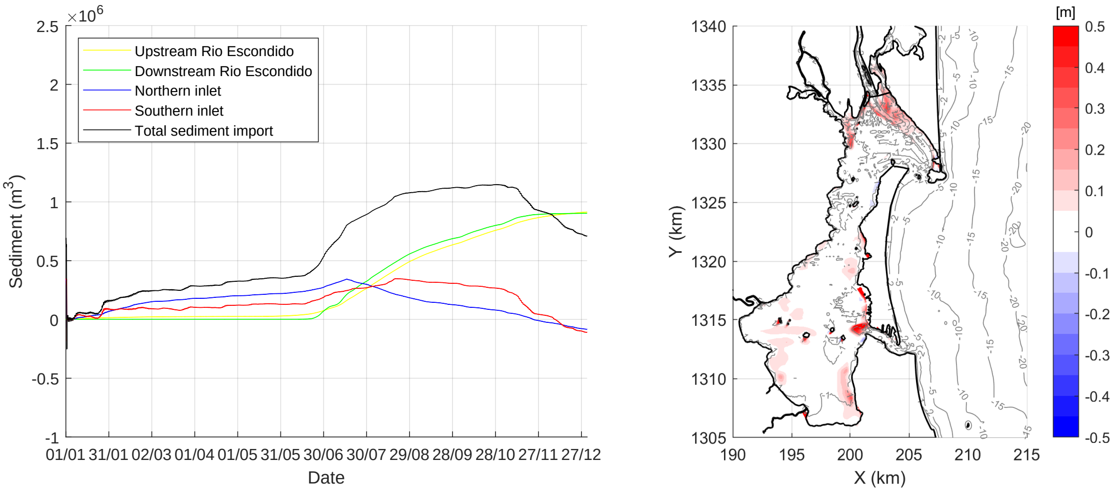

(a) Sediment balance

(b) Deposition pattern

Figure 4.10: Sediment balance and deposition for the existing situation

Figure 4.11 shows the deposition patterns in the dry and wet period for the existing situation. In the blue areas, erosion occurs, and in the red areas, sedimentation takes place. In the dry season, waves resuspend the mud, and the tide transports it back into the tidal basin due to the flood dominance. Mud deposits on the riverbanks and, southward, on the shallower areas as it enters through the northern inlet. There is also some deposition in the river and tidal channel. The flow velocities here are slow enough to let the sediment rest in the dry season. There is some erosion on the riverbanks near the river mouth. Wind-induced waves and the tide erode and transport the mud deposited here in the wet period due to the high bed shear stresses indicated in Figure 4.5b.
At the coast, mud is transported southward due to the wave-current and passes the southern inlet. When the mud passes this inlet, it is imported into the tidal basin. The flood transports into the system, depositing directly due to the mild hydraulic climate.
Figure 4.11b shows the erosion and sedimentation in the wet period. In the wet period, sediment is transported out of the system. Fluvial sediment originating from the river is deposited on the riverbanks. Sediment imported during the dry season and deposited in the tidal channel is eroded due to the higher currents. This erosion is seen at both the northern and southern inlet.

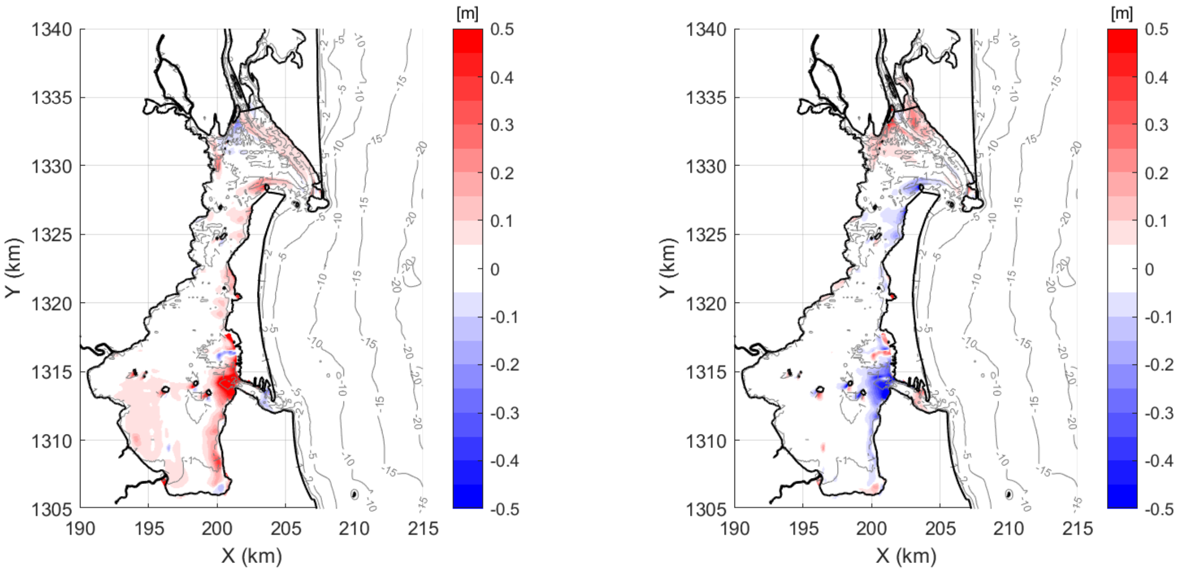

(a) Dry period (b) Wet period

Figure 4.11: Deposition of the silt

4.2.2 Suspended sediment concentrations

The suspended sediment concentrations at measuring stations indicate the amount of sediment coming across certain areas. The stations from Figure 4.2 are used again. The concentrations for these stations are presented in Figure 4.12 for the dry season and wet season. Although the absolute numbers should be considered cautiously, the relative transport of sediment for each place can still be analysed.

Station 1 has low concentrations in the dry season, which might be explained by low river discharge and, thus, low input of fluvial sediment. However, the low concentrations for Station 1 in the wet season are of the same order of magnitude as the dry season. The sediment originating from the river only leaves the river channel in small quantities. Most of the sediment follows the river channel and exits the lagoon through the northern inlet.

Stations 2 and 3 have higher suspended sediment concentrations than does Station 1. This sediment explains the high import rates of the sediment balance during the dry period. The transport of sediment depends heavily on the tidal current. The concentrations are slightly higher during the dry period than during the wet period. The force of the tidal current is opposed by the river discharge in the wet period, as shown in Section 4.1. The shallow areas remain flood dominant, but the supply of sediment is less in the wet period than in the dry period.

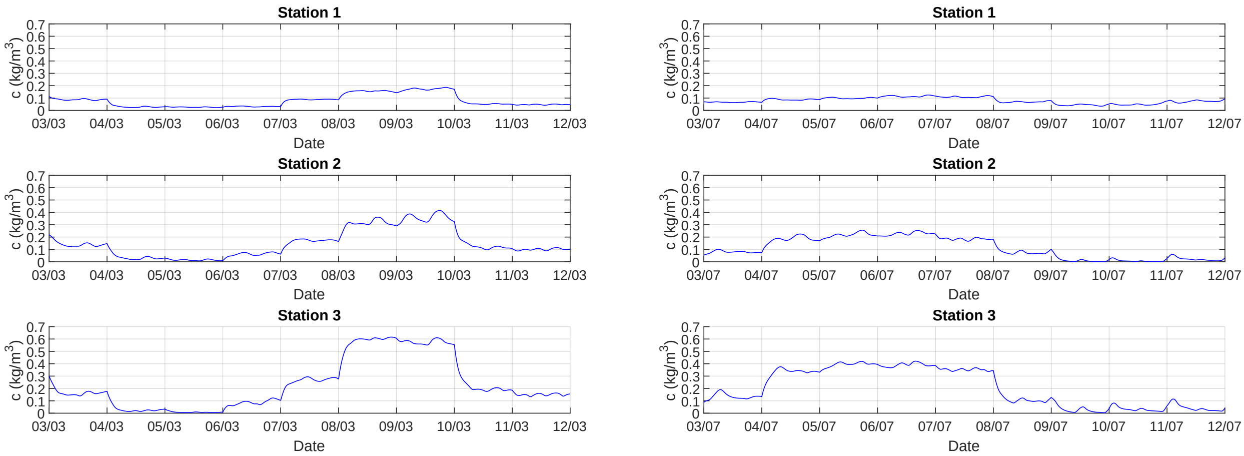

(a) Dry period (b) Wet period

Figure 4.12: Suspended sediment concentrations at the stations

4.2.3 Distribution of sand

The conceptual model suggests, through historical investigation, that the coastline is in dynamic equilibrium. The sediment transport at the coast exists out of suspended transport and bedload transport. Bedload transport happens mainly in the cross-shore direction and influences beach state and its profile development. The beach profile is a response of wave energy (Wright and Short, 1984). Low wave energy is responsible for reflective beach states, while high wave energy is responsible for dissipative beaches. The conceptual model proposes that the swell waves in the area are of moderate height, indicating a mild wave condition. The waves should be of the plunging type, creating a slightly reflective beach. Swell waves push the coarser material ashore, while the finer materials are transported offshore. However, the bathymetry in front of the barrier island has a dissipative slope. As the shore is in a tropical storm area, the bathymetry may be in a dissipative beach state due to a storm creating an energetic wave climate somewhat recently.
Figure 4.13 presents the mean spatial bedload transport and the cumulative transport through the transects. The highest cumulative transport for the bedload is on the most northern and southern transects. These are places of high transport because the transects are not perpendicular to the shore for these points. As the bedload transport moves mainly cross-sectionally, the cross-sections that are perpendicular (i.e., the black, blue, and green) have the lowest cumulative transport through their transects.
Figure 4.13a shows a broader stretch of cross-shore transport rates in front of the barrier island compared to the coast north of the northern inlet. One explanation is that the waves are pushing the beach back into a more reflective beach state, by pushing the coarser sediment more onshore. However, as the study and numerical model concentrate on large sediment fluxes, the area, and thus also cross-section area of the beach, is assumed to be in dynamic equilibrium. The bed slope resulting from the bathymetry data may not be in equilibrium, but this model is not capable of analysing this possibility in detail.

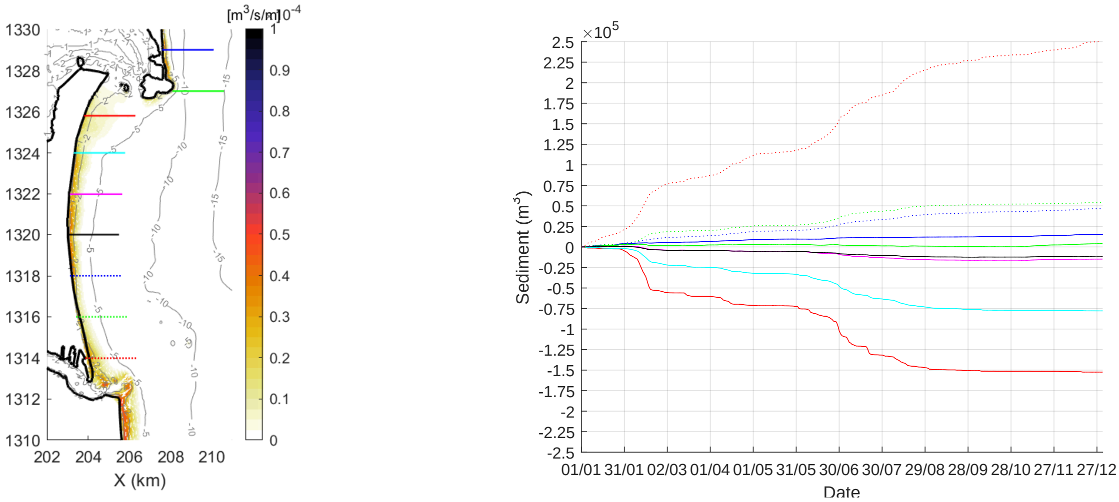

(a) Transport rates of the bedload transport of sand

(b) Cumulative sediment transport through the transects

Figure 4.13: Bedload transport

Longshore transport consists mainly of suspended sediment. This transport of sand is in dynamic equilibrium. As explained, the deposition and erosion patterns are difficult to use to test dynamic equilibrium. Therefore, it is preferred to analyse transport through the transects. Figure 4.14 shows longshore transport rates in space and cumulative transport in time. The difference in transport through both transects should not be too large. If this gradient is kept low, the erosion and sedimentation are low, and the transport is thought to be in equilibrium in the model.

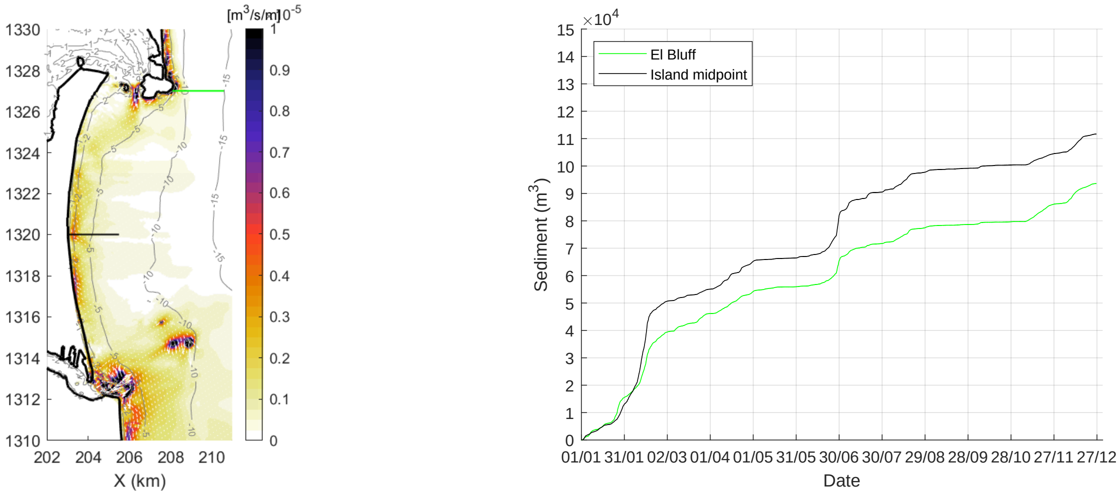

(a) Transport rates of the longshore transport of sand

(b) Cumulative sediment transport through the transects

Figure 4.14: Suspended longshore transport

As suggested in the conceptual model, the transport of the sediment is southward, the whole year-round. This direction is the case due to the wave climate originating from the north-east and east-northeast throughout the year. With a transport of 110,000 m^3 for the island midpoint, the amount of sediment that is transported is moderate. As the average mean wave height is around 1 m, the amount of transport is expected to be moderate. Steeper gradients in transport are seen in the months with a more severe storm climate. Moreover, the hurricane season lasts from June through November. The gradients during this period are also steeper, due to more extreme waves.

As Figure 4.14 depicts, the transport is substantial, with an amount of 95,000 m^3 north of El Bluff. This substantial transport is due to the severe wave dissipation north of the split. The beach slope is steeper in this area, creating plunging waves. This type of wave induces higher stresses when breaking than do spilling waves. The difference in the longshore transport between the transects is quite large, at 15,000 m^3. How-

ever, this difference is partly due to the rectangular grid at the coast. Grid cells block the transport, as there is a staircase structure of grid cells. The errors due to the grid are further discussed in Chapter 5.
In front of the barrier island, the conceptual model indicated that the beach is dissipative. For a dissipative beach, the wave height does not increase over a wide stroke due to wave dissipation. The wave dissipation starts far offshore, in the case of the island, as Figure 4.9 indicated. This wide stroke of dissipation induces a wide zone of littoral drift. The sediment transport in Figure 4.14a shows a wide range between the 10 m and 15 m depth lines. However, the suspended sediment at these depth lines are transported offshore from the coast, or the sediment originates from the north of El Bluff. This proposed origin is probably accurate, as at this depth the bed friction prompted by waves is too small to suspend new sediment.
Near the northern inlet, the transport rates are somewhat lower. The wave height decreases here, due to refraction. A lower wave height, and thus energy, induces lower sediment transport rates, as explained in Appendix A.1. Halfway around the island, the transport ratios are the highest since also sediment from the north reaches this shore. The transported sediment combines sediment locally suspended and sediment from upstream. Near the southern inlet, tidal currents exiting the lagoon reach high interactions with the longshore currents and waves in this area. The directions of the sediment transport are dispersed, inducing a blow of sediment offshore.

4.2.4 Sediment balance

Figure 4.15 shows the sediment balance of mud and sand for the area. The left figure shows the dry season and the right figure shows the wet season. The numbers shown are the model results multiplied with the calibration factors from Section 3.5.2. For the mud balance, it is only possible to make a sediment balance of the inner basin. When the mud leaves the lagoon, it diffuses over a too large area to monitor it.
The lagoon imports a large amount of mud (indicated with the red arrows) during the dry season. This mud originates from the wet season the year before. An amount of 0.25 Mm^3 is imported by the northern and southern tidal inlet in the first six months. This amount deposits for the most part near the inlets. When this mud is imported through the northern inlet, it is also partly transported to the shallower areas located to the south of the northern inlet. During the wet period, the circulation currents in the ebb direction increase and the imported mud is exported through both inlets. Part of the mud that is deposited during the dry period at the northern inlet is transported to the south during the wet period. The southern inlet exports this mud during this period. The same amount of 0.70 Mm^3 is exported at the northern and southern inlet.
The river delivers an amount of 0.90 Mm^3 of mud to the lagoon during the wet period. The largest fraction of this mud follows the river channel through the basin and is exported through the northern inlet. Only a small amount of this mud is transported directly over the shallower areas to the south.
Sand (indicated with the green arrows) moves to the south from north of El Bluff with an amount of 143,000 m^3/yr and at the midpoint of the barrier island with 165,000 m^3/yr. The first half-year, the longshore transport has a higher rate and is more than twice as high than the second half-year. The average wave heights are higher in this period of the year, inducing higher sediment transport. Figure 4.15 shows the sediment balance over annual period.

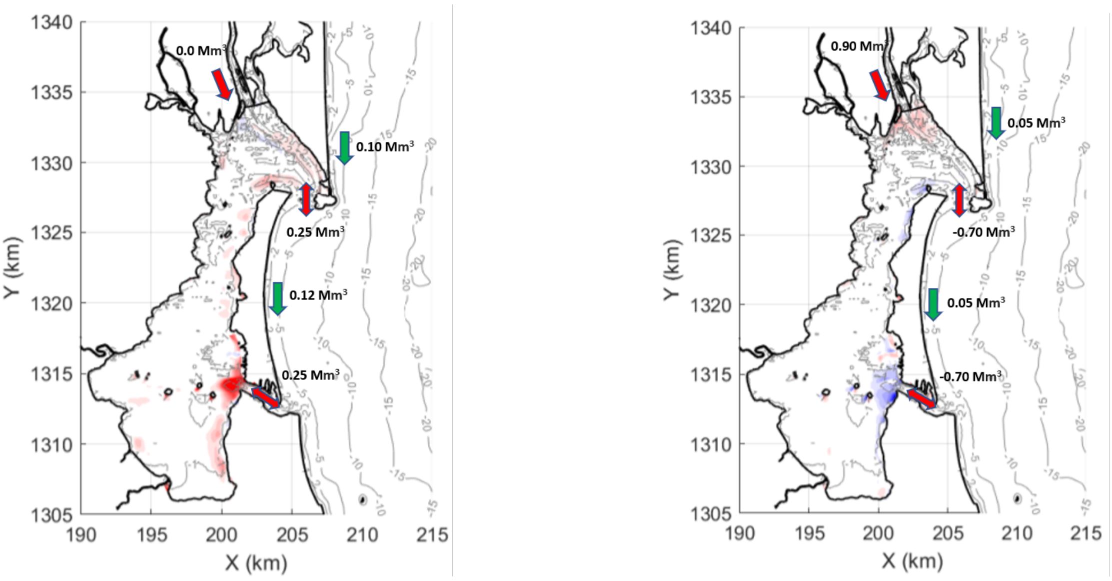

(a) Dry period (6 months)

(b) Wet period (6 months)

Figure 4.15: Sediment balance existing situation

4.3 Alternatives

In this section, the hydrodynamic and morphodynamic results of the cases with the alternatives are analysed. Firstly, the changes in residual currents and bed shear stresses are analysed. These changes indicate the new sediment fluxes and areas of erosion and sedimentation. Subsequently, the changes in the distribution of mud and sand are analysed. For the inner basin, the mud balance is important. For the adjacent coast, longshore transport is the dominant force of sedimentation.

4.3.1 Hydrodynamics

Firstly, the changes in hydrodynamics are analysed to explain the eventual sediment transport. The changes in the velocity of the tide in the inlet clarify sedimentation in this area. Due to a change in the hydraulic factors of the tide, the residual currents in the tidal basin alternate. Furthermore, velocity changes indicate whether the tidal basin changes from flood dominance to ebb dominance and explains how much sediment the basin imports. Finally, bed shear stresses are analysed to investigate to what degree sediment motion is initiated.

Discharge and velocity in the inlets

Changes in the cross-sectional area of the inlet influence flow velocity and discharge passing through the tidal inlet. Flow velocities in the entrance significantly influence the size of the cross-section of the inlet, as explained in Appendix A.3.2. For Alternative 1A, the depth is increased in the main channel. Figure A.4 shows that for an increase in the cross-sectional area, flow velocity decreases. In the conceptual model, it was stated that by enlarging the cross-sectional area, the dynamic equilibrium is disturbed. Through sedimentation, it is forced back into balance. The cross-sectional area at the northern inlet is 4000 m^2 in the existing situation and is increased to 5270 m^2 for Alternative 1A. The cross-section increases by 32%. Alternative 1B creates a new inlet in the barrier island with a cross-sectional area of 1810 m^2, where the tidal wave flows through. Figure 4.16 shows the results of the computed discharge through the northern tidal inlet and the velocity in the main channel. In the case of decreasing flow velocity and, thus, bed shear stresses, sedimentation more easily occurs in the channel.

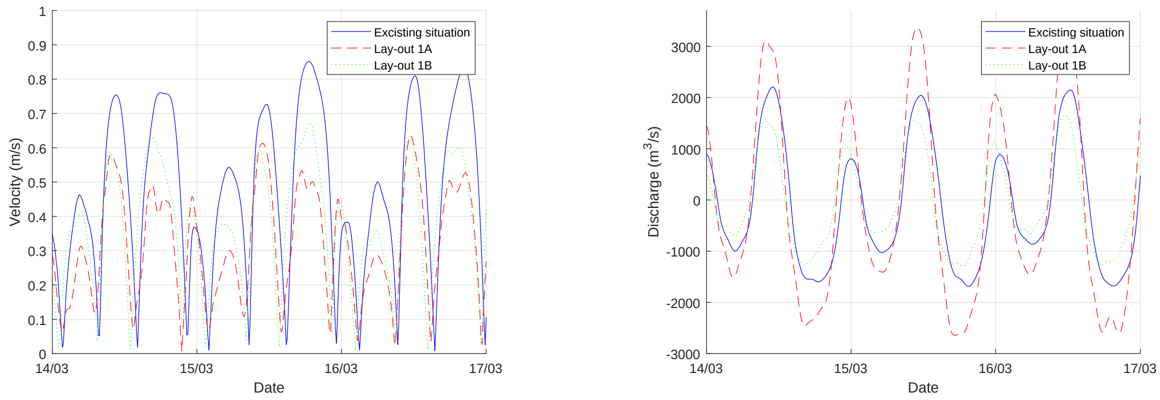

(a) Flow velocities (b) Discharges

Figure 4.16: Discharge in the northern tidal inlet for the existing situation and the alternatives

The discharge in the inlet increases substantially for Alternative 1A. This increase is a consequence of the decrease in resistance by deepening the bathymetry. Due to the smaller resistance, the water level increases slightly. The tidal basin is a discrete system. In a discrete system the water level increases and decreases simultaneously over the entire area. The water level is about the same for the whole system. If the water level increases slightly due to less resistance when the flow enters the opening, the water level increases slightly over the full length of the navigation channel in the basin. With the increase of water level, the discharge through the inlet also increases. Because the length of the channel is long, the discharge increases substantially. The formulas for this phenomenon and a more in-depth explanation can be found in Appendix G.1. Figure G.4 shows changes in discharge and flow velocity in the southern inlet. The discharge does not change when the alternatives are constructed. The flow velocity does decrease in the inlet. This decrease in flow velocity indicates that sedimentation takes place after the construction of the alternatives.

Residual currents

Due to changes in the bathymetry of the tidal basin after the construction of Alternative 1A, the properties of the tidal wave change. Water flow follows the path of the least resistance, which are the deeper areas. Because the bathymetry is deepened in the path of the access channel, the tidal flow follows the new channel geometry in the inlet.
Figures G.5 and G.6 show the trajectory of the tide during flood and ebb in the dry and wet season for Alternative 1A. As the tide follows the channel west and subsequently southward, it receives less resistance from the river discharge and vice versa compared with the existing situation in Figures E.2 and E.3. Due to lower resistance, both hydraulic components reach higher flow velocities. The flow velocities in the area south of the channel increase during ebb and flood due to the tide. Higher velocities are observed here in Figures G.5 and G.6 during ebb and flood in comparison with the existing situation. North of the channel the velocities also increase, as the river discharge receives less resistance from the tidal wave. Higher flow velocities, mainly during ebb, are observed north of the channel, as compared to the existing situation. This effect is especially notable in the wet period, when the river discharge is higher. Changes in the tide entering the tidal basin result in fluctuations in the residual currents within the basin. Figure 4.17 shows the residual currents after Alternative 1A is modelled. These residual currents are taken over a spring tide. South of the dredged channel, residual currents are directed southward for Alternative 1A in the dry season. This is the flood direction. North of the tidal channel, the currents have increased, as compared to the existing situation in Figure 4.1a. In this area, the river discharge has less resistance due to the alternating direction of the tidal wave. The influence of the river increases and a stronger ebb dominant and southward current is the result.
During the wet season, the currents south of the channel alternate to ebb dominance, as the residual currents are directed towards the channel. The river discharge mainly follows the river channel, as a result of this discharge not influencing the southern area. However, compared to the existing situation in Figure 4.1b, stronger southward directed currents are observed north of the navigation channel for the new alternative.

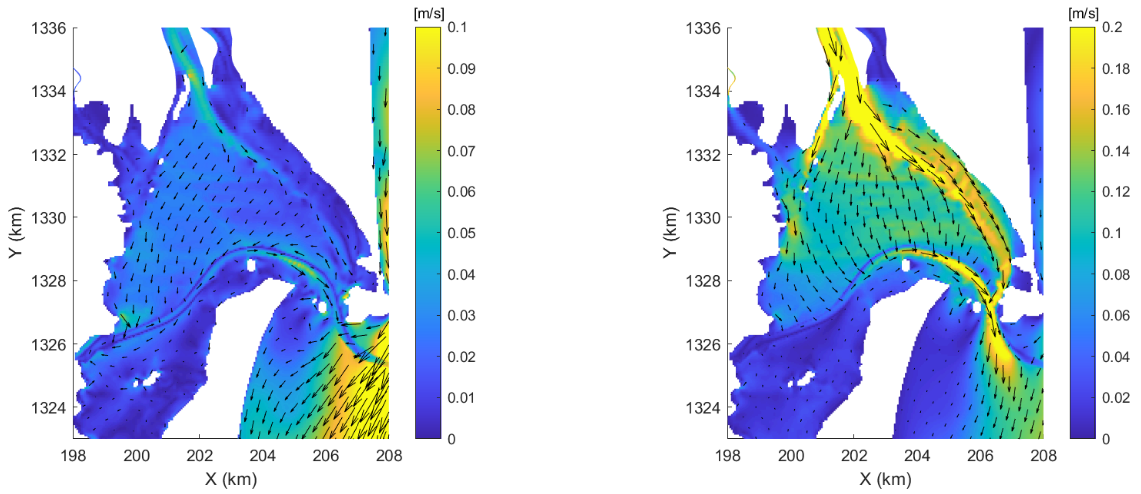

(a) Dry period

(b) Wet period

Figure 4.17: Residual currents for Alternative 1A

Figures G.7 and G.8 show the trajectory of the tide when Alternative 1B is modelled. Due to the new opening, a part of the tidal wave force no longer goes through the northern gap. The flow velocities have decreased, imparting less resistance to the river discharge. The river discharge also induces stronger southward currents for Alternative 1B, as compared with the existing situation. South of the new gap, the currents are more severe for the new situation. During ebb, the currents above the new entrance are southward directed, flowing out of the newly created gap. Before the construction, these currents are northward directed. When the currents are followed for Alternative 1B in Figures G.7 and G.8, they flow in a circle. As they enter through the northern inlet during flood, they are directed towards the newly created gap. During ebb, the currents leave through the new gap. The sediment that enters through the northern inlet is transported to the new channel. In the ebb-tidal channel, where the currents of the tidal wave meet, the flow velocities have decreased.

Figure 4.18 shows the residual current for Alternative 1B. Around the newly created channel, the currents have an ebb dominant direction. In some areas south of the channel, residual currents are close to zero. In the original ebb channel, the ebb-directed current has decreased in velocity compared to the existing situation in Figure 4.1a. This decrease is expected, as the velocity has dropped around the inlet in Figure 4.16a. For the wet season, the same southward-directed current of the river discharge is observed. For both the alternatives, the residual currents drop southward of the newly dredged channels in the wet season. The residual current for both the alternatives at the southern inlet are shown in Figures G.9 and G.10. The currents during the dry period do not change severely compared to the existing situation in Figure E.4a. In the wet season, residual currents in ebb direction decrease in velocity. This decrease is mainly as the river discharge from the Rio Escondido does not reach the southern inlet in the same quantity as the existing situation. When the river discharge flow south, it encounters the newly dredged channel, and it follows as it is the path with the least resistance. A less strong residual current coming from the north is the result for both the alternatives. The discharge of the Rio Kukra is the only discharge with a substantial quantity that leaves through the southern inlet. The southern inlet becomes less ebb dominant during the wet period than for the existing situation.

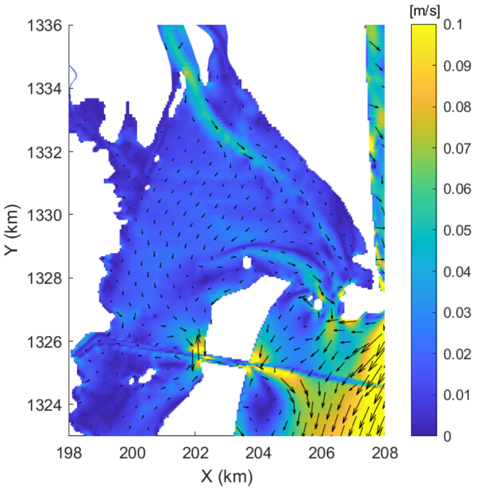

(a) Dry period

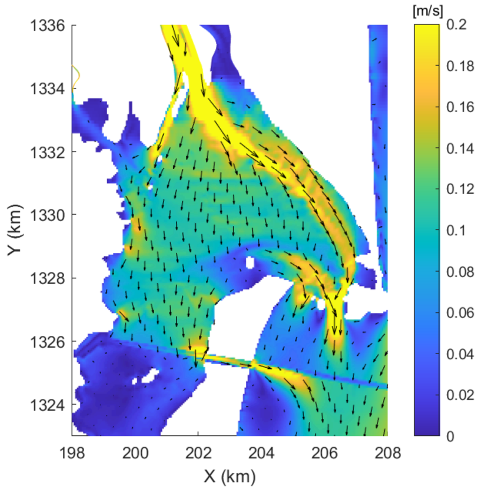

(b) Wet period

Figure 4.18: Residual currents for Alternative 1B

The metering stations in Figure 4.2 are also analysed for the alternatives. Figure 4.19 shows the water levels and flow velocity for Alternative 1A. In a comparison of the tidal asymmetries of Figure 4.19 with those of Figure 4.4, which presents the existing situation, differences are found in flow velocities.
For the existing situation, the stations create greater differences in the magnitudes of flood and ebb and, hence, are more flood dominant in the dry season. This decrease in the difference between ebb and flood flow velocity in Figure 4.19a emerges from the greater influence of the river discharge. Because the tidal wave follows the dredged channel, the river discharge becomes the dominant hydraulic forcing for Stations 1 and 2. The discharge forces these areas into ebb dominance. For Station 3 the velocities and fluctuations are higher for Alternative 1A than for the existing situation. South of the channel, where Station 3 is located, the tidal wave has a greater influence. Furthermore, Station 3 is now located near the channel, and is thus easily reached by the tidal wave.
In the wet season, the flow velocity during ebb is higher than during flood at Stations 1 and 2. For the existing situation, the flow is more constant, originating from the river discharge. For Alternative 1A, the river pushes the station into ebb dominance, as it then has a greater influence. The tidal wave counteracts the river discharge less strongly. At Station 3, the flow velocities have increased, as the tidal wave reaches it more easily. Sediment is transported further away in the basin. At Stations 1 and 2, a relatively stable constant flow speed is visible due to the rive discharge. At Station 3, the flow speed due to the river is lower, and it is mainly the tide that influences the velocity.

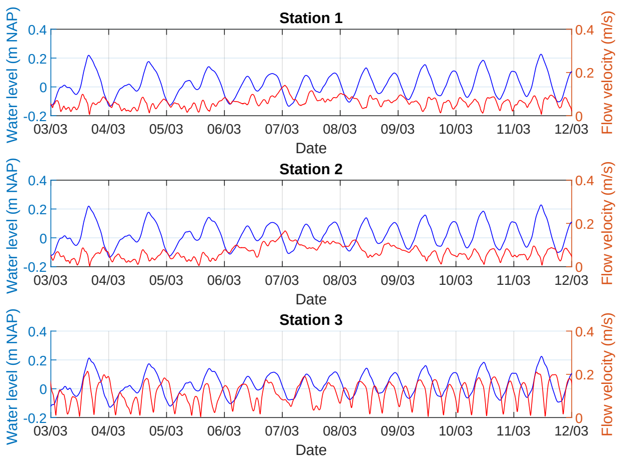

(a) Dry period

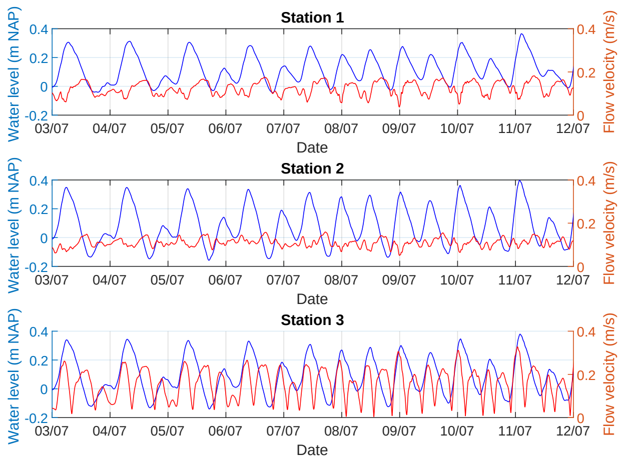

(b) Wet period

Figure 4.19: Flow velocity and water level for Alternative 1A

For Alternative 1B, the same patterns are observed as for Alternative 1A. Stations 1 and 2 are pushed further into ebb dominance by the river discharge, as the discharge amplitude that enters the northern inlet decreases, compared to the existing situation. This effect is somewhat more substantial for Alternative 1B, as the flow velocities are higher for ebb than in Alternative 1A. For Station 3, the same patterns are observed as in the case of Alternative 1A.

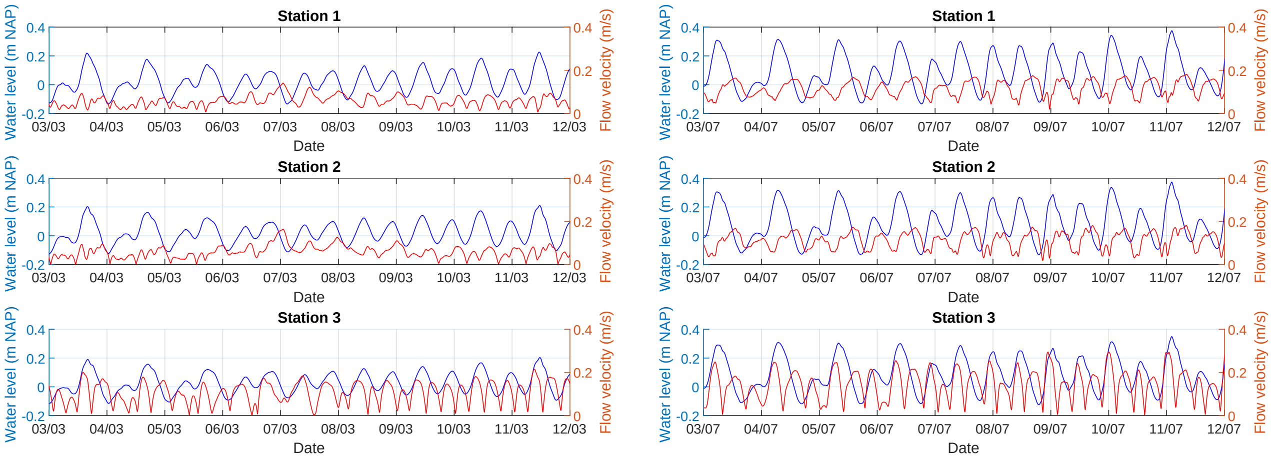

(a) Dry period

(b) Wet period

Figure 4.20: Flow velocity and water level for Alternative 1B

Bed shear stresses

With changes in the flow directions and magnitudes, the bed shear stresses in the basin also change. Figure 4.21 shows the bed shear stresses for the stations, as compared to those of the existing situation. Whereas the bed shear stresses for the existing situation are high during flood, the bed shear stresses for ebb are also high for both the alternatives. This higher bed shear stresses during ebb occur because the river discharge has less resistance. During ebb, the river discharge increases in velocity compared to the existing situation. For Station 1 the bed shear stresses have a constant value indicating the river discharge is the primary hydraulic forcing here. For Station 2, the river discharge also creates constant hydraulic forcing in the case of the alternatives. As the river discharge is the dominant hydraulic process north of the channel in the new situation, it forces the system in ebb dominance, and the high bed shear stresses during ebb are clarified. For Station 3, the bed shear stresses are substantially higher than for the existing situation. The bed shear stresses are tide-induced, in an analysis of the curves. Station 3 is located at a shallow area near the newly dredged channel. The tidal flow reaches the more land-inward shallow areas with more ease, as it follow the newly dredged channel. Around the channel higher bed shear stresses occur.
High bed shear stresses during ebb indicate transport takes place during ebb. The system was at first mainly flood dominant in the shallower areas, whereas the system is now forced slightly into ebb dominance north of the channel according to the flow velocities. Due to the higher bed shear stresses during ebb, the system is capable of transporting mud.

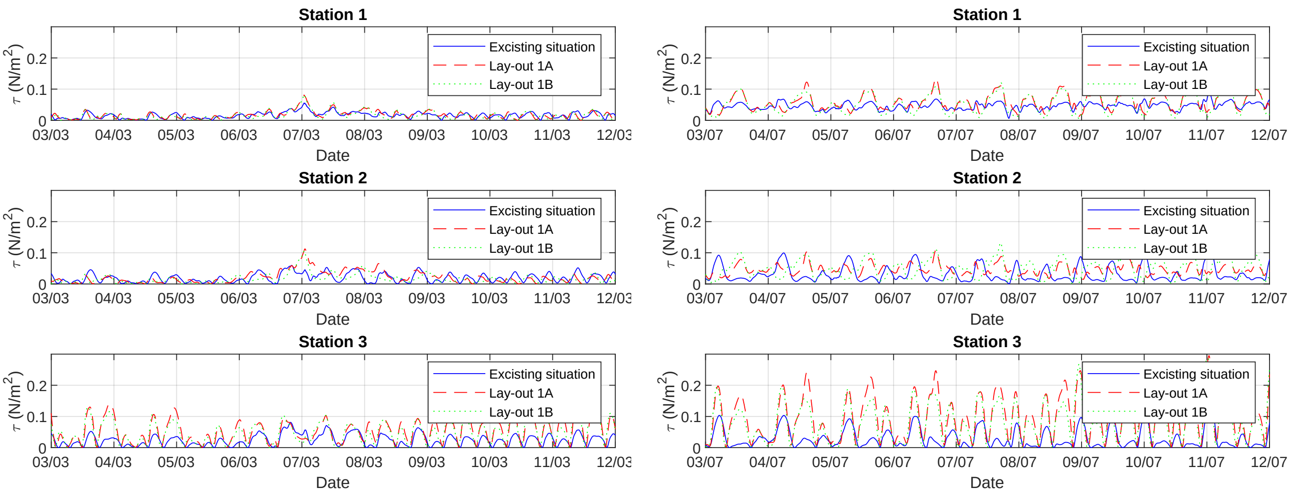

(a) Dry period (b) Wet period

Figure 4.21: Bed shear stresses for the Alternative 1A and 1B during a neap and spring tide

4.3.2 Morphodynamics

The conceptual model in Section 2.5 explains that the channel forces the dimension of the dynamic system out of balance. By analysing the sediment balance, the new sediment fluxes are observed. For the coast, longshore and cross-shore transport are analysed. The channel layouts are in the path of both the transport routes.

Deposition mud

The sediment balance for Alternative 1A is shown in Figure 4.22. Figure 4.22b shows the deposition pattern of the mud accompanying the sediment balance.
According to the results of the mud transportation of the existing model depicted in Figure 4.10a, mud enters the tidal basin in high quantities during the dry season. For Alternative 1A, slightly less mud enters through the tidal inlets in the dry season. These quantities are lower because the flow through the inlet is not strong enough to carry as much mud as in the existing situation. The flow velocities have decreased, as shown in Figure 4.16. The stations in the shallower areas are also less flood dominant (see Figure 4.19) for Alternative 1A, as compared to the existing situation (see Figure 4.4). The system, in total, imports less mud. In addition, Figure 4.22b shows that mud is trapped in the outer channel before it reaches the tidal inlet and can be imported.
When the river discharge increases during the wet season, the sediment input through the river increases substantially, and the northern inlet starts to export sediment. This export, however, does not occur with a steeper gradient than in the existing situation. Figure 4.19b showed that the ebb dominance is enhanced, as compared to the existing situation. The mud is transported to the navigation channel and is trapped before it leaves the basin.
Additionally, during the wet season mud starts to be transported south, exiting through the southern inlet in the existing situation. For Alternative 1A the mud that is transported south is deposited in the dredged channel. A shortage arises south of the channel, so south of the channel areas of erosion are observed. Another explanation is that parts of this area are now ebb dominant. Erosion takes place, and the sediment is deposited in the channel. When less mud reaches the southern channel, it exports less mud. The mud is predominantly deposited in the port and where the channel crosses the shallower areas in the basin. In these areas, the flow velocities are less severe than are those in the area around the inlet. The flow going southward over the shallower areas is less than that in the existing situation. A hydrodynamic explanation is that the water flow elects the path of lesser distance and follows the dredged channel. Due to the smaller current, the erosion of mud at the southern inlet is diminished, as compared to the existing situation.
The deposition pattern in the river channel is enlarged in Figure 4.22b, as compared to the existing situation in Figure 4.10b. The river discharge has less resistance from the tidal wave transporting the mud further in the basin, as compared to the existing situation.
Most of the sedimentation in the channel is found in the land-inward part, where the tidal wave loses power.

In the northern inlet, velocity has decreased, so mud also has the chance to deposit in this area, although in lower rates than occurs further offshore and land-inward. At the coast, areas of erosion are observed. As less mud leaves the northern inlet, shortages arise around these areas. The outer channel also traps mud that is transported northward by the tide.
For the southern inlet, the import of mud is less intense for the Alternative 1A in Figure 4.22 than for the existing situation in Figure 4.10a. The southern inlet is left unaltered. The velocity decreases a little, as Figure G.4 shows. The lower amount of import is probably because the southward mud transport along the coast has decreased, as the channel traps it at the northern inlet.

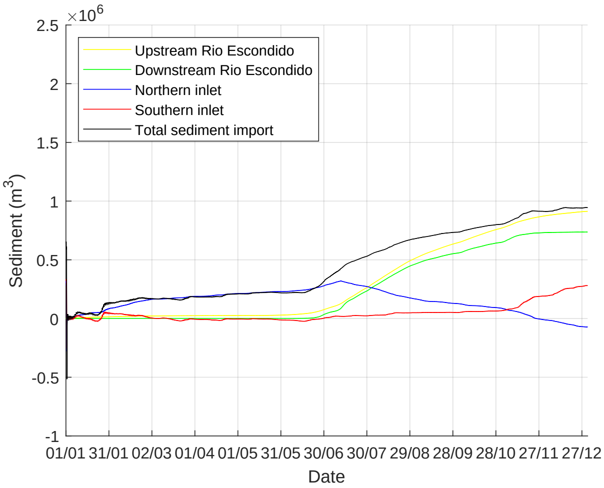

(a) Sediment balance

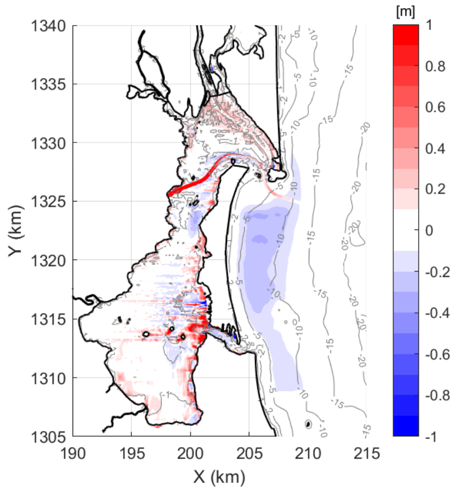

(b) Deposition pattern

Figure 4.22: Sediment balance and deposition for Alternative 1A

Figure 4.23 shows the sediment balance for Alternative 1B. For Alternative 1B, the import through the northern inlet during the dry season is small, as compared to the existing situation, which is due to the reduced flow velocities in Figure 4.16a. The tidal wave is not capable of transporting the same amount of mud through this inlet, as compared to the existing situation. Figure 4.23b shows that the mud entering through the inlet deposits in the ebb channel. The residual currents are close to zero around this area in Figure 4.18b. Figure 4.28 also shows that the new opening starts to import sediment. This sediment is mainly deposited in the navigation channel.
In the wet season, the river transports mud into the basin. The residual currents in the direction of the northern tidal inlet have altered, as compared to the existing situation in Figure 4.1b. The residual currents are mainly directed to the newly dredged channel. Due to this new direction of the currents, the mud is transported mainly to the newly created opening now. Here, the sediment deposits in the channel or leaves through the opening. When the mud reaches the shore, the waves are incapable of taking all sediment away. Some of the mud is transported back through the northern inlet and, after that, transported towards the channel again. This circulation of transport is why the northern inlet has a relatively high import of mud in the wet period.
In Figure 4.23b, the same deposition and erosion patterns are observed for Alternative 1B as for Alternative 1A. Different deposition patterns are observed in the ebb channel at the northern inlet. The velocity decreased at the northern inlet, as observed in Figure 4.16b, making possible the deposition of mud in these areas. In the navigation channel, mud deposits over the full stretch, except for the direct openings. The mud is transported mainly during the tide, reaching the port. The outer channel attracts the mud that is deposited offshore, creating areas of erosion around it.

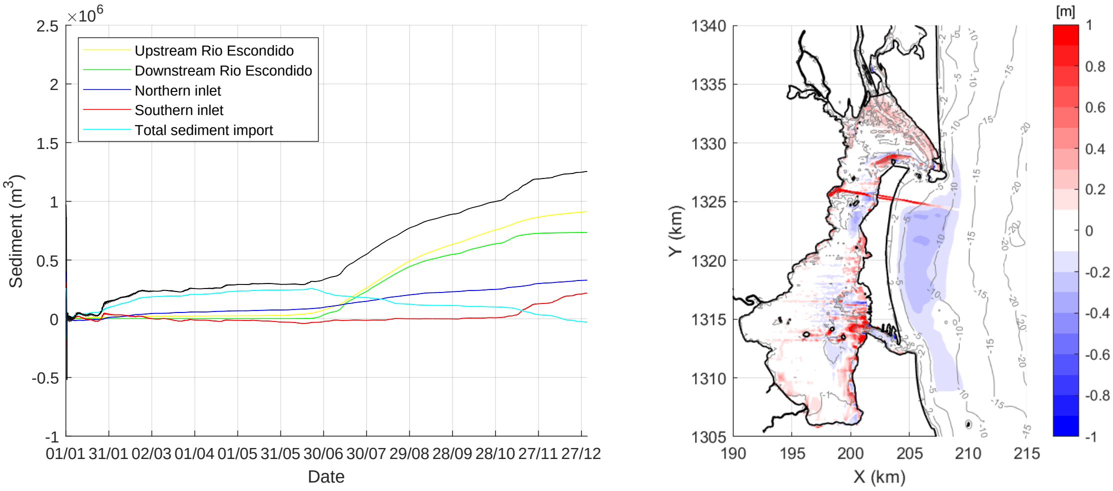

(a) Sediment balance

(b) Deposition pattern

Figure 4.23: Sediment balance and deposition for Alternative 1B

Distribution sand

As explained in Section 4.2.3, the transport of sand is divided into longshore and cross-shore transport at the adjacent coast. Cross-shore transport is mainly bedload transport, and longshore transport is mainly suspended-load transport. As the layout of each alternative has a different trajectory, suspended load and bedload are unequally essential for them. Notably, the bedload transport is a factor of 10 higher than the suspended load transport in the figures.

Figure 4.24 depicts the transport rates of the suspended load and bedload transport for Alternative 1A. As the trajectory of the alternative curves around El Bluff, the bluff partly protects it from longshore transport. The suspended sediment and deposits that reach the channel originate from the northern shore. However, there are substantial sediment transport rates around the channel. These high rates are induced locally due to the construction of the channel, as these did not occur in the existing situation (see Figure 4.14).

Aside from the suspended load, the channel is in the route of the bedload transport, as Figure 4.24b shows. The bedload transport is important for Alternative 1A, where the channel starts curving into the inlet. The trajectory of the channel moves to a position parallel to the shore, and thus is in the route of the cross-shore transport. Figures 4.24a and 4.24b show that the stretch of the channel into which the sand is transported is short. However, around the inlets, the transport rates signal high quantities.

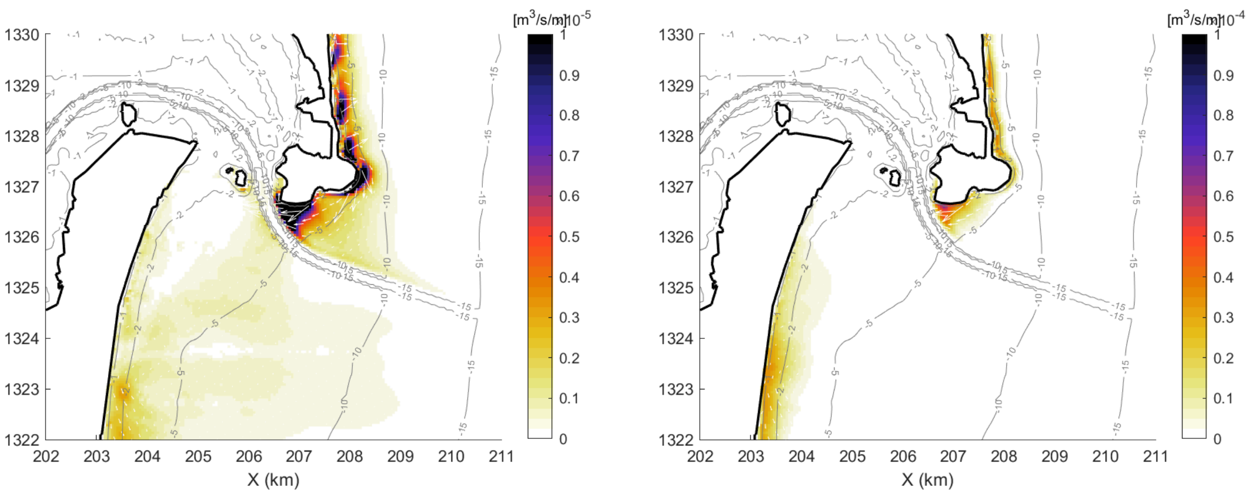

(a) Suspended load transport

(b) Bedload transport

Figure 4.24: Transport rates of the suspended load and bedload transport of sand for Alternative 1B

The suspended load and bedload transport for Alternative 1B are presented in Figure 4.25. The suspended load transport reaches the channel over a wider stretch, as compared to Alternative 1A. In Alternative 1B, more suspended sediment deposits in the access channel, as compared to Alternative 1A. This higher quantity is mainly because the transport zone is wider in Alternative 1B than in Alternative 1A. Furthermore, north of the channel, waves reach the coast and put new sediment in suspension. However, the wave climate is mild around this area, as Figures 4.7 and 4.8 show. This mild climate is due to the refraction of waves. The suspended sediment between the 5 m and 10 m depth line originated mainly from the north of El Bluff. The bedload transport reaches the channel over a smaller transport zone, as compared to Alternative 1A. The zone is smaller because the channel is perpendicular to the coast, and thus the bedload transport is parallel to the channel.

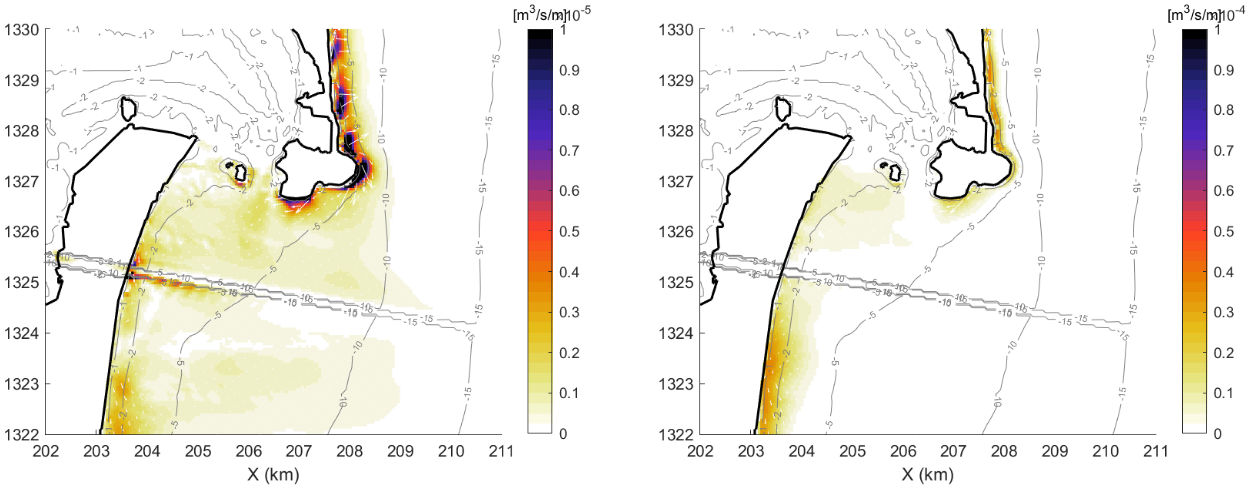

(a) Suspended load transport

(b) Bedload transport

Figure 4.25: Transport rates of the suspended load and bedload transport of sand for Alternative 1B

4.3.3 Sedimentation and erosion

This section presents the results for the sedimentation and erosion in the area after implementing the alternatives. First, a sediment balance of the mud and sand transport is presented to locate the origin of sediment that deposits in the port and channel. Additionally, the sedimentation rates in port and its channel are given by combining the sedimentation results of mud and sand. Finally, the coastal regression of the adjacent coast is analysed to determine the influence of the ports on the coast.

Sediment balance

A sediment balance is made for Alternative 1A and for 1B. Figure 4.26 presents this for Alternative 1A. The left figure presents the dry period, and the right figure presents the wet period. The longshore transport is indicated with the large green arrow at the coast. The mud transport is presented with the large red arrows at the river and the tidal inlets. These longshore and mud transport are consistent on the long-term. When a port and its navigational channel are constructed, the morphodynamic equilibrium is disturbed, and sediment transport will also be locally initiated. This locally induced sediment transport is a short-term process, as this stops once the bed has degraded substantially and the bed shear stresses are too low. The small yellow arrows indicate locally induced sand transport and the small orange arrows indicate mud transport. In the dry period, the sedimentation of mud in the port and channel is 0.23 Mm^3 (presented in red numbers) and the import of mud into the basin is 0.24 Mm^3. The tide follows the dredged channel and deposits the sediment once the flow velocity decreases. However, the tidal flow also follows the river channel and deposits sediment in here. Not all the sedimentation in the dredged channel originates from the import through the northern inlet. Places of erosion are observed around the channel in Figure 4.26a. It is estimated that sedimentation due to locally induced sediment is about 25% of the sedimentation in the dredged channel. The sediment that enters the basin through the southern inlet does not reach the channel in the north, as the residual currents are directed southward.
During the wet period, the total net import through the northern inlet and Rio Escondido is just 0.02 Mm^3

higher than the wet period. Most of the sediment from the river is transported directly to the northern inlet and leaves the basin. The sedimentation of mud in the port and inner channel during this period is 0.09 Mm^3, which is lower than in the dry period. Figure 4.26b shows a small amount of erosion around the channel. It is therefore assumed that about 90% of the sedimentation in the channel is from the influx through the Rio Escondido.
The sedimentation of mud in the outer channel during the dry period is from local sediment as the northern inlet does not export sediment. The sediment is transported by the tide to the navigation channel from downstream, as the erosion in Figure 4.26a indicates. During the wet period, the sedimentation in the outer channel is only 0.01 Mm^3, while the northern inlet exports 0.24 Mm^3 of mud. A large part of the mud is transported directly away from the channel.
The sedimentation of sand in the outer channel is 0.14 Mm^3 (presented in green numbers) in the dry period. This quantity is higher than the total longshore transport of 0.10 Mm^3 passing it. This means about 30% of the sedimentation in the outer channel originates from sediment around the channel. In Figure 4.24a the transport rates north of the channel are high, and much of the sediment originates from here. In the wet period, the total sedimentation decreases to 0.03 Mm^3 of sand, which is a smaller quantity than the longshore transport. The model grid cells at the coast have a staircase structure blocking a fraction of the longshore transport. Deviations in the model grid are further elaborated in Chapter 5.

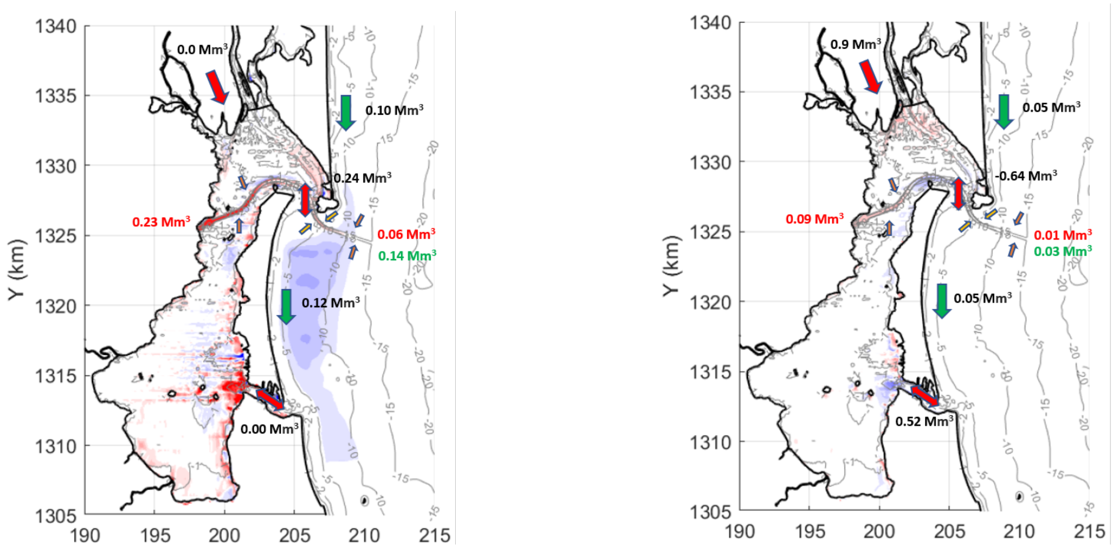

(a) Dry period (6 months)

(b) Wet period (6 months)

Figure 4.26: Sediment balance Alternative 1A

Figure 4.27 shows the sediment balance for Alternative 1A for annual period. The sedimentation in the inner channel and port is 0.34 Mm^3/yr and the total net import of mud in the lagoon is 0.50 Mm^3/yr. About 50% of this import deposits in the dredged channel and port, when the locally induced sediment is subtracted from the total sedimentation. Only a small fraction of the mud that exits the northern inlet deposits in the outer channel, as the Figure 4.26b shows. The mud in the outer channel originates for 85% from locally induced sediment. The longshore transport is deposited for 100% in the outer channel. This means 0.02 Mm^3 originates from locally induced sediment.

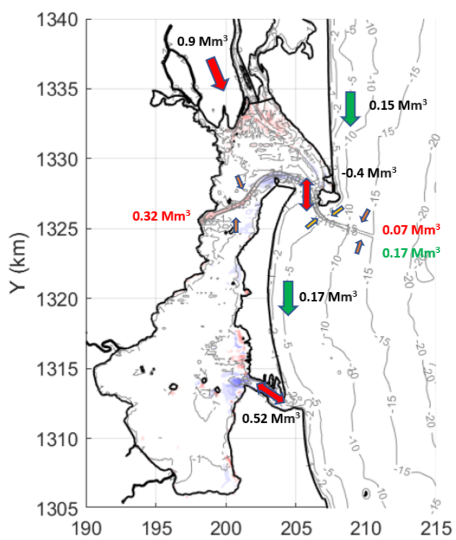

Figure 4.27: Sediment balance of a year for Alternative 1A

Figure 4.28 shows the sediment balance for Alternative 1B. In the left figure, the northern inlet imports a quantity of 0.08 Mm^3 of mud during the dry season. The mud that enters through the northern inlet deposits for a large part in the ebb channel. The rest of this mud is transported to the new channel. After all, the residual currents are directed from the northern inlet to the new channel, according to Figure 4.20b. The total import in the dry season is larger for Alternative 1B than for Alternative 1A, as the newly created gap imports 0.19 Mm^3 of mud. The mud that enters through the newly created gap deposits directly in the channel. The mud is not transported to the areas around the channel, as the residual currents around the channel are in the ebb direction according to Figure 4.20a. Figure 4.21 shows the bed shear stresses increases in the area where the channel is dredged, and thus sediment movement is induced. An estimation is made that about 25% of the sedimentation in the dredged channel is from locally induced sediment. The total sedimentation in the port and inner channel during the dry season is much smaller for Alternative 1B than for Alternative 1A. The sedimentation in the channel is lower than import trough the newly created gap and the locally induced sediment, the tidal flow velocity seems strong enough to also export a fraction of this sediment in the dry period.

In the wet period, the import through the northern inlet is high, and the river starts to supply a large quantity of mud. The sedimentation in the inner channel of 0.08 Mm^3 is not as high as the total net import of mud, which is 0.94 Mm^3. This means about 90% does deposit in the lagoon but outside the channel, as the hydrodynamics have changed considerably. Due to the newly created gap, sedimentation occurs at specific places like the ebb channel, as the flow velocity in this area is not high enough anymore to transport the mud.

The sedimentation of mud in the outer channel originates from local sediment, as there is no supply of sediment through the inlets. In the wet season, the newly created inlet exports a large quantity of sediment. The sedimentation in the outer channel is small with 0.03 Mm^3 during this period. This small quantity is probably from the export through the new inlet.

The sedimentation of sand in the outer channel has the same amount for Alternative 1B as for alternative 1A. About 30% is from longshore transport. In the wet period, the sedimentation in the outer channel is, however, higher for Alternative 1B than for Alternative 1A. Local sediment deposits in higher quantities in the channel for Alternative 1B, as the longshore transport, is not smaller for Alternative 1B. About 50% of the deposition is from locally induced sediment. Figure 4.25a shows the trajectory has a longer stretch in the breaker zone than Alternative 1A in Figure 4.24a. By implementing a channel in this dynamic area, the sediment transport is disturbed more significantly, but the hydraulic processes restore it at a higher rate.

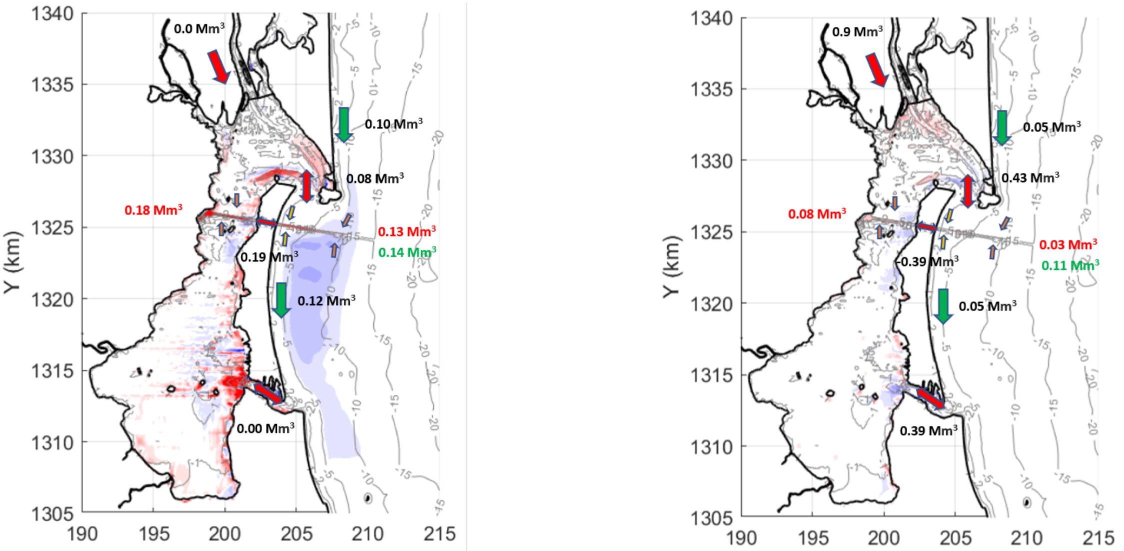

(a) Dry period (6 months)

(b) Wet period (6 months)

Figure 4.28: Sediment balance Alternative 1B

Figure 4.29 shows the sediment balance of a year for Alternative 1B. The total net import in the tidal basin is 1.21 Mm^3/yr, while the sedimentation is only 0.26 Mm^3/yr, which is about 20% of the net import. The tide is able to flush a large quantity out the channel in the wet period. The mud that deposits in the inner channel and port originates for about 80% from the import fluxes. The outer channel has higher rates of sedimentation than Alternative 1A. The outer channel catches more locally induced sediment as it is in the breaker zone.

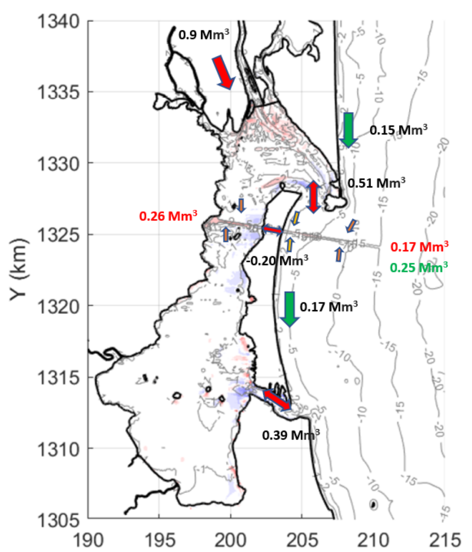

Figure 4.29: Sediment balance of a year for Alternative 1B

Sedimentation port and channel

The sedimentation in the access channel and the port basin is a result of the combination of the sediment transport processes of mud and sand in the bay and along the shore. In Section 4.3.3 the sedimentation for sand and mud in the channel are given separately and relatively to the large sediment fluxes. The sediment quantities are given in the specific density of 2650 kg/m^3. However, for dredging purposes the dry bulk density of the mixture of sand and mud must be computed. The dry bulk density of the mixed sediment depends on the ratio of the sand and mud. To compute this dry bulk density the channels are divided into sections, as the sedimentation of sand and mud is different over the channel. Each section has a different ratio of mud to sand with a different new dry bulk density. The new density is computed according to

Equation 4.1. The number 500 is the dry bulk density of mud, and the number 1600 is the dry bulk density of sand.

$$\rho_{sediment} = 500 + (1600 - 500) * (1 - \frac{p_{mud}}{p_{mud} + p_{sand}})^2 \tag{4.1}$$

$\rho_{sediment}$	=	Dry bulk density	$[kg/m^3]$
p_{silt}	=	Fraction mud	$[-]$
p_{sand}	=	Fraction sand	$[-]$

Figure 4.30 represents the sections for both channels. In Tables H.1 and H.2, the sedimentation of sand and mud are presented per section. Figures H.1 and H.2 show the numbering of the sections. The sedimentation rates in tables are divided into quantities for the dry and wet period. This division is made because each period requires different calibration factors, as explained in Section 3.5.2. The highest sedimentation is observed for the dry period when the tide is the dominant hydrodynamic forcing component. The mud is transported along the total length of the channels and reaches the port, inner channel, and outer channel. At the sections around the inlet, a mixture of sand and mud is found. The sedimentation of the sand is the highest here. The transport of sand is greatest at the outer channel and near the tidal inlet, as the longshore transport is the most severe near the coast to a depth of 5 m. The tidal wave is not strong enough to transport the sand deep into the basin. Further offshore, the ratio of mud increases, as mud is transported offshore by the swell waves. Within the basin, the transport of sand under year-round conditions is negligible.

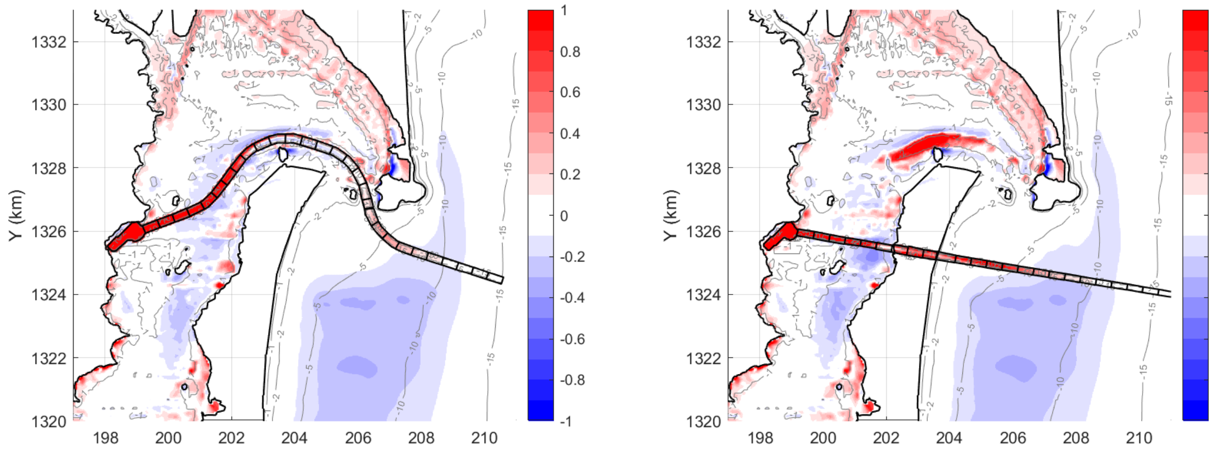

(a) Alternative 1A

(b) Alternative 1B

Figure 4.30: Sections of the alternatives and the deposition pattern of silt

In Table 4.1, the total sedimentation quantities of the alternatives are shown. The total sedimentation in the inner channel is larger for Alternative 1A than for 1B. The sedimentation in this area is mostly due to the tide. When mud leaves the northern inlet, it is transported back into the basin with more ease for Alternative 1A than for 1B. The mud does not leave the dredged channel of Alternative 1A, as explained in Section 4.3.3. The tide flushes the channel of Alternative 1B, with more ease. At the outer channel, more sand and mud are captured by Alternative 1B than by 1A. The navigation channel for this alternative is located over a longer stretch in the breaker zone inducing more local sediment transport. The difference in the deposition in the outer channel is so large that the total sedimentation for Alternative 1B is greater, with a difference of 650,000 m^3/yr.
The annual sedimentation is about 11% of the capital dredging volume for Alternative 1A and 17% for Alternative 1B. This quantity matches the expectation of the conceptual model, which estimated a sedimentation rate of 10% to 15% for the outer channel. The outer channel of Alternative 1B is refilled in about 6 years, which is a high rate. The outer channel, however, is located in the breaker zone of the adjacent coast. The annual siltation in the inner channel and the port consists of main mud and is on the order of 6% to 9% of the capital dredging volume. These percentages are much lower in quantity than the 25% to 75% represented in the conceptual model. An explanation for this difference is that the port and largest part of the navigation channel is located outside of the large mud transport routes. Most of the mud input is from the

Rio Escondido. This mud follows the river channel to the northern inlet. About 50% of the net import of mud for annual period is deposited in the inner channel. The port and the most land-inward part of the channel are reachable only by the mud transport of the tide. Only 10% of the mud influx of the Rio Escondido reaches the dredged channel directly.
For Alternative 1B, a higher refill rate in the inner channel is found than for Alternative 1A. Although the total sedimentation quantity is smaller than for Alternative 1A, the length of Alternative 1B and thus capital dredging is much smaller. There are high sedimentation rates in the sections of the new inlet for Alternative 1B, indicating that tidal flow is not strong enough to flush these sections fully.

		Port	Inner channel	Outer channel	Total
Alternative 1A	Total sedimentation (10^6 m^3)	0.49	1.22	1.08	2.79
	Percentage of the capital dredging (%)	8	6	11	
Alternative 1B	Total sedimentation (10^6 m^3)	0.45	0.94	2.05	3.44
	Percentage of the capital dredging (%)	8	8	18	

Table 4.1: Total sedimentation of sand and silt combined for the Alternatives

Erosion of the coast

The navigation channel at the coast traps the sand from the longshore transport. Subsequently, a shortage in the sediment supply arises at the downdrift side of the channel. In the areas of a shortage, there is erosion to compensate for the sediment supply. The longshore transport rates at the island midpoint in the sediment balance of Figure 4.27 and 4.29 are of the same quantity as for the existing situation in Figure F.1. As the sediment transport quantities are the same, erosion has occurred to compensate for the sedimentation in the dredged channel.
Figure 4.31a shows the relative difference in transport rate for Alternatives 1A compared to the original situation. In red areas, the transport ratios for the alternative are higher. For the blue areas, the transport ratios for the existing situation are higher. The areas with a local surplus of transport potential based on available (wave) energy erosion might take place. The main transport direction is from north to south.
The red area just upstream of the channel shows that the construction of the channel leads to a local increase of sediment transport towards the channel. The channel induces sediment transport around the channels as explained in Section 4.3.2. A fraction of the sediment in the outer channel is because of the erosion in this area. This increase leads to some erosion of the foreshore in front of El Bluff. A certain fraction of the total longshore transport is deposited in the channel, leading to a decrease in longshore transport directly south of the channel. This is the blue area directly south of the channel. In this blue area exists a surplus of potential transport leading to local erosion in this area to supply new sediment to the longshore component.

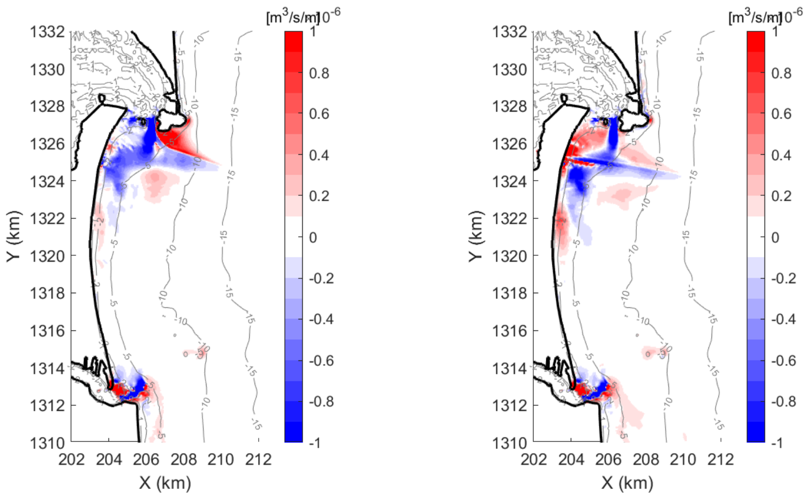

(a) Alternative 1A (b) Alternative 1B

Figure 4.31: Areas with erosion due to the navigation channels

The loss in transport by sedimentation in the channel is compensated by erosion indicated as the blue area of Figure 4.31a. The total sedimentation in the outer channel is 330,000 m3/yr (Table H.1). The blue area stretches from 1327 km to 1323 km. The total erosion in this area is at most the same as the total sedimentation in the channel. At the northern and southern ends of this erosive zone, the erosion is zero, as it builds up and decays in this zone. In the middle of the area, it is assumed to be two times the mean erosion of the area. The coastal regression is computed with Equation H.1. The mean erosion regression in the area is 5.27 m/yr, assuming the full surplus of potential transport is eroded over the blue area. The peak in shoreline regression is then 10.54 m/yr in the middle at 1325 km.
Figure 4.31b shows the relative difference in transport rates for Alternative 1B compared to the original situation. Higher transport rates for Alternative 1B are observed near the coastline. The channel initiates a local increase of sediment transport in the direction of the channel, directly north and south of it. In the blue area south of the channel, a surplus of potential transport leads to local erosion in this area to supply sediment to the longshore component. Directly north and south of the channel, erosion of the shoreline is expected, as the area consists of a sandy beach. South of the channel, the surplus of potential transport may lead to more local erosion. The total sedimentation in the outer channel is 420,000 m^3/yr (Table H.2). Based on the sedimentation volume in the outer channel, the mean erosion depth in the area is computed as 6.61 m/yr. The shoreline can retreat by about 12.22 m/yr until a new equilibrium has been established. Notably, the calculated erosion is initial. In reality, the point of erosion moves slowly south; otherwise the shoreline would rotate. This rotation is not assumable, as the wave climate does not change. The shape of the coastline depends mostly on the direction of the wave climate. There is a blockage of sediment, but this shortage is compensated by coastal regression. The erosion of the coast means it retreats. Additionally, in Figure 4.31, erosion is seen north of the channels. The erosion directly north of the channel is locally induced, which means the surplus of supply south of the channel does not compensate for this fraction of the sedimentation in the channel. For reasons of design safety the extremes are chosen, and the sedimentation due to this erosion is used in the calculations.

5 Discussion

This chapter presents critical reflection on the research. When analysing the hydrodynamics and morphodynamics of the area choices are made of the processes to account for. These choices are assumptions and simplifications to gain reasonable results from the complex model simulation problem. Moreover, every numerical model has limitations in its capacity to simulate reality. In this chapter, the background of the assumptions and simplifications is explained. An elaboration on the limitations from the numerical model and data analysis is also given. Finally, the results are discussed.

5.1 Natural processes

In the study of the area, certain assumptions and simplifications are made, based on the relevant influence of specific hydrodynamic and morphodynamic processes. This section discusses simplifications which could have substantially influenced the results.

5.1.1 Extreme conditions

The hydraulic processes considered in the model are tide, waves, river discharges, and wind. The input parameters for these processes are based on a representative year. According to the hydrodynamic and morphodynamic results, these processes all have a substantial influence. Tide and the wind-induced waves are important in the dry season, and river discharge changes the currents substantially in the wet season. Extreme conditions are not considered. Heavy storms leading to higher wind velocities, waves, and river run-offs are excluded in the model. Hydrodynamic processes induce sediment transport. With higher river run-offs, more mud enters the basin, and with higher wind speeds higher bed shear stresses are induced. Higher bed shear stresses resuspend more sediment. With higher suspended sediment concentrations in the lagoon, more mud can be transported out of tidal inlets. A potential cause of high sedimentation in the lagoon in the model results may be that no extreme weather conditions are considered in the model. When the extreme conditions are modelled, sediment resuspends more often and is thus exported in higher rates out of the lagoon.

Taking extreme conditions into account can also influence the sedimentation of the navigation channels. The area is a muddy environment, and a storm can speed up the refill of the channels substantially. When much sediment is resuspended, larger quantities of mud are transported to the channels. Higher sedimentation rates in the channel can occur.

Notably, extreme hydraulic conditions mostly influence sediment transport quantities. The qualitative processes that this model does represent accurately do not change. As the extreme conditions persist only a few days, a qualitative comparison can be made between the existing situation and the alternatives with reference to a representative year. The ratios of the sediment fluxes do not change, but the quantities resulting from these fluxes do.

5.1.2 Salinity

A natural process that is not accounted for is salinity. Salt water initiates horizontal stratification, as is explained in Section A.3.1. This horizontal stratification induces gravitational circulation and has a strong effect in estuaries with substantial water depth. The depth in the basin is beneath the 5 m, which is too shallow to induce strong gravitational circulation due to horizontal stratification. However, when a 15 m deep channel is dredged through an area of 1 m, the bathymetry is to be changed considerably. In Section 2.3.6 it is analysed the area has substantial horizontal stratification in the wet period. Further, as the discharge increases by the enlarged depth, so will the salinity intrusion. The horizontal stratification moves more land-inward. The import of mud during the dry season is already substantial, increasing with gravitational circulation due to horizontal stratification. The constant flow near the bottom that has a land-inward direction increases. This bottom flow will transport mud constantly land-inward, so mud reaches the port and inner channel not only by the tide but also due to this horizontal stratification. When the depth is enlarged from 5 to 15 m, the sedimentation results in the channel and port can increase by a factor 2.

Aside from the land-inward bottom flow, there is a seaward surface flow of fresh water. The salt water does not mix with this fresh water flow. The mud originating from the river moves as a flume near the surface in the direction of the sea. In the model, much sediment deposits on the riverbed when it enters the lagoon.

These sedimentation rates can thus partially be reduced by including salinity in the model. The calibration factor needed in the wet season would decrease.
Another influence of salinity is floc creation. This floc creation is not depth-dependent, but is more affected by concentration amount, as explained in Section A.2. Flocculation influences the fall velocity of sediment substantially at suspended sediment concentrations of 100 mg/l (Mhashhash et al., 2017). During the dry period, the suspended concentrations are not very high, with 0.3 mg/l according to Table 2.2. There are no data on suspended sediment concentrations in the wet period. Fluvial sediment input is estimated to increase suspended concentrations to 234 mg/l. Flocculation can be influential at these concentrations. Larger quantities deposit inside the lagoon with floc creation, so less mud exits the tidal inlets. Fresh water and salt water do not mix easily, so much of the mud follows the fresh water surface flow directed out of the lagoon. When the salinity intrusion increases due to the dredged channel, the salinity of the basin increases. Floc creation can increase, and larger quantities can deposit in the channel than the model shows. Salinity was not modelled though, due to the long hours of computation time required. To model salinity, multiple vertical layers are included. These layers substantially increase computation time. This study is done in an early phase of the feasibility study of the port. It was not time-efficient to study salinity intrusion.

5.1.3 Sand–mud interactions

Assumptions are also made regarding sediment properties and transport processes. Since this study concentrates on sediment fluxes, one of the main governing processes of interest is the exchange between the bed and the water. It focusses on mud transport for the inner basin and sand transport at the adjacent coast. This division seems to be legitimate, as the hydrodynamics are too mild for large quantities of sand to transport in the inner basin. The area of the port and the channel is only reachable for suspended materials. For the adjacent coast, the bed was composed of sand. Longshore transport consists mostly of heavier materials as mud is carried offshore.
However, the interactions between sand and mud do influence total sediment fluxes. Interaction between water and bed in shallow waters is essential and critical bed shear stress depends on percentage of clay in the bed, as Section A.3.2 explains. The bed composition of the lagoon differs widely along the area. When mud is deposited it can consolidate, if the bed shear stress for erosion is not exceeded, as explained in Section A.2. In this study, these interactions are not considered. The right adjusted parameters for a bed composition consisting of sand and mud did not emerge in the sensitivity analysis. With the addition of a sand fraction in the model, the critical erosion shear stress of the area becomes too high, and no mud is moved in the model. At the same time, removing the sand from the layer, too much mud is suspended in the model. In the dry period, the calibration of the results is based on sediment concentrations. A relative comparison is made with measurements in the Wadden Sea, and a calibration factor of 0.75 is chosen. However, a comparison with another area is arbitrary, as many factors contribute sediment suspension. In the wet season, the calibration factor is based on the fraction of fluvial mud transported directly out of the basin. About 50% of fluvial sediment deposits directly in the basin. The choice is, therefore, made to multiply sedimentation in the inner channel by 1.85 in the wet season. However, in reality not all the sediment that is deposited in the channel during this period is from the fluvial sediment. Sediment that is already present and locally induced by the dredged channel is also multiplied with 1.85. This factor of 1.85 for the total sedimentation during this period can, therefore, be considered too high.
Specific critical processes such as consolidation and fluid mud development are not considered in this study, as the bed composition was not modelled in detail. These processes are important for siltation studies in harbours. When fluid mud occurs, a large flume of sediment can be transported to the navigation channel and deposited there. In the investigation of the bed shear stresses in the area, values no more than 0.3 N/m^2 seem too low to constantly resuspend mud and thus induce fluid mud.
Although by modelling a complex bed composition and thereby reducing the calibration factors mentioned above here are also specific reasons not to do so. By including multiple bed layers, the model becomes more complex, and the computational time of the model increases. The calibration process of the model is also complicated, as more parameters need to be adjusted. For this stage of the project and study modelling, a complex bed composition would be too time-consuming.

5.1.4 Bed-level updates

Next to neglecting sand-mud interactions, bed level updates are not considered. In reality, when sedimentation or erosion occurs, the bathymetry changes, and the flow velocities are influenced. Flow velocities on

its turn influence the sediment transport. For the used model, using bathymetry update results in a more equally diffusive erosion and deposition patterns in the area. From the model results, areas of high erosion and sedimentation rates are observed. These areas exist because no bathymetry update is used in the model. For example, the sedimentation in the navigation channel is in specific sections, while in reality, this would have been more evenly spread along the channel. The decision to spread the deposited sediment by expert judgement is arbitrary.
The inclusion of morphodynamic modelling is relevant when the time scales of interest cover the time scale of morphodynamic development. These time scales are usually from years to decades. The area of interest was considered in dynamic equilibrium, and thus it is computationally more efficient to exclude bed-level updates. However, in constructing a port, the area is put out of its dynamic equilibrium. The results presented show the initial response sedimentation and erosion during a year. When bed-level updates are included, the flow velocities decrease, and less sediment is suspended around the channel after a certain time. The sedimentation numbers from the model result can, therefore, be too high, as there is not bed degradation. Changes in the coastal line, erosion around the channel in the basin and smoother sedimentation in the channel are, however, better modelled with morphodynamic modelling, as these processes take many years.

5.2 Numerical model limitations

In this section, the limitations of the numerical model used are mentioned. Delft3D is a process-based numerical model which simulates nature's physical behaviour with mathematical formulations. In terms of coastal and estuaries, the physics are still not fully understood. The model that simulates the situation cannot truly and correctly represent it. Furthermore, the conditions that occur in nature, including wave heights and quantities of sediment, are not consistent (Lesser, 2009).

5.2.1 2D/3D modelling

Modelling in 2D rather than 3D imparts certain limitations. The choice between the two model types is based on the added accuracy of a 3D model and the increase in computational time. As river discharges, tide, wind, and waves are considered the primary sediment transport drivers in this area that cannot be neglected, computation time is already substantial. It is possible to model the area in 2D with the mentioned processes. Other processes that can be included in 3D modelling add value to the results, but they do not outweigh the increase in computation time.
Some of the effects of estuarine circulation and thus suspended sediment transport depend on varying vertical flow, but these effects are considered small due to the low depths in the tidal basin. However, these processes can add the most value for detail studies of sediment concentrations. The use of a 3D model is relevant for the vertical spreading of suspended materials. As not many measurements are taken, predicting the sediment concentration profile is difficult. A 3D model is challenging to validate, as the measurements are not available. When the profiles of concentrations have a logarithmic shape, 2D models can be used. However, this is mostly the case for the sand-dominated areas. This study concentrates predominantly on sediment fluxes and less on precise suspended sediment concentrations. The modelled area is too large to consider these processes. Therefore, 2D modelling has been preferred.

5.2.2 Grid

An existing grid of the area is used for the model. In the area of interest, the grid resolution is about 50 m, which is low, so the deposition patterns in Figures 4.10b, 4.22b, and 4.23b seem to be in blocks. The grid is set up for large hydrodynamic currents. Furthermore, the grid is rectangular in the area of interest. The resulting numerical computations are diffusive for this reason, and the computations result in sharp deposition and erosion patterns. The grid should be curvilinear in the direction of the currents to compute the sediment-transport directions. At the coast, the grid has a staircase structure. The boundaries of the grid are in wet cells. Due to this staircase structure, longshore transport is constantly interrupted after about 2 km. Near the coast, especially north of El Bluff, areas of high erosion are observed. These places influence quantities in longshore sediment transport. Transects to monitor sediment transport and calibrate the model, can only be placed at specific places, where the coast is not abruptly interrupted by grid cells. The calibration factors needed for the model results are partly due to the selected grid. As the study consists of such a large area, and since detailed results are not critical, making the model more complex by increasing the grid resolution was not considered. Some of these deviations can, however, be solved without increasing resolution and, thus, computation time.

5.2.3 Wave-related transport factor

The wave-related transport factor has a value of 1 in the model, resulting from the sensitivity analysis from Section D.3. This high factor means that sediment movement is sensitive to wave-related energy. When the influence of waves disappears, sediment can stop moving abruptly, as it is less sensitive to other hydrodynamics than the waves. For this study, this means the longshore transport stops moving once it reaches the channel. As the channel is around 15 m deep, the waves do not influence the shear stress of the bed. An overestimation of the deposition in the outer channel results from this lack of influence.

5.3 Results

The discussion of the results is based on the deviations from what is anticipated in the conceptual model. These expectations are based mostly on rules of thumb and expert judgement.

5.3.1 Long-term and short-term sedimentation

The model results show erosion patterns around the channel, as the channel attracts local sediment once it is implemented. When the channel is modelled, the dynamic equilibrium is disturbed, and the channel attracts sediment from these specific areas. The channel is filled with surrounding sediment, and not just from the river. In the model results these short-term effects are only seen in the first half year of the simulations. The sedimentation rates in the wet period, the second-half year, due to locally induced sediment transport are very small compared to the first half year. This is the case for the inner and outer channel. Most of the sediment around the channel originates from the spin-up time of the model. The model required many repetitive simulations before dynamic equilibrium in the model was reached. During these repetitive runs, the sedimentation in specific areas increased. The larger part of this sediment is thus transported away in the first half year. Only the mud fraction from the bed composition with a critical bed shear stress of 0.5 N/m2 stays behind. The critical bed shear stress for this fraction is too high, for these sediment particle to be put into movement. In reality, sedimentation originating from directly around the channel takes longer than a half year and diminishes when the depth around the channel has decreased substantially. Larger quantities of sedimentation due to sediment that originate from areas around the channel probably exist in reality. A calibration factor can be used to increase the sedimentation due to the short-term processes.

At the adjacent coast, the same patterns can be seen for sand. Higher sedimentation quantities than in longshore transport are found in the channel. A fraction of this sediment also originates from the direct surroundings. In the long-term, erosion directly surrounding the channels is diminished. Due to deeper depths due to erosion, the flow velocities decrease, and the top layer of erodible mud and sand runs down. In the long-term, the sedimentation in the channel and port is due to sediment input from outside the system. These inputs include mud originating from the Rio Escondido and sand from longshore transport. One long-term effect is that total sedimentation in the channel and port decreases.

The sedimentation results from this study are thus more focused on long-term sedimentation. The long-term sediment transport are the mud from the Rio Escondido and sand from the longshore transport. The calibration and validation of the model concentrated on these fluxes and thus the model is to be mostly used for the sedimentation quantities from these processes.

Finally, all the sedimentation in the inner channel and port is mud. This high mud fraction arises because the tidal force is not strong enough to transport the sand from the coastal zone directly into the tidal basin. According to Equation A.8, the dynamic equilibrium of the tidal inlet and somewhat land-inward are also determined by the longshore transport of sand. The sand fraction in the model has a diameter of 200 μm and is too heavy to be transported. In reality, the fraction of sand is probably higher for the land-inward channel, as the bed samples from Figure 2.7 show. Nonetheless, the port is located too far for sand to reach.

5.3.2 Qualitative or quantitative

The model is set up first to be used for qualitative comparisons, after which it is also tuned to be used quantitatively. The relative sediment transport fluxes are trusted in terms of time and direction. Nonetheless, the sediment concentrations do seem too high for the area. The model is fit to use qualitatively and to compare the reactions when adding port layouts. However, to use the sedimentation numbers, calibration factors are applied. The outcome of the model is only an approximation of reality, and the comparison was thus relative. The comparative study could indicate the preferred option for the location of the port between Alternative 1A and 1B. The sedimentation numbers were analysed meticulously, however, precise numbers of sediment transport are hard to produce for the stage of the project. Nonetheless, approximate numbers, including a range of accuracy, can be given regarding the sedimentation and erosion volumes. The model, as always, should be used as support to assess the area. With this in mind, it is assumed that the model can be used to compute quantitative numbers with expert judgement to calibrate the results and back them up.

6 Conclusions and recommendations

6.1 Conclusion

In this chapter, the research is concluded by addressing the main research question:

How would the potential locations of a newly constructed port and its channel affect the hydrodynamics and morphodynamics in Bluefields Bay and its adjacent coast, and how would the sediment transport in Bluefields Bay and its adjacent coast affect the potential locations of a port and its channel?

The answer to the main research question is found by answering the sub-questions. By answering these sub-questions, the objective of the research is obtained.

1. What transport processes of sand and mud occur under the influence of the hydrodynamics of the tidal basin, discharging rivers, and adjacent coast?

The dominant hydrodynamic processes differ around the area. The area can be split between the inner tidal basin and adjacent coast. When analysing the past morphological development, the area seems to be in dynamic equilibrium. The meteorology shows a distinct dry and wet period, influencing the dominant hydrodynamic components. There are periods with more extreme wind velocities and even hurricanes. These extreme conditions intensify sediment transport processes.
For the inner tidal basin, the dominant hydraulic process occurring during the dry period is the tide and during the wet period is the river discharge. Because the inner tidal basin has large areas of shallow depths, wind-induced waves influence the bed shear stresses in these areas. The primary transport of sediment consists of mud, as the inner basin has a mild hydrodynamic climate. Residual currents due to the tide are the main drivers, especially in the dry season. The tidal basin has large shallow areas and deep channels, causing it to be flood dominant during the dry period. The river discharge is too low for the residual currents to be ebb dominant. During this period, mud is imported through the tidal inlets because of the flood dominance of the lagoon. These fine sediments are deposited on the shallower areas.
In the wet season, the river begins to add fluvial sediment to the lagoon. The river discharge begins to influence the currents, thereby changing the residual currents to an ebb dominant direction. The mud that is imported in the dry season is exported by both the tidal inlets. A large part of the mud that deposited on the shallow areas in the dry period is transported to the south and exported by the southern inlet. The mud supplied by the Rio Escondido is transported directly to the northern inlet and exported from there. A small fraction goes southward along the shallower areas of the basin and exported by the southern inlet.
At the coast, the dominant hydrodynamic process driving sediment transport is the swell wave climate. The median wave climate is around 1 m all year. The direction from the waves is predominantly east-northeast. Therefore, longshore transport has a southward directed current. During different periods in the year, storms occur, inducing more extreme waves. Due to the swell wave climate, fine sediment is transported offshore, while large sand fractions move onshore due to cross-shore transport.

2. How can an efficient numerical model compute the dominant transport processes of sand and mud in the area of interest?

The main hydrodynamic processes that influence sediment transport are river discharge, tide, waves, and wind. All these components must be modelled to assess the entire area. The modelling of these components is possible with the process-based model Delft3D. Delft3D-FLOW and Delft3D-WAVE must be coupled, as at the coast waves are of importance and in the lagoon wind-induced waves are of influence. As the depths in the tidal basin are shallow, gravitational circulation and stratification by salinity are not of substantial importance. Therefore, it is possible to model the area as a 2D model. After implementing the navigation channel in the model, the depths do increase substantial and gravitational circulation due to stratification by salinity can become of importance. However, it should be noted that a 3D model best assesses mud transport. As the computational grid size, the number of hydraulic components, and the period assessed are all substantial; it is not computationally efficient to model in 3D. In the area of interest, the grid size must have a relatively high resolution. The model is set-up to assess the large sediment fluxes and contains a large area. The level of detail in sediment transport is, therefore, qualitative.

The essential sediment fractions for transport is a mud fraction from the Rio Escondido for the inner basin and a sand fraction for the longshore transport. A bed composition of multiple fractions is preferred, as the sand-mud interactions are of importance when analysing the bed composition.
The data available for the area is scarce. Therefore multiple sensitivity analysis have to been done to find acceptable sediment transport patterns. The model can be calibrated and validated by analysing the large sediment fluxes in the model.
Because the area is in morphodynamic equilibrium, and the relative sediment fluxes are of importance on a large-scale, bed-level update is not necessary. Besides this, a comparison is made between the sedimentation in the port alternatives, making the bed-level updates less critical. However, a future port and its channel do disturb the dynamic equilibrium. To analyses the morphodynamic behaviour over a more extended period, it is therefore advisable to include bed-level updates.

3. What are the dominant hydrodynamics and dominant transport patterns of sand and mud transport in the area of interest?

The coast and the lagoon are in dynamic equilibrium on a large-scale basis, according to past morphological development. In the dry period, there is a total net import of 0.25 Mm^3 for both inlets. The main hydrodynamic process of sediment transport is the tide during this period. The residual currents show a southward flood dominant direction. The mud is transported to the south when it enters the northern tidal inlet. The wind-induced waves resuspend sediment on the riverbanks that deposit there in the wet period. However, the residual currents of a maximum of 0.1 m/s in the shallower areas indicate that the sediment transport is small.
In the wet period, the river discharge increases and counteracts the flow of the tide. The flow velocity during flood decreases, and the ebb directed flow velocity increases. Because this change in flow circulation, the northern area is pushed into ebb dominance. From suspended sediment concentrations at measuring stations, it is observed that most of the sediment transportation in the basin is due to the tide. Low concentrations are found at the stations at the riverbank. The fluvial mud follows the river channel through the basin and is exported directly. The fluvial sediment input of the river is about 2.5 to 3.44 million t/yr. The river also increases the southward directed currents in the shallower areas. Mud that deposits in the shallower areas during the dry period is transported to the southern inlet. In the wet period, there is a net export of mud through the northern and southern inlet. Because the mud of the river and the sediment that is imported in the dry season are exported in the wet season, a total export quantity of 0.75 Mm^3 is found for both inlets.
At the coast, the longshore transport is moderate, with a quantity of about 150,000 m^3/yr. This quantity is explainable for a moderate wave climate with a mean significant wave height of 1 m. A broad zone of longshore transport is observed in front of the barrier island. North of El Bluff, the zone of littoral drift is much smaller, as the bed has a steeper gradient. Near the northern tidal inlet, the longshore transport is small, as a split shelters it and as wave refraction occurs. The longshore transport originating from north of El Bluff is partly transported directly to the sea and partly to the barrier island. Halfway, the island the transport rates are about as high as at El Bluff.

4. What would be the dominant hydrodynamics in the area of interest after the potential constructions of the port and its structures?

When the port and its navigation channel are constructed, the hydrodynamics change since the directions of the hydraulic processes are altered. By implementing Alternative 1A, the tidal flow has less resistance in the opening at El Bluff. A larger discharge amplitude enters the basin. The tidal flow follows the navigation channel to the west and subsequently south-west when it enters the basin. The tidal wave needs less effort to reach the areas south of the newly dredged channel, compared to the existing situation. Stronger currents are observed in these areas, and the bed shear stresses are increased. South of the channel the area is still dominated by the tide and remains flood dominant. However, the velocities during ebb have increased and the flood dominance is weakened.
When the tidal flow enters the northern inlet and follows the dredged channel, it has a less strong current to the north. Subsequently, the river discharge has less resistance of the tidal flow now and thus induces a stronger southward current north of the channel. The dominant hydraulic forcing factor in the northern area becomes the river discharge. The ebb dominance increases compared to the existing situation north of the channel.
By constructing Alternative 1B, a new opening is created through the barrier island. The flow velocities and discharge have decreased in the northern inlet, as the tidal wave also flows through the new opening.

The river discharge becomes the dominant forcing factor in the north of the basin, as it has less resistance from the tidal flow. The northern part in Alternative 1B is even more ebb dominant than Alternative 1A. The residual currents are in the direction of the newly dredged channel.
In the areas north and south of the newly dredged channel, the velocities of the tidal currents have increased compared to the existing situation. The tidal flow reaches these areas with less resistance in the new situation. The bed shear stresses have also increased in these areas. Both north and south of the channel the residual currents are ebb dominant now, while the currents south of the channel were flood dominant in the existing situation.
At the southern inlet, the discharge does not change when the alternatives are constructed. The flow velocity does decrease at the inlet for both the cases. This decrease in flow velocity indicates that sedimentation takes place after the construction of both the cases. Additionally, the southward directed residual currents halfway the lagoon have decreased. The discharge of the Rio Escondido follows the dredged channel to the northern inlet once the flow reaches it. In the existing situation, a larger fraction of the river discharge exits through the southern inlet. The residual currents south of the channel are thus forced less in ebb dominance for the new situations. The area around the southern inlets is less ebb dominant, with some areas even becoming flood dominant during the wet period.

5. What would be the dominant sand and mud transport patterns in the area of interest after the potential constructions of the port and its structures?

When Alternative 1A is implemented, the lagoon becomes more ebb dominant in the northern part and less flood dominant south of the channel compared to the existing situation. The decrease in mud import is 0.01 Mm^3 in the dry season. The tidal flow has less energy to carry mud from outside the basin into the system, as the velocities at the entrances have decreased. Moreover, the navigation channel catches the mud outside of the basin before it gets carried in. The export of mud through the northern inlet has decreased with 0.06 Mm^3 in the wet season. However, for a more ebb dominant system, it is expected that the area exports more mud. This increase in export is not the case, since the channel traps the mud. The tidal flow generates higher bed shear stresses in the areas around the channel than there were for the existing situation, putting sediment into movement because.
At the southern inlet, almost no mud is imported during the dry period. The residual currents on the shallower areas are less flood dominant for the new situation than for the existing situation. The residual current in the southern half of the lagoon does not have the extra forcing of the river discharge in the ebb direction anymore. The residual currents direction become less strong southward, and the southern inlet starts to import mud in the wet period. This import has an amount of 0.52 Mm^3. Less sediment also reaches the southern inlet as the sediment flowing southward deposits in the channel.
When Alternative 1B is implemented, the import through the northern inlets decreases substantially, because a new opening is created through the barrier island. Mud is now imported for the biggest part by the new opening. When the mud is imported it deposits directly in the channel, as the residual currents around the channel are ebb dominant. The mud that enters through the northern inlet begins to deposit in the ebb channel. In the wet season, the import through the northern inlet continues. The residual currents inside the lagoon are directed to the newly dredged channel. The system imports mud through the northern inlet and subsequently transports it to the navigation channel. The mud supply in the wet season is higher than the amount of sedimentation in the channel. This means the mud deposits in other areas inside the lagoon as the hydrodynamics have changed due to the new opening. The tidal flow is not capable of transporting the same amount of mud in the northern area. There is sedimentation in the new opening, so this opening will be closed in the future, restoring the dynamic equilibrium of the lagoon. The southern inlet shows the same import and export pattern as for Alternative 1A.
Both alternatives catch all the longshore transport. For Alternative 1B the sedimentation of sand is higher, as the channel has a longer trajectory in the breaker zone. In this area with strong morphodynamic processes, the channel is sooner pushed in its dynamic equilibrium.
The total sedimentation of mud in the inner channel and port is 0.32 Mm^3/yr for Alternative 1A. About 50% of the net import of mud in the inner basin, which is 0.50 Mm^3/yr deposits in the port and the dredged channel. The sedimentation due to locally induced sediment transport is 0.09 Mm^3/yr and is 25% of the total sedimentation. About 85% of the sedimentation of mud in the outer channel is due to locally induced transport. Most of the sediment that exits through the northern inlets leaves the area before it deposits in the channel. The outer channel catches all the longshore transport, which is 0.15 Mm^3/yr. Local sand also deposits in the channel in a quantity of 0.02 Mm^3/yr.
For Alternative 1B the inner basin has a higher import quantity than for Alternative 1A, 1.21 Mm^3/yr and 0.50 Mm^3/yr respectively. However, the sedimentation quantity of 0.26 Mm^3/yr is smaller than the quan-

tity of 0.32 Mm^3/yr for Alternative 1A. The tide is able to flush a large quantity out the basin, especially in the wet season. The sedimentation of mud in the outer channel exists out of 80% due to locally induced sand. As Alternative 1B has a longer stretch in the breaker zone, it accumulates more sediment, namely 0.25 Mm^3/yr, in comparison with Alternative 1A, namely 0.17 Mm^3/yr.
After converting the sedimentation quantities with a dry bulk density formula the total to be dredged sedimentation for Alternative 1A is 2.79 Mm^3/yr against 3.44 Mm^3/yr for Alternative 1B. This difference is mainly because the outer channel of Alternative 1B catches more sediment. The outer channel of Alternative 1B takes about 6 years to fill up and for the outer channel of Alternative 1A this period is about 9 years. The total sedimentation for the inner channel is, however, smaller for Alternative 1B with a quantity of 0.94 Mm^3/yr against a total of 1.22 Mm^3/yr for Alternative 1A. For both alternatives, coastal regression can take place north and south of the channel, as a fraction of the sedimentation originates from the areas around the channel. Downstream of the coast, erosion can take place throughout 5 km for both alternatives. This coastal retreat is in the order of 10 m/yr for Alternative 1A and 12 m/yr for Alternative 1B.
Based on the sedimentation quantities from the results, it is more beneficial to construct Alternative 1A. There is a difference in yearly total sedimentation of 0.65 Mm^3/yr. From the section study, the sedimentation in specific sections is higher for Alternative 1B than for Alternative 1A, which means the channel for Alternative 1B must be dredged more frequently. For both alternatives, coastal regression of about 11 m is large. It may be recommended to release the dredged sediment from the channel into the areas of coastal regression.

6.2 Recommendations

This section offers recommendations for further study to quantify the results in more detail. The applied model is thought to be detailed enough to study the large sediment fluxes and to make comparison possible between different alternatives once modelled. Nonetheless, recommendations are provided to increase applicability and more detail . Additionally, reliability can be improved to get smaller compensation factors when using quantitative results.

- Some issues arise when the bed composition is determined. The bed composition substantially affects the model result, so the model can be improved by fixing this. In the model, the interaction between sand and mud are neglected. These interactions can be modelled by constructing multiple sediment fractions and bed layers. A sensitivity analysis of this component is recommended. However, attention should be paid to keep the model time efficient. Aside from improving bed composition, a further sensitivity analysis can improve the results for the sediment fluxes and sediment concentrations. The sediment concentrations are considered too high, partly due to the bed composition.
- When bed composition is improved, bed-level updating can be added to the model. The current results show mostly initial erosion and sedimentation. The future influence of the morphological response of the port and its structures can be derived more accurately. The future development and the associated time scale can then be derived in more detail. Additionally, the short-term sedimentation in the channel due to locally induced sediment transport can better be analysed. The results for these processes are probably too low in this model.
- Some crucial processes of sediment transport that have a considerable influence on the port can be investigated. Fluid mud is not considered in this study. Fluid mud is, however, known to have a substantive impact on dredging strategies. Although the bed shear stresses in the area do not seem high enough for fluid mud to occur, this possibility should be examined .
- No extreme conditions are considered. Mud transport is highly affected by extreme river run-off and wind-induced waves in the shallow areas. With heavy hurricane storms, the bathymetry can be changed considerably, as a large fraction of the bed composition is mud. Sediment and especially mud, with its low critical erosion stresses, are sensitive to extreme conditions. As the model is already in dynamic equilibrium, only the hydraulic input must be changed to simulate extreme events.
- The effects of salinity intrusion on the area can be studied in greater depth. Salinity intrusion can substantially affect horizontal stratification when the channel is deepened. Sedimentation through this effect has to be studied, as sediment is pushed into the channel due to this process. It might also be interesting to investigate salinity intrusion for environmental reasons. The assessment of salt intrusion can be used on different aspects of the ecological response within the tidal basin. For this purpose, model calibration must be improved, as the obtained results are not yet detailed enough.

- The grid can be updated. In the area of interest, the grid seemed to be too coarse. For the deposition of mud, the areas are not alternating each other fluently. Blocks of sedimentation and erosion are observed. Moreover, as the grid shows a staircase structure at locations with wet cells, sediment tends to stay behind grid cells and cannot be carried away by the flow. These blockages show interruptions in the gradients of the sediment transport. This improvement is mostly for quantitative results.
- The validation of the model is based mainly on observing the phenomenological results of the processes and on expert judgement. This method is used because the field data of the area is scarce. More data samples on the bed composition and suspended sediment concentrations can be useful. Further, only the data from the dry period is available. Data measurements of the wet period can help to assess this period better.

References

Alkyon. Feasibility study for increasing the cargo flow through El Rama Port. Technical report, Alkyon and Damen Shipyards Gorinchem and Van Oord, 2004.

J. Battjes and R. J. Labeur. *Unsteady Flow in Open Channels*. Cambridge University Press, 2017.

J. Bosboom and M. J. F. Stive. *Coastal Dynamics I Lecture notes CIE4305*. Delft Academic Press, 2015.

C. L. Brenes and E. Castillo. Hidrografia de la bahia de Bluefields, 1999.

C. L. Brenes, A. Hernandez, and D. Ballestero. Flushing time in Perlas Lagoon and Bluefields bay, Nicaragua. *Invest. Mar., Valparaíso*, 2007a.

C. L. Brenes, A. Hernandez, and D. Ballestero. Estructura hidrográfica de la Bahía de Bluefields, Nicaragua. *Ciencia y Tecnología*, 2007b.

H. Burchard and H. Baumert. The formation of estuarine turbidity maxima due to density effects in the salt wedge. a hydrodynamic process study. *Physical Oceanography*, 1998.

R. W. G. Carter. *Coastal environments: An introduction of physical, ecological and cultural systems of coastlines*. Academic Press, Londen, Londen, 1988.

B. De Vries, P. Dankers, and J. Vroom. Slib in de waddenzee. Technical report, Royal HaskoningDHV and Deltares and Arcadis, 2018.

Deltares. *3D/2D modelling suite for integral water solutions; Delft3D*, 2014.

G. D. Egbert and Y. E. Svetlana. Efficient inverse modeling of barotropic ocean tides. *Journal of Atmospheric and Oceanic Technology*, 2002.

F. F. Escoffier. The stability of tidal inlets. *Shore and Beach*, 1940.

S. Fagherazzi and P. L. Wiberg. Importance of wind conditions, fetch, and water levels on wave-generated shear stresses in shallow intertidal basins. *Journal of Geophysical Research*, 2009.

Google Earth, 2020. Retrieved from Google Earth: https://earth.google.com/ Accessed: 2020-02-15.

L. Guo. *Modeling estuarine morphodynamics under combined river and tidal forcing*. PhD thesis, Delft University of Technology, 2014.

A. Hastie, R. Tibshirani, and J. Friedman. *The Elements of Statistical Learning*. Springer, 2008.

R. G. W. Hisgen and R. W. P. M. Laane. *Geheim van het Getij*. Sdu Uitgevers bv, Den Haag, The Netherlands, 2004.

L. H. Holthuijsen. *Waves in Oceanic and Coastal Waters*. Cambridge University Press, 2007.

C. Jiang, J. Li, and H. E. de Swart. Effects of navigational works on morphological changes in the bar area of the Yangtze Estuary. *Geomorphology*, 2011.

R. Jiménez Van Patten. Evaluación de la metodología empleada en Costa Rica para la determinación del transporte de sedimentos en los ríos. Technical report, Universidad de Costa Rica. Facultad de Ingeniería. Escuela de Ingeniería Civil, 1975.

R. B. Krone. Flume studies of the transport of sediment in estuarial shoaling processes; Final report. *Journal of the Hydraulics Division*, 1965.

G. R. Lesser. *An Approach to Medium-term Coastal Morphological Modelling*. PhD thesis, Delft University of Technology, 2009.

G. R. Lesser, J. A. Roelvink, J. A. T. M. Van Kester, and S. G. S. Development and validation of a three-dimensional morphological model. *Coastal Engineering*, 2004.

W. M. Lewis Jr and J. F. Saunders III. Concentration and transport of dissolved and suspended substances in the Orinoco River. *Biogeochemistry*, 1985.

LIVSET. Atlantic Port and highway study. *LIVSET*, 1963.

K. Mangor. *Shoreline Management Guidelines*. DHI, Denmark, 2004.

A. Mhashhash, B. Bockelmann-Evans, and S. Pan. Effect of hydrodynamics factors on sediment flocculation processes in estuaries. *Physical and Ecological aspects of mobile sediments*, 2017.

J. Mil-Homens. *Longhshore Sediment Transport; Bulk Formulas and Process Based Models*. PhD thesis, Delft University of Technology, 2016.

S. Muis, M. Verlaan, H. Winsemius, J. Aerts, and P. Ward. A global reanalysis of storm surges and extreme sea levels. *Nature Communications*, 2016.

E. Partheniades. Erosion and deposition of cohesive soils. *Journal of the Hydraulics Division*, 1965.

J. Perez, M. Menendez, and I. J. Losada. GOW2: A global wave hindcast for coastal applications. *Coastal Engineering*, 2017.

J. F. Richardson and W. N. Zaki. Edimentation and fluidization: Part I. *I. Trans. Institution of Chemical Engineers*, 1954.

S. Saha, S. Moorthi, X. Wu, J. Wang, S. Nadiga, P. Tripp, and E. Becker. The NCEP climate forecast system version 2. *Journal of Climate*, 2014.

M. L. Schwartz. *Encyclopedia of Coastal Science*. Springer, 2005.

US Army Corps of Engineers, 2020. Retrieved from USACE Digital Library: https://usace.contentdm.oclc.org/ Accessed: 2020-09-20.

M. Van der Wegen and J. A. Roelvink. Reproduction of estuarine bathymetry by means of a process-based model: Western Scheldt case study, the Netherlands. *Geomorphology*, 2012.

L. Van Rijn, D. Walstra, B. Grasmeijer, J. Sutherland, S. Pan, and J. Sierra. The predictability of cross-shore bed evolution of sandy beaches at the stim scale of storms and seasons using process-based profile models. *Coastal Engineering*, 2003.

L. C. Van Rijn. *Principles of Sediment Transport in Rivers, Estuaries and Coastal Seas*. Aqua Publications, 1993.

L. C. Van Rijn. *Principles of sedimentation and erosion engineering in rivers, estuaries and coastal seas*. Aqua Publications, 2006.

J. Van Veen, A. J. F. Van der Spek, M. Stive, and T. J. Zitman. Ebb and Flood Channel Systems in the Netherlands Tidal Waters. *Journal of Coastal Research*, 2015.

A. Verruijt. *An Introduction to Soil Dynamics*. Springer Netherlands, 2010.

C. K. Wentworth. A Scale of Grade and Class Terms for Clastic Sediments. *The Journal of Geology*, 1922.

J. Winterwerp and B. v. Prooijen. *Sediment Dynamics Lecture Notes*. Delft Academic Press, 2017.

J. C. Winterwerp. The physical analyses of muddy sedimentation processes. *Elsevier*, 2011.

J. C. Winterwerp and W. G. M. Van Kesteren. *Introduction to the Physics of Cohesive Sediment Dynamics in the Marine Environment*. Elsevier Science, 2004.

L. Wright and A. Short. Morphodynamics variability of surf zones and beaches: a synthesis. *Marine Geology*, 1984.

L. Zuo. *Modelling and Analysis of Fine Sediment Transport in Wave-current Bottom Boundary Layer*. PhD thesis, Delft University of Technology, 2018.

C. Álvarez Díaz, E. G. Alonso, C. P. S. J. R. Gómez, and B. T. Vega. Aplicación de un modelo logístico triparamétrico a la estimación de caudales diarios en la cuenca del río Nam Ngum (Laos). *IV Jornadas de Ingeniería del Agua*, 2015.

List of Figures

List of Tables

A Theoretical Background

The theoretical background that is important for the morphodynamics of the area is elaborated on in this chapter. Firstly, the general mechanisms of hydrodynamics, sediment, and their interaction are presented. After this, the specific dynamics for a tidal basin and its adjacent coast are explained. Finally, the impact of human interventions on coastal dynamics is analysed.

A.1 Hydrodynamics

The primary hydrodynamics that induces sediment transport are focussed on in this section. For the study area, the hydrodynamics are river discharges, tides, and waves. For each of these physical processes, an evaluation is given how they contribute to the morphology in the area.

A.1.1 Waves

Waves initiate sediment transport through interaction with the seabed. When waves move in the direction of the shore, they deform due to this interaction. Friction occurs due to these interactions. The influence of friction starts when the water depth is about 0.5 of the wavelength by a rule of thumb. The friction also influences the energy balance of the wave energy, which is represented in Equation A.1 (Holthuijsen, 2007).

$$E = \frac{1}{8}\rho g H_{rms}^2 \tag{A.1}$$

E	$=$	Wave energy	$[J/m^2]$
H_{rms}	$=$	Significant wave height	$[m]$
g	$=$	Gravity	$[m/s^2]$
ρ	$=$	Water density	$[kg/m^3]$

The wave energy (E) is dependent on the significant wave height (H_{rms}), specific weight of the water (ρ), and gravity (g). When a wave, with its energy, propagates with a group velocity, it has an energy flux in the direction of propagation. The amount of energy it loses over a distance x is the wave dissipation. This is shown in Equation A.2 (Holthuijsen, 2007).

$$D_f = \frac{d(c_g \dot{E})}{dx} \tag{A.2}$$

D_f	$=$	Wave dissipation	$[N/ms]$
c_g	$=$	Group velocity	$[m/s]$
E	$=$	Wave energy	$[J/m^2]$
x	$=$	Distance	$[m]$

The wave dissipation (D_f) is dependent on the group velocity (c_g), wave energy (E), and distance (x). From this dissipation eventually, sediment transport is induced, which will be further elaborated on in Section A.2. Wave dissipation primarily happens through wave breaking, which on its turn is caused by either steepness or depth- induced wave breaking (Holthuijsen, 2007).
For wave dissipation, the depth- induced wave breaking is the essential factor for sediment transport. This breaking is initiated at a ratio of $\frac{d}{H}$ of 0.8 of the wave as a rule of thumb. When waves break bed shear stresses occur, which are the main drivers for the movement of sediment (Holthuijsen, 2007).
Besides the above-described mechanisms bed shear stresses also occur due to the orbital flow beneath the surface. Equation A.3 shows that bed shear stresses (t_w) are dependent on the bottom friction (f_w) and wave orbital velocity (u_0) and specific density of water (ρ) (Holthuijsen, 2007).

$$\tau_w = 0.5\rho f_w u_0^2 \tag{A.3}$$

τ_w	=	Bed shear stresses	$[N/m^2]$
ρ	=	Water density	$[kg/m^3]$
f_w	=	Bottom friction	$[-]$
u_0	=	Wave orbital velocity	$[m/s]$

The orbital flow velocity influences the bed shear stress as follows. The area of the flow is called the boundary layer, and the bed roughness causes turbulent flow in this layer. Under a wave, the flow constantly reverses in an orbital motion. This flow reversal initiates velocity gradients in the boundary layer, which induces stresses. Due to this, turbulence occurs, and energy is dissipated, stirring up the sediment. The thickness of the boundary layer is time-dependent, and so the wave period influences the magnitude of the bed shear stresses (Bosboom and Stive, 2015).
Outside of the breaker zone, additional onshore sediment transport occurs inside the boundary layer. This transport is through Longuet-Higgens flow, which is an averaged non-zero flow and manifests itself next to the oscillating flow (Bosboom and Stive, 2015).

A.1.2 Tides

The sediment transport of the adjacent coast is mainly dependent on waves. In the area of the tidal basin that is covered by the barrier island, other hydrodynamics are dominant forcing in the sediment transport. For this area, the tide in combination with the river discharge are the primary drivers of sediment transport.
When a tide enters a tidal basin, deformation of the tidal wave occurs. This deformation is due to friction and varying basin geometry and topography. When the tidal wave enters the basin, the geometry becomes less wide, increasing the amplitude of the tidal wave. Besides this, the basin has areas with smaller depth, where the friction magnitude differs. Loss of energy occurs due to friction, making the tidal wave amplitude smaller. Next to that, the water depths and geometry are different for flood and ebb. Through these differences, the tidal wave becomes asymmetrical. Asymmetric means the flow velocity and slack duration are different on locations during flood and ebb. Figure A.1 represents this process. It shows that the flow velocity during flood is higher than during ebb, which is called vertical asymmetry. Besides this, the slack duration, flow reversal from flood to ebb, after flood is larger than after ebb, which is called horizontal asymmetry (Bosboom and Stive, 2015).

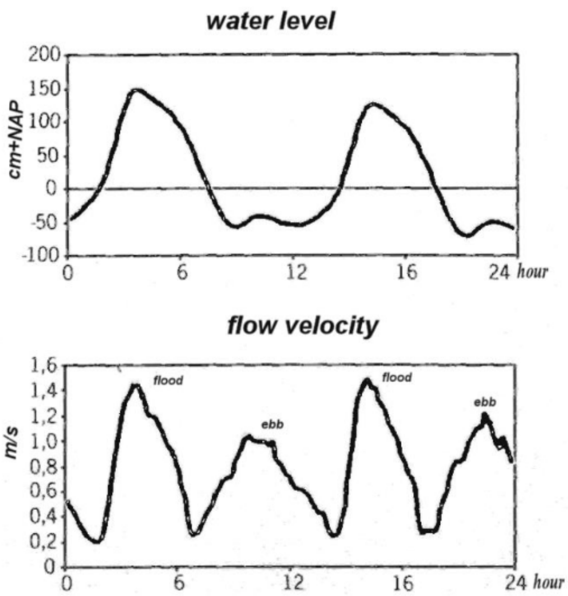

Figure A.1: Water level and current velocity measured at the entrance of the Rotterdam harbour (Hisgen and Laane, 2004)

Tides contribute to sediment transport through these tidal asymmetries. The asymmetry can be categorised in horizontal asymmetry and vertical asymmetry.
Vertical asymmetry indicates that the rising period of the tide is faster or shorter than the falling period.

When the rising period is faster, the flood velocity exceeds the ebb velocity, and a residual of sediment is transported in the flood direction. When the falling stage is faster, the ebb velocity is higher than the flood velocity and a residual of sediment is transported in the ebb direction. The vertical asymmetry is dominant for medium to coarse sediment (Bosboom and Stive, 2015).
With horizontal asymmetry, the slack durations are not equal. The slack duration is the duration between the rising and falling stages. For example, if the high-water slack, which is preceding ebb, is longer than the low-water slack, which is before a flood, more sedimentation occurs after a flood. Horizontal asymmetry is essential for net residual transport of fine sediments (Bosboom and Stive, 2015).

A.1.3 River discharge

Rivers transport sediment into the system, to be described in the next section. The influence of the river discharge on the morphology of the estuary and subsequentially the tidal basins is subject to its relative magnitude compared to the tide. Through the river discharge, an extra ebb directed velocity is present (Guo, 2014). Next to that, the river discharges damp through friction with the tidal wave. Finally, due to the fresh water flow, the saline water is pushed back. At the meeting point between fresh water and salt water, gravitational circulation patterns will occur.

A.2 Sediment

The transport of sediment depends the most on hydrodynamic conditions and sediment properties. In this section is elaborated the different kinds of sediment fractions and how they are transported.

A.2.1 Sediment fractions

Coastal zones contain different kinds of sediments. When looking at sizes, four types can be distinguished: gravel, sand, silt, and clay. Gravel and sand classify as non-cohesive sediments and silt and clay as cohesive (Winterwerp and Van Kesteren, 2004). Sediment transportation depends partly on this classification (Van Rijn, 1993). Cohesive soils are mainly transported in suspended load. They consolidate slowly, and the surface erodes in aggregates. In salt water, cohesive sediments tend to form sediment flocs, with a degree of flocculation dependent on the concentration of salinity in the medium. These flocs, much larger than individual sediment particles, have a higher sedimentation rate. Non-cohesive soils are transported mainly in bedload transport. They consolidate instantaneously, and the surface erodes particle by particle (Zuo, 2018).

A.2.2 Transport

For bedload transport, the sediment particles stay in contact with the bed, and transportation is mainly dependent on bed shear stresses. If the bed shear stress or the bed shear velocity exceeds a specific value, transport occurs. Currents and waves fuel this kind of stress. The equations of bed shear stress exist of bed shear stress due to currents and waves and sometimes a term for the initiation of motion. Besides this, the equations are time-averaged or instantaneous, dependent on whether inertia plays a role. Inertia is dependent on particle size (Bosboom and Stive, 2015). When the shear stresses are high enough, particles close at the bed move in multiple layers. The sediment moves as a sheet over the immovable bed, instead of jumping and rolling the layer of sediment. This movement is called sheet-flow transport.
Fine sediments are mostly transported as suspended load transport; the particles are moved higher up in the water column. The particles stay in the water column and move with the speed of the flow. Suspended sediment transport is mostly modelled as a product of the sediment concentration c and the horizontal velocity u. Turbulence is responsible for the upward flux of sediment and the fall velocity for the downward flux (Bosboom and Stive, 2015). As stated in Section A.1, the vertical asymmetry is essential for the movement of suspended sediment.

Erosion and deposition

The interaction with the bed and flow is conceptualised with the difference between the erosion (E) and deposition (D). Sedimentation occurs when the gross flux of deposition exceeds the flux of erosion. The erosion of fine sediments is dependent on the threshold for incipient motion (Winterwerp and Van Kesteren, 2004). In this case, the Partheniades formula is regularly applied (Partheniades, 1965):

$$E = M\frac{(\tau_b - \tau_e)}{\tau_e} \tag{A.4}$$

E	$=$	Erosion flux	$[kg/m^2s^1]$
M	$=$	Erosion flux parameter	$[kg/m^2s^1]$
τb	$=$	Bed shear stress	$[N/m^2]$
τ_e	$=$	Critical shear stress threshold for erosion	$[N/m^2]$

In this formula the erosion rate (E) is dependent on the erosion rate parameter (M), the bed shear stress (τb), and critical shear stress threshold for erosion (τ_e)
The deposition of fine sediment is dependent on the sediment concentration and the settling velocity (Winterwerp and Van Kesteren, 2004). The formula of Krone is used for deposition (Krone, 1965):

$$-D = -W_s c_b(1 - \frac{\tau_b}{\tau_d}) \tag{A.5}$$

D	$=$	Deposition flux	$[kg/m^2s^1]$
W_s	$=$	Settling velocity	$[m/s]$
c_b	$=$	Suspended sediment concentration	$[kg/m^3]$
τ_b	$=$	Bed shear stress	$[N/m^2]$
τ_d	$=$	Critical shear stress threshold for deposition	$[N/m^2]$

The deposition rate (D) is dependent on the settling velocity (W_s), the suspended sediment concentration (c_b), the bed shear stress (τ_b), and the critical shear stress threshold for deposition (τ_d).
Through turbulent mixing, sediment is brought up in suspension, while the settling flux is responsible for deposition. This settling velocity can be described with Stokes' law. In Stokes' law (Equation A.6), the settling velocity is dependent on the grain size diameter (D), the specific density of the sediment (ρ_s) and water (ρ_w), the gravity (g), and the viscosity of the fluid (μ). The gravity forms an equilibrium with hydraulic drag forces.

$$W_s = \frac{(\rho_s - \rho_w)gD^2}{18\mu} \tag{A.6}$$

W_s	$=$	Settling velocity	$[m/s]$
ρ_s	$=$	Sediment density	$[kg/m^3]$
ρ_w	$=$	Water density	$[kg/m^3]$
g	$=$	Gravity	$[m/s^2]$
D	$=$	Grain size diameter	$[m]$
μ	$=$	Viscosity of the fluid	$[m^2/s]$

During the settling process, floc sizes grow due to aggregation, which indicates higher settling velocities. With increasing sediment concentrations towards the bed, the falling flocs start to hinder each other, and the settling velocity decreases, which is called hindered settling. The settling process of flocs is characterised by an initial increase of the settling velocity due to flocculation. After this initial stage, the velocity decreases because of hindered settling. Consequently, the settling velocity of mud flocs varies in time (Winterwerp, 2011).
When mud is deposited, it can consolidate, if the bed shear stress for erosion is not exceeded. The bed volume will decrease due to the gravitational forces. Water is pressed out of the pore volumes. Eventually, the internal strength increases due to compression (Verruijt, 2010).
The critical bed shear stress of the whole bed also depends on the percentage of clay in the bed. The bed can act cohesively or non-cohesively as a whole. When the clay content is less than $5-10\%$, the bottom acts non-cohesively. The mud and sand erode independent from each other. If the percentage of clay is above this threshold, the bed behaves cohesively. The sand and mud erode simultaneously. Because in the cohesive case, the critical bed stress for erosion is different from that of sedimentation, the reaction of the bed is essential. The difference in erosion and sedimentation is the result of a sizeable binding force between particles. The bed shear stress for sedimentation is lower than that for erosion. For a range of bed shear stresses, this means that there are no exchanges with the bed (Bosboom and Stive, 2015).

A.3 Tidal basin morphodynamics

In this section, the morphodynamics in the tidal basin is described. Firstly, the hydrodynamics that work as forcing factors of the morphodynamics is explained. Hydrodynamics influences how to characterise a tidal basin. After this, the sediment transport due to the hydrodynamics is explained.

A.3.1 Hydrodynamics

Dependent on the type of tidal basin, different hydrodynamics take place inside the basin. A tidal basin that is sheltered by, for instance, barrier islands, is protected against wave influences. For estuaries, the fresh water that flows into the basin initiates hydraulic dynamics which are absent when there is only salt water. Bosboom and Stive (2015) distinguish a different kind of tidal basins. These differ mainly in terms of the importance of the fresh water run-off and the characteristics of the entrance. Table A.1 shows this distinction.

Environment	Distinctive attributes
Tidal bays	High level of wave energy dissipation; little fresh water run-off
Tidal lagoons	Waves excluded by barriers; tidal flows via passes; infilling wetlands; little fresh water run-off
Estuaries	Waves possibly excluded by barriers or sand shoals; high fresh water run-off

Table A.1: Distinctive attributes of tidal environments (Carter, 1988)

As stated in the previous sections, tides cause sediment transport due to tidal asymmetries and other residual currents. When the tide enters the basin, they are deformed by bottom friction and other non-linear effects due to the geometry of the basin. These deformations strengthen the asymmetries that are associated with sediment transport.
In the estuary, a transit region between salt water and fresh water is present with different water densities which form layers that act as barriers to water mixing stratification occurs. Two types of stratification can be distinguished, namely horizontal and vertical stratification. Horizontal stratifications induce gravitational circulation when the density of salt water is higher than the density of fresh water. As a result of this density difference, the pressure on the seaside is higher than on the riverside (Winterwerp and Prooijen, 2017). A slope in the water level compensates this. The flow is presented in Figure A.2. The effect of this gravitational circulation depends on the mixing conditions of the estuary and the water depth. In estuaries with significant water depth, the gravitational circulation is more extensive due to the vertical distance between the flows. The effects are also substantial in partly stratified water.

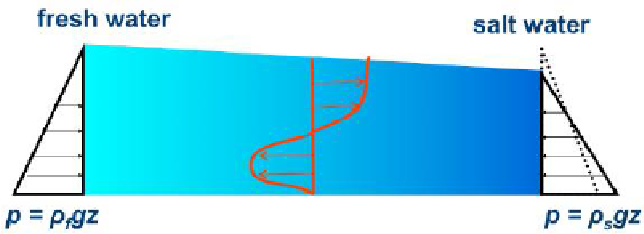

Figure A.2: Horizontal stratification (Winterwerp and Prooijen, 2017)

Vertical stratification causes tidal straining. During the flood, salt water advances landward over layers of less dense water. This instability in density will lead to more vertical mixing and intensified bottom velocity in the profile. During ebb, fresh water moves on top of layers of more dense water leading to less vertical mixing. The velocity profile is intensified at the surface. So, during the flood, the velocities are higher near the bottom, resulting in a net residual transport (Burchard and Baumert, 1998).
At the entrance of the basin, the tides and waves are the dominant hydraulic dynamics. Because these two conditions occur independent of the entrance, classification of the entrance is based on these conditions (Bosboom and Stive, 2015). Figure A.3 depicts this classification based on the wave height and tidal range.

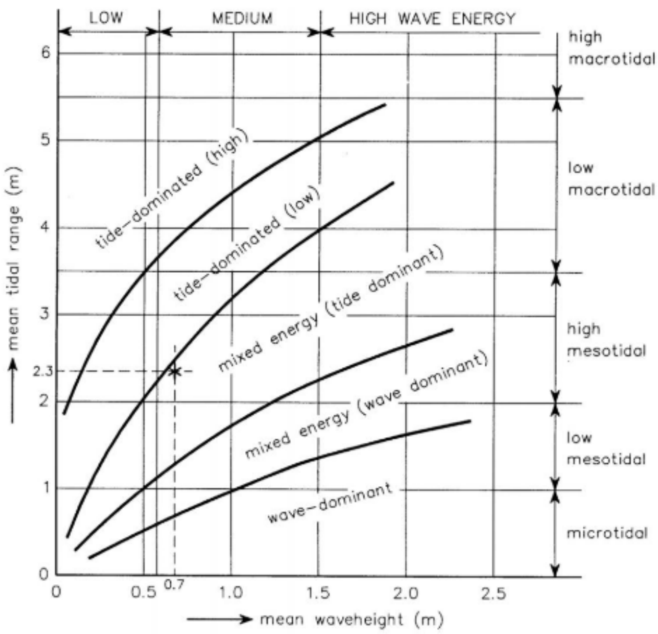

Figure A.3: Hydrodynamical classification of an inlet (Bosboom and Stive, 2015)

Waves can generate currents that will influence the morphodynamics of the adjacent coast. Barrier islands and outer deltas will, however, act as barriers for the tidal basin and estuary against waves (Bosboom and Stive, 2015). The waves will influence the tidal basin when they enter through the inlet.
In the tidal basin, waves induce currents which have an along-shore and cross-shore momentum. This momentum is because of the complicated topography that is present in the tidal basin. The onshore net flow travels different paths than the offshore net flow (Bosboom and Stive, 2015). Currents of the tide and waves can have strong interactions with waves and even block the waves.
Waves also influence the bottom shear stress experienced by currents. Because of enhancement of the bed shear stress through waves, tidal currents tend to seek deeper areas. In shallow water, the wave action and bed shear stress enhancement have the highest impact (Bosboom and Stive, 2015).

A.3.2 Morphodynamics

This section elaborates on the sediment transport due to the hydrodynamics in the tidal basin.
Different components of the tidal basin are dependent on equilibrium relations. The geometric properties are linked to hydraulic boundary conditions. The components are the stability and cross-sectional area of the entrance, the sand volume of the ebb-tidal delta, and the relation between the tidal channels and flats. The extent of the tidal delta, especially the ebb-tidal delta, depends on the dominance of waves or tide. A balance of the net onshore directed sediment flux caused by offshore waves and a net offshore directed sediment flux by inlet currents create the ebb-tidal delta. The onshore directed sediment flux mostly creates the flood-tidal delta. The dominance of waves or tide is decisive on which of the two delta's is relatively larger to one another. The flood dominant systems, which have shallow channels and limited intertidal storage, fill their channels with coarse material through their landward near-bed transportation. For ebb dominant systems, with deep channels and large intertidal storage, flush coarse sediment seaward. The amount of sediment the outer delta can absorb depends on the tidal prism and empirical coefficient (Bosboom and Stive, 2015). Equation A.7 represents this relation.

$$V_{od} = C_{od} P^{1.23} \tag{A.7}$$

V_{od}	$=$	Sand volume stored in the outer delta	$[m^3]$
C_{od}	$=$	Empirical coefficient	$[m^{-0.69}]$
P	$=$	Tidal prism	$[m^3]$

Where V_{od} is the sand volume stored in the outer delta in m^3, C_{od} the empirical coefficient in $m^{-0.69}$ and P the tidal prism in m^3 (Bosboom and Stive, 2015).

Sediment from the adjacent coast is transported to the inlet through the flood channel of the outer delta. If the state of the tidal basin is out of balance, the sediment is transferred into the basin. Otherwise, it passes into the main ebb channel and then towards the outer delta from which it moves to the adjacent coast. Besides this process, a part of the transported sediment ends up in the shoals in the outer delta. These shoals move in the direction of the longshore drift in a short process (Bosboom and Stive, 2015).
The ratio between the tidal prism and the magnitude of the littoral drift determines the amount of sediment that bypasses the outer delta direct and the amount that passes through the delta. Equation A.8 represents this relation.

$$r = \frac{P}{M_{tot}} \tag{A.8}$$

r	$=$	Parameter to indicate the bypass	$[-]$
P	$=$	Tidal prism	$[m^3]$
M_{tot}	$=$	Total littoral drift	$[m^3/year]$

Where r is a parameter to indicate the bypass, P the tidal prism in m^3 and M_{tot} the total littoral drift in $m^3/year$ (Bosboom and Stive, 2015).
Escoffier's model determines the cross-section area of the inlet. Escoffier determined an expression for the cross-sectionally averaged entrance channel velocity (u_e) for an inlet. He combined the parameters hydraulic radius of the channel (R), the cross-sectional area (A_e), and the tidal range (Δh) in the tidal basin in x. A larger cross-section results in a larger x. He found that u_e is a function of x. Figure A.4 shows this. Escoffier's model uses the empirical relation of Equation A.9 to find the equilibrium cross-sectional area.

$$A_{eq} = CP^q \tag{A.9}$$

A_{eq}	$=$	Minimum equilibrium cross-section of the entrance channel	$[m^2]$
C	$=$	Coefficients obtained for observational data	$[m^{2-3q}]$
P	$=$	Tidal prism	$[m^3]$
q	$=$	Coefficients obtained for observational data	$[m^{2-3q}]$

Where A_{eq} is the minimum equilibrium cross-section of the entrance channel, measured below the water level in m^2, and P the tidal prism in m^3. The dimensionless q and C in m^{2-3q} are coefficients obtained for observational data (Escoffier, 1940).

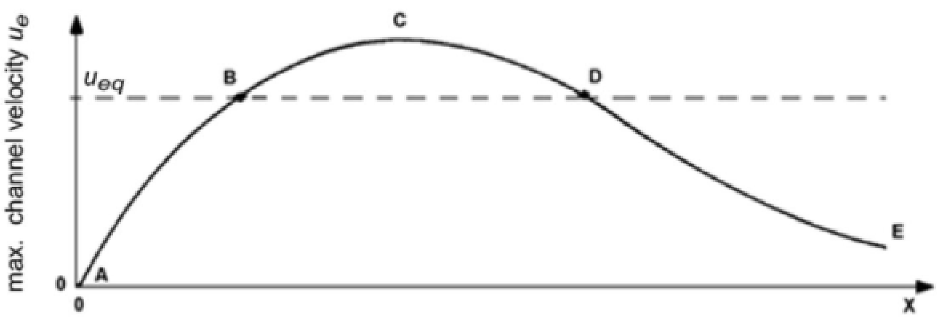

Figure A.4: Relation between channel velocity and channel geometry (Escoffier, 1940)

As stated before, the sediment transport in the inner basin occurs through the circulation currents in the channels of the inner basin. The tidal channels and tidal flats can be explained with the Equation A.10. In this empirical explanation, the flow area is related to the tidal volume passing the local cross-section (Bosboom and Stive, 2015).

$$A_{MSL} = C_A P_{AB} \tag{A.10}$$

A_{MSL}	=	Equilibrium flow area in the cross-section (AB)	$[m^2]$
C_A	=	Empirical coefficient	$[m^{-1}]$
P_{AB}	=	Tidal prism landward of a certain cross-section (AB)	$[m^3]$

P_{AB} is the tidal prism landward of a certain cross-section (AB) under consideration in m^3. Where A_{MSL} is the equilibrium flow area in the cross-section (AB) of the basin, measured below mean sea level in m^2. C_A the empirical coefficient in m^{-1} (Bosboom and Stive, 2015).

A.3.3 Net import or export of sediment

The net sediment import or export of tidal basins and estuaries is also dependent on the asymmetries of the tide, as stated in Section A.1. Vertical asymmetry is essential for residual sediment transport for tide dominated areas. When the flood or the ebb velocity exceeds the other, a residual transport of sediment occurs. For coarse sediment, this is the primary way of transportation. For fine sediments, the horizontal asymmetry is essential. The fine sediments need time to settle. When the slack durations before ebb and flood are not equal, the sediment has more time to settle before the flood or ebb. In this way net-import or export of sediment takes place.

A.4 Longshore transport

The hydrodynamics and morphodynamics of longshore transport are explained in this section. As stated before, longshore transport influences the part of the navigation channel located outside the tidal basin. Longshore transport influences inlet closures, rapid build-up of ebb/flood shoals and bypass of large volumes of sand. When the longshore transport is stopped by, for instance, a groyne, coastline recession takes place on the downdrift side. This recession is seen as a significant problem if it impacts populations who live in this part of the coast (Mil-Homens, 2016).
The longshore transport is dependent on the hydrodynamics in the breaker zone (Bosboom and Stive, 2015). Through wave breaking, turbulence is generated, and the sediment in suspension is increasing as explained in Section A.1. Sediment transport only occurs if there is enough sediment available. Sediment transport usually happens in bedload transport for low bed shear stresses and as a suspended load for high bed shear stresses. The transport appears in two directions: the cross-shore and longshore direction. Bedload transport is a small fraction of the total longshore sediment transport compared to suspended transport (Mil-Homens, 2016).
The longshore current is the dominating current in the nearshore zone. This current runs parallel to the shore. The longshore current is generated by the transfer of momentum of wave motion to the mean flow. This transfer is associated with the breaking process for obliquely incoming waves, the so-called radiation stresses, and by the surplus water which is carried across the breaker zone towards the coastline. Equation A.11 shows the wave-induced net force (F_x), that is dependent on the radiation stress perpendicular to the x-axis (S_{yx}) and the length of a uniform coast (dx). When waves break, the energy-momentum is transferred to the water column, inducing the longshore current. Besides this, tide or wind also induces a longshore current.

$$F_y = -\frac{dS_{yx}}{dx} \tag{A.11}$$

F_y	=	Wave-induced net force	$[N]$
S_{yx}	=	Radiation stress perpendicular to the x-axis	$[N/m]$
x	=	Length of a uniform coast	$[m]$

There are roughly two ways to predict the longshore transport, namely through bulk transport formulas and process-based models. The bulk transport formulas are equations based on simplified physical processes. They are calibrated on empirical coefficients and provide an estimate of the total longshore transport. The bulk transport formulations are mainly used for rough estimations. Process-based models, on the other hand, include a lot of physical processes and are used to simulate the longshore transport in more detail. They do, however, need more input than the bulk transport (Mil-Homens, 2016).

A.5 Natural processes and mechanism and human impact

Human activities change the bathymetry, hydraulic regime, and sediment transport pattern. Some estuaries lose their physical and morphological balance and their natural patterns of flow and sedimentation change (Jiang et al., 2011).

When disruption of the equilibrium state takes place, the morphological system will react and can try to either redress its balance or aggravate it. For instance, ebb dominance is enhanced when a tidal channel is deepened through dredging. The equilibrium in Equation A.10 will be forced out of balance when this dredging is performed. A net sediment export is initiated to redress this. However, when a channel is widened, the intertidal areas get smaller, the disturbance is opposed, and a net sediment import is enhanced. When a navigation channel is dredged through the outer delta, the equilibrium state of Equation A.7 is disturbed. Because the tidal prism and the protrusion rate do not change, the supply of sand from the flooded delta does not change. (Bosboom and Stive, 2015).

B Area study

B.1 Hydraulic data

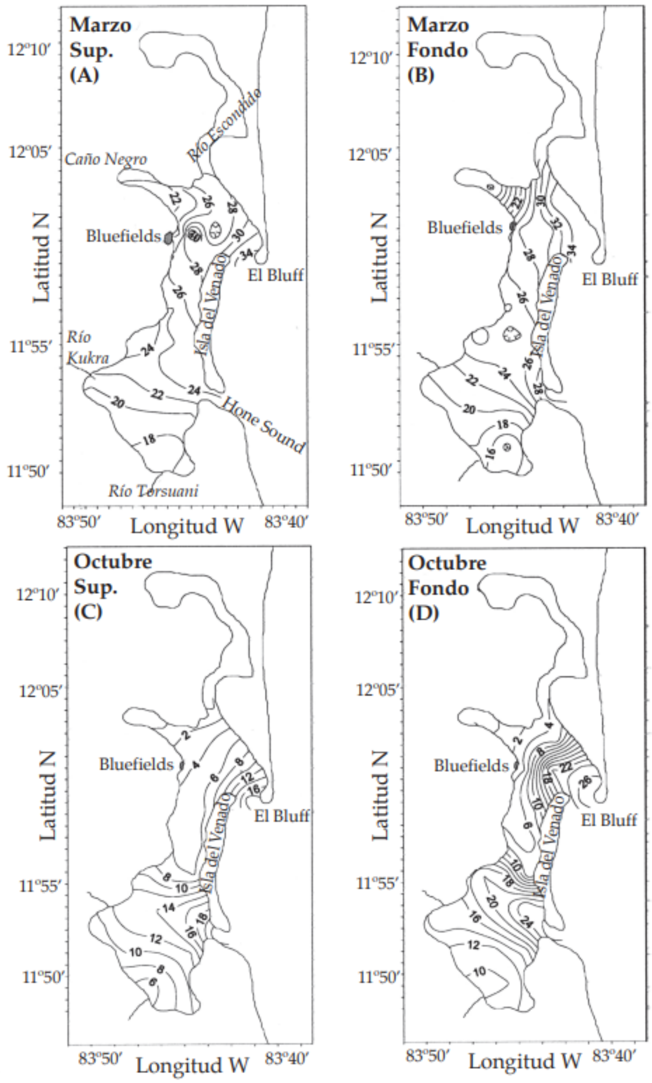

Figure B.1: Salinity measurements in October and March (Brenes et al., 2007b)

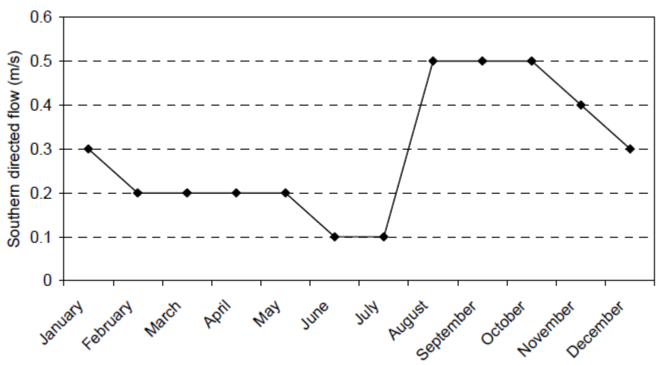

Figure B.2: Longshore current (Alkyon, 2004)

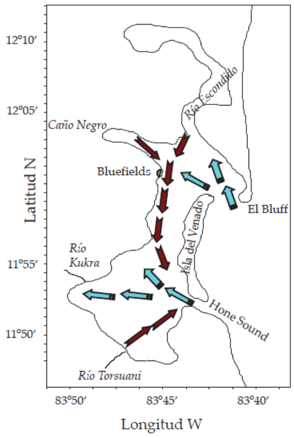

Figure B.3: Surface circulation model for Bluefields Bay. The lines represent fresh water flows and arrows represent salt water flows. (Brenes et al., 2007b)

B.2 Sediment data

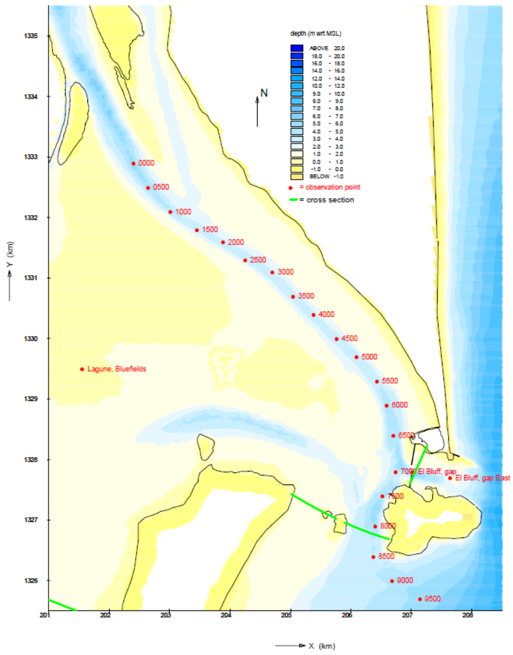

Figure B.4: Points of depth measurements in the study by Alkyon (Alkyon, 2004)

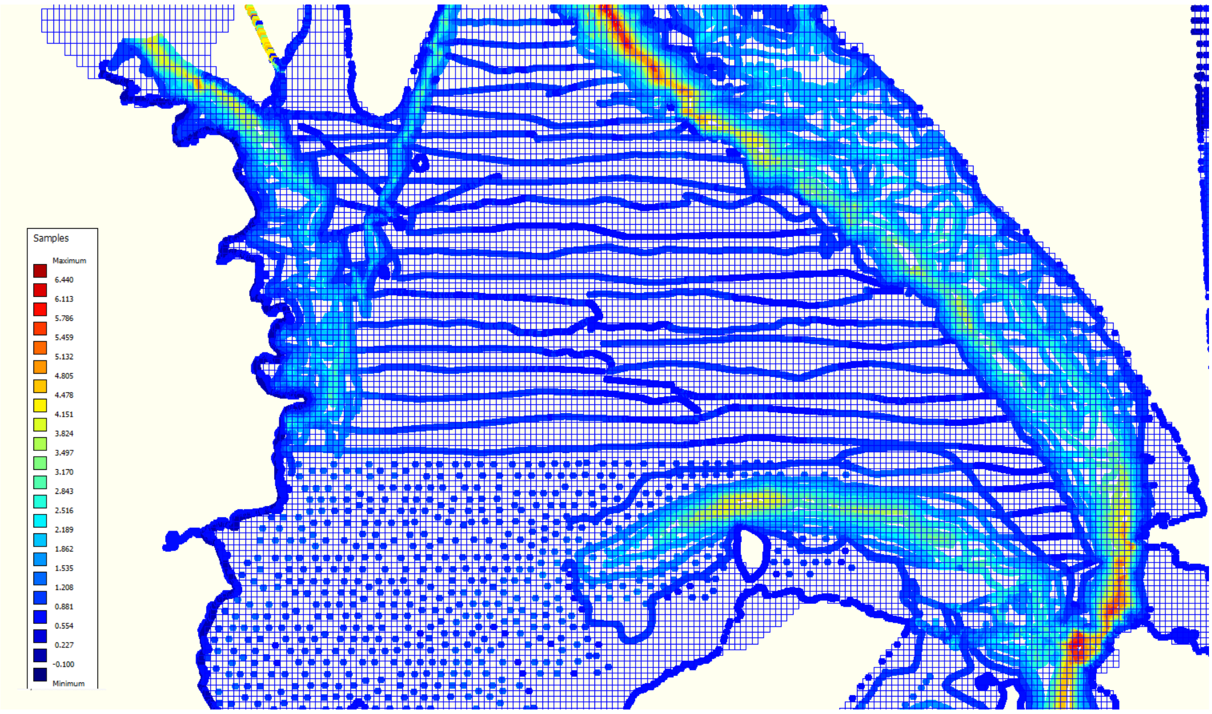

Figure B.5: Depth samples of the northern part of the lagoon

C Port dimensions

Port 1A

Channel section	Channel Width	Actual depth (m -MSL)	Dredged depth (m -MSL)	Length (m)
Coastal area	137	4.5 - 18	16.9	6815
Inner Bay	123	1 - 4.5	14.7	10125
Port Basin	-		13.8	

Table C.1: Port dimensions alternative 1A

Port 1B

Channel section	Channel Width	Actual depth (m +MSL)	Dredged depth (m +MSL)	Length (m)
Coastal area	137	4.5 - 18	16.9	8300
Inner Bay	123	1 - 4.5	14.7	4620
Port Basin	-		13.8	

Table C.2: Port dimensions alternative 1B

D Model setup

D.1 Delft3D formula's

D.1.1 Suspended transport formula's

The sediment source function of Equation 3.2 is computed with Equation D.1.

$$S = \frac{\overline{c}_{eq} - \overline{c}}{T_s} \tag{D.1}$$

The erosion and deposition step functions of Equations 3.3 and 3.4 are computed with Equations D.2 and D.3.

$$S(\tau_{cw}, \tau_{cw,e}^{(l)}) = \begin{cases} (\frac{tau_{cw}}{\tau_{cw,e}^{(l)}} - 1) & tau_{cw} > \tau_{cw,e}^{(l)} \\ 0 & tau_{cw} \leq \tau_{cw,e}^{(l)} \end{cases} \tag{D.2}$$

$$S(\tau_{cw}, \tau_{cw,d}^{(l)}) = \begin{cases} (1 - \frac{tau_{cw}}{\tau_{cw,d}^{(l)}}) & tau_{cw} < \tau_{cw,d}^{(l)} \\ 0 & tau_{cw} \geq \tau_{cw,d}^{(l)} \end{cases} \tag{D.3}$$

For the non-cohesive suspended sediment transport, the Van Rijn (1993) method is followed. An erosive flux (Equation D.4) due to upward diffusion and a deposition flux (Equation D.5) due to settling velocity are the main drivers.

$$E = \epsilon_s * \frac{\delta c}{\delta z} \tag{D.4}$$

$$D = w_s * c \tag{D.5}$$

When concentrations are high of suspended sediment, hindered settling can happen. Hindered settling is calculated with the Equation D.6 (Richardson and Zaki, 1954).

$$w_s = (1 - \frac{c_s^{tot}}{C_{soil}}) * w_{s,0} \tag{D.6}$$

Where β is the effective Van Rijn's 'beta' factor of the sediment fraction, which on its turn is dependent on the fall velocity and the local bed shear stress due to currents.
The non-cohesive settling velocity is computed through the method Van Rijn (1993) (Equation D.7), where the fall velocity is dependent on the diameter of the fraction.

$$w_s = \frac{10 * v}{D_s}(\sqrt{1 + \frac{0.01 * (s-1) * g * D_s}{v^2}} - 1) \tag{D.7}$$

D.1.2 Bedload transport formula's

Where sediment mobility number M and excess sediment mobility number M_e are calculated by Equations D.8 and D.9.

$$M = \frac{v_{eff}^2}{(s-1) * g * D_{50}} \tag{D.8}$$

$$M_e = \frac{v_{eff} - vcr}{(s-1) * g * D_{50}} \tag{D.9}$$

$$v_{eff} = \sqrt{v_R^2 + U_{on}^2} \tag{D.10}$$

With the concentration that is transported calculated with the following formula:

$$c_a = 0.015 * \rho_s * \frac{D_{50} * (T_a)^{1.5}}{a * (D_*)^{0.3}} \tag{D.11}$$

Where T_a is dependent on the bed shear stresses due to currents (Equation D.12 and D.13).

$$\tau_{b,cw} = \rho_w * u_*^2 \tag{D.12}$$

$$\tau_{b,w} = \frac{1}{4}\rho_w f_w(\widehat{U}_\delta)^2 \tag{D.13}$$

D.2 Delft3D parameter settings

Unchanged settings

Parameter	**Unit**	**Value**
Domain		
Time step	min	0.5
k-layers	-	1
Physical parameters		
Gravity	m/s^2	9.81
Water density	kg/m^3	1025
Air density	kg/m^3	1
Bottom roughness		Manning
Uniform bottom roughness in u-direction	-	0.02
Uniform bottom roughness in v-direction	-	0.02
Horizontal eddy viscosity	m^2/s	1
Horizontal eddy diffusivity	m^2/s	10
Morphology		
Update bathymetry during FLOW simulation		False
Include effect of sediment on fluid density		False
Equilibrium sand concentration profile at inflow boundaries		True
Morphological scale factor	-	1
Spin-up interval before morphological changes	min	720
Minimum depth for sediment calculation	m	0.1
Van Rijn's reference height factor	-	1
Threshold sediment thickness	m	0.05
Factor for erosion of adjacent dry cells	-	0
Current-related reference concentration factor	-	1
Current-related transport vector magnitude factor	-	1
Waves		
Generation mode for physics		3-rd generation
Depth-induced breaking (B&J model)		True
Alpha	-	1
Gamma	-	1
Non-linear triad interactions (LTA)		False
Bottom friction		True
Type		Jonswap
Coefficient	m^2/s^3	0.067
Wind growth		True
Quadruplets		True
White capping		Komen et al.
Refraction		True
Frequency shift		True

Table D.1: Main model settings

Mud from the Rio Escondido

Parameter	*Unit*	*Value*
Reference density for hindered settling	kg/m^3	1600
Specific density	kg/m^3	2650
Dry bed density	kg/m^3	500
Fresh settling velocity	mm/s	0.129
Critical bed shear stress for sedimentation	N/m^2	1000
Critical bed shear stress for erosion	N/m^2	0.1
Erosion parameter	kg/m^2s	0.001

Table D.2: Cohesive fraction setting for sediment fraction 1

Mud in the initial bed composition

Parameter	*Unit*	*Value*
Reference density for hindered settling	kg/m^3	1600
Specific density	kg/m^3	2650
Dry bed density	kg/m^3	500
Fresh settling velocity	mm/s	0.129
Critical bed shear stress for sedimentation	N/m^2	1000
Critical bed shear stress for erosion	N/m^2	0.5
Erosion parameter	kg/m^2s	0.0001

Table D.3: Cohesive fraction setting for sediment fraction 2

Sand in the initial bed composition

Parameter	*Unit*	*Value*
Reference density for hindered settling	kg/m^3	1600
Specific density	kg/m^3	2650
Dry bed density	kg/m^3	1600
Median sediment diameter (D_{50})	μm	200

Table D.4: Non-cohesive fraction settings for sediment fraction 3

D.3 Sensitivity analysis

No bed composition is used for the first few steps of the sensitivity analysis. Elected is to first find the right parameters of the silt fraction, without bed composition. By setting the model up with one fraction by each step, the influence of different parameters is better understood. It must be noted that the direction of the positive sediment flux of the blue line, representing the northern inlet, is to the sea. This direction is opposite of the direction of the sediment flux in Figures 3.8b, 3.3a, and 3.3b.

D.3.1 Sensitivity analysis critical erosion parameter

For freshly deposited mud, the critical erosion parameter can vary between $0.05N/m^2$ and $0.5N/m^2$. Figure D.1 shows the sensitivity analysis of a varying critical erosion parameter between the range $0.05N/m^2$ and $0.2N/m^2$. The yellow line represents the input of the sediment in the Rio Escondido near the boundary. The green line represents the cumulative transport at the mouth of the river, and the blue line represents the cumulative transport going through the northern tidal inlet.
The amount of sedimentation increases significantly for higher erosion shear stress. For a critical erosion shear stress $0.10N/m^2$ the sedimentation is already about 50% in the river, increasing further with higher critical erosion shear stresses. Since as much sediment as possible should exit the river, a critical erosion shear stress of $0.05N/m^2$ is chosen. A lower value is not represented in the literature study.

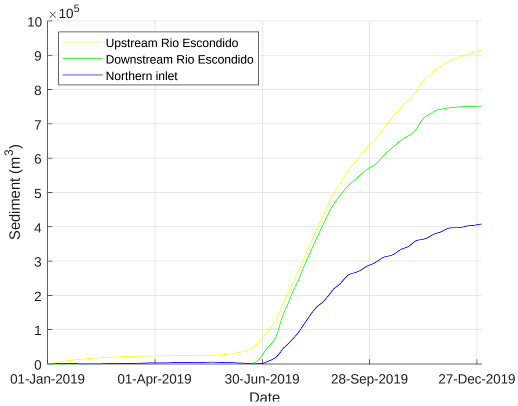

(a) Critical erosion shear stress $0.05 N/m^2$

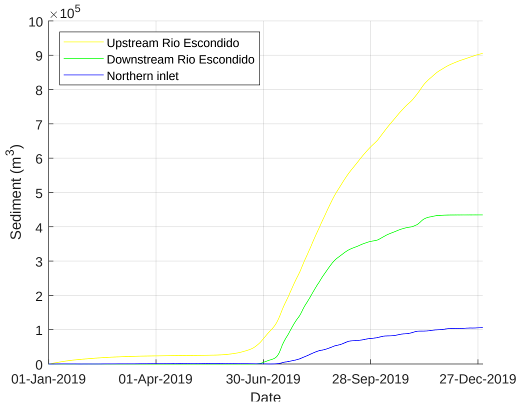

(b) Critical erosion shear stress $0.10 N/m^2$

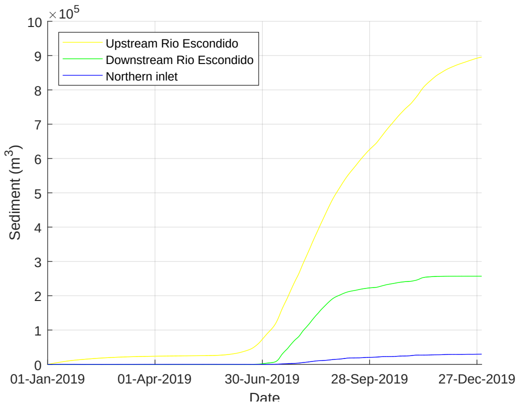

(c) Critical erosion shear stress $0.15 N/m^2$

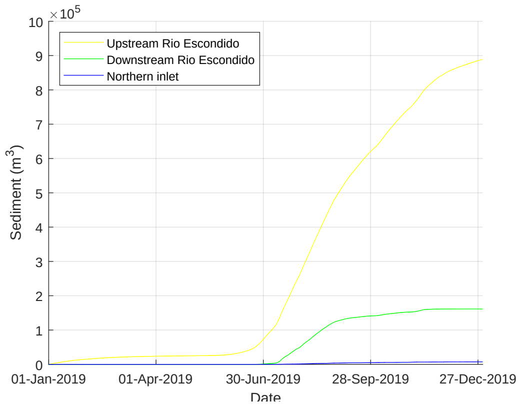

(d) Critical erosion shear stress $0.20 N/m^2$

Figure D.1: Cumulative amount of sediment going through the cross-sections with a different critical erosion shear stress

D.3.2 Sensitivity analysis sediment size

Besides the critical erosion parameter, the fall velocity is an adjustable parameter. The data analysis in Section 2.4 estimates a D_{50} of $17 \mu m$. However, the size is derived from a bed sample, whereas the sediment in the suspension probably has a lower fall velocity. A sensitivity analysis compares the amount of sedimentation for different D_{50} in the Rio Escondido. The different sediment sizes are $8 \mu m$, $12 \mu m$, $17 \mu m$ and $22 \mu m$. Figure D.2 shows the results of the sensitivity analysis of changing the D_{50} in the model. The graphs show that the D_{50} does not influence the cumulative amount of sediment transport through these sections. About 80% of the total input of the Rio Escondido exits the river. Besides this, about 45% of the sediment input exits the tidal basin. A sediment size of $12 \mu m$ for the cohesive fraction that enters the boundary is the sediment size modelled from now on, as the size is not relevant.

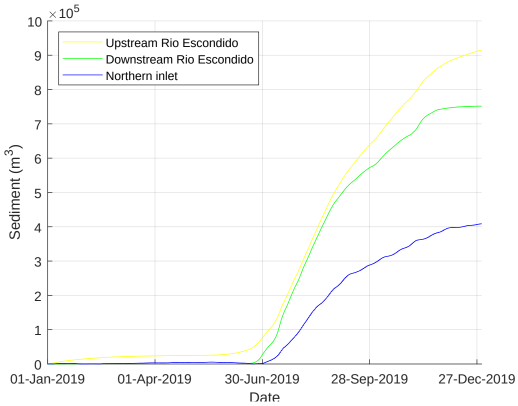

(a) Sediment size $8\mu m$

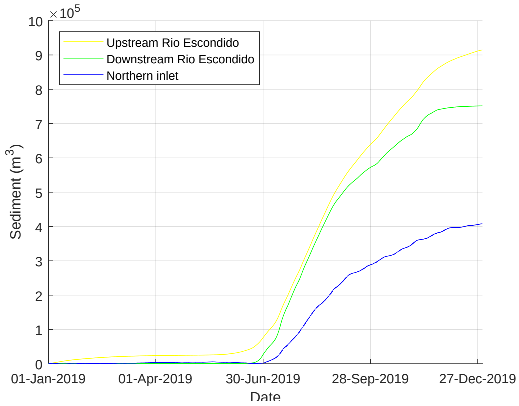

(b) Sediment size $12\mu m$

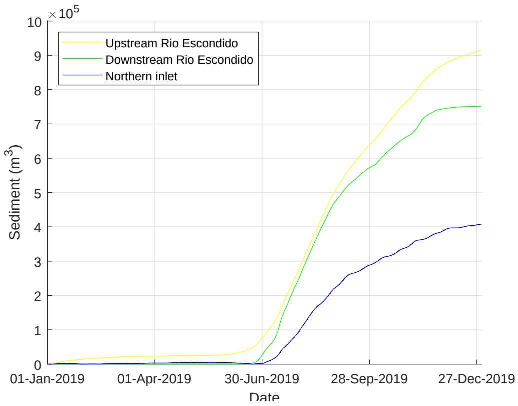

(c) Sediment size $17\mu m$

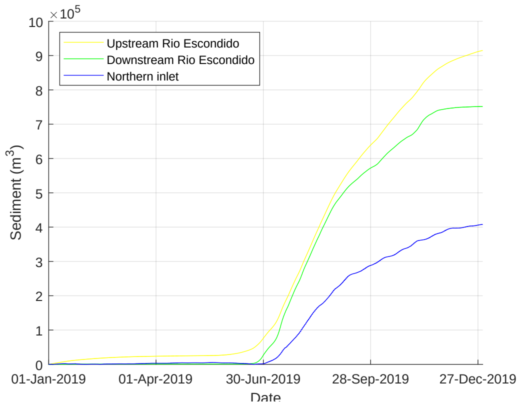

(d) Sediment size $22\mu m$

Figure D.2: Cumulative amount of sediment going through the cross-sections with a different fall velocity

D.3.3 Sensitivity analysis erosion parameter

The erosion parameter is calibrated with values of 10^{-3} and 10^{-4}. The results are seen in Figure D.3. In both the results, the basin exports silt in the dry period. Besides this, the basin starts to import sediment in the wet season. This is physical not possible according to the conceptual model. This error is probably because of the too high critical erosion shear stress due to the sand in the bed composition.

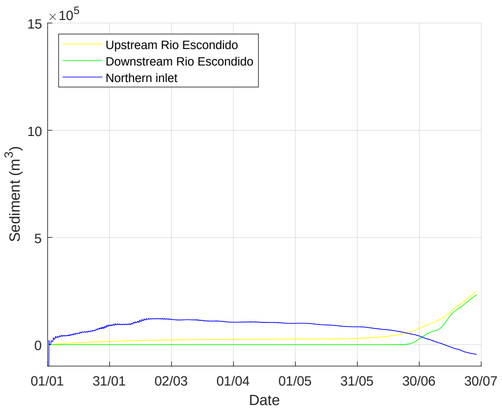

(a) Erosion parameter 10^{-3}

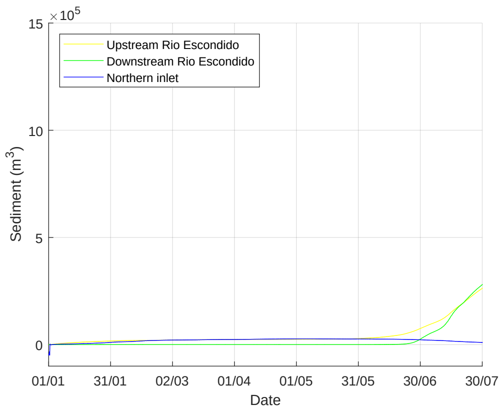

(b) Erosion parameter 10^{-4}

Figure D.3: Cumulative amount of sediment going through the cross-sections with a different erosion parameter

D.3.4 Silt originating from the bed composition

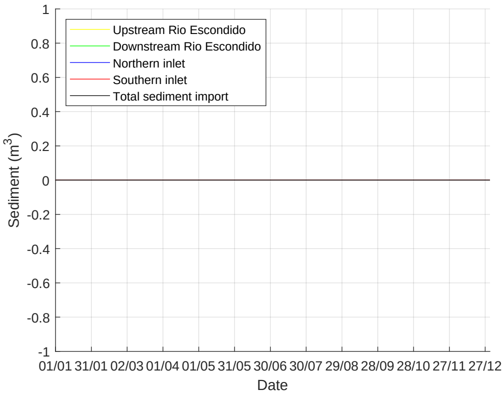

Figure D.4: Cumulative amount of the silt with a higher critical erosion shear stress going through the cross-sections

D.4 Analytical calculations for the longshore transport

Longshore sediment transport can be calculated with different bulk transport formulas and process-based transport formulas, as explained in Section A.4. The bulk transport formulas are used for rough estimations. In these formulas, the transport is mainly dependent on wave height and angle of incidence. For this conceptual model, a bulk transport formula is sufficient, as an indication of sediment transport is needed. Eventually, this will be used to validate the process-based model from Delft3D. The sediment transport was calculated using the Van Rijn transport formulas D.14 and D.15.

$$Q_{kg} = 0.00018 * \rho_s * \sqrt{g} * D_{50}^{-0.6} * H_{br}^{3.1} * \sin(2 * \theta_{br}) \tag{D.14}$$

$$Q_{m^3} = Q_{kg} * \frac{1}{(\rho_s - \rho)(1 - \rho)} \tag{D.15}$$

The parameters that influence the transport quantities are the diameter size of the sediment (D_{50}), the wave height at breaker point (H_{br}), and the angle of incidence at breaker point (θ_{br}). These input parameters vary over the year with the changing conditions. The dataset available, as explained in Section 2.3.4 has data of the wave height, wave period, and angle of incidence. To calculate H_{br} and θ_{br}, the offshore wave data must be transformed into onshore waves quantities. When these waves come in the breaker zone, they transform into the wave quantities that eventually initiate the sediment transport as explained in Section A.1. Shallow water equations were used to calculate the offshore to onshore wave transformation (Holthuijsen, 2007). These formulas that are used are shown in Appendix D.5.

A couple of locations along the shore are studied to obtain insight in the sediment transport; respectively, a point northward on the adjacent coast, a midpoint, and a northern and southern point of the island. The normal line to the shore of these locations can be seen in Figure D.5a.

Because of the differences in bathymetry per location plus differences in angle of approach to the island compared to the normal to the shoreline, the waves will have different values for the onshore significant wave height, wave period, angle of incidence and wave celerity. The wave profiles for the different locations can be in seen in Figure D.5. Over the year, the waves are from the same angle, with minimum variance. At each location, the angle of incidence is slightly smaller than the normal line perpendicular to the shoreline seen from the north, meaning the mean transport direction will be from north to south at each location the year around. The angle of incidence varies between $2°$ to $16°$, which will initiate small quantities considering Equation D.14. and because of the small value, small transport capacities will go to the north.

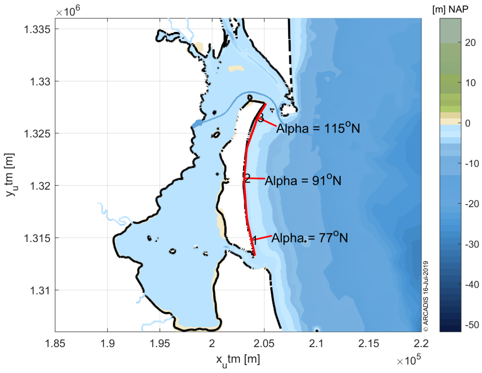

(a) Profiles along the shore

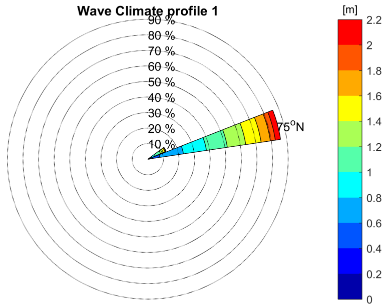

(b) Wave profile for location 1

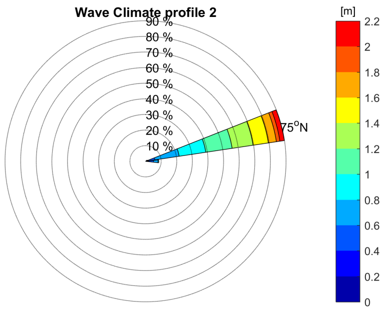

(c) Wave profile for location 2

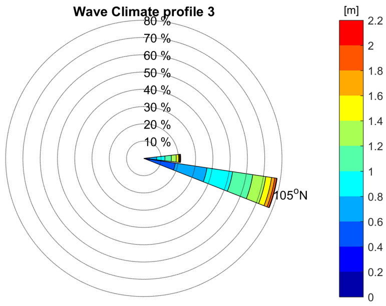

(d) Wave profile for location 3

Figure D.5: Wave climate at the beach

The sediment size also influences sediment transport quantities. A $D50$ of $100\mu u$, $200\mu u$ and $300\mu u$ is used. The results of Formula D.14 with the different sizes as input parameter and the onshore wave conditions can be seen in Table D.5. The quantities of the littoral drift to the south at location 4, are about the same size as for the littoral drift quantities in the middle of the island. A large part of the sediment that comes from the north of El Bluff will be swept to sea, taking the sharp angle of the coastline at El Bluff into account.
The distribution of the sediment transport over the year can be seen in Appendix D.6 for a sediment size of $200\mu u$. A remark must be made that Van Rijn formula is a potential transport formula, meaning it tends to overestimate the longshore sediment transport.

Transport quantities longshore transport

Profile	$100\mu m$	$200\mu m$	$300\mu m$
Southern point Island	$418.583m^3$	$276.377m^3$	$216.525m^3$
Midpoint Island	$757.836m^3$	$499.985m^3$	$392.015m^3$
North point Island	$348.096m^3$	$229.658m^3$	$180.064m^3$
El Bluff	$687.255m^3$	$453.419m^3$	$355.505m^3$

Table D.5: Longshore sediment transport at the different profiles

D.5 Wave transformation formulas

Offshore wavelength [m]:

$$L_0 = \frac{g}{2 * pi} * T_{p0}^2 \tag{D.16}$$

Offshore wave celerity [m/s]:

$$c_0 = \frac{L_0}{T_{p0}} \tag{D.17}$$

Water depth at breaker line [m]

$$h_{br} = {\frac{H_{s0}^2 * c_0 * \cos\theta_0}{\alpha * \gamma^2 * \sqrt{g}}}^{4}; \tag{D.18}$$

Wave celerity at breaker line [m/s]:

$$c_{br} = \sqrt{h_{br} * g}; \tag{D.19}$$

Wavelength at breaker line [m]:

$$L_{br} = c_{br} * T_{p0} \tag{D.20}$$

Significant wave height at breaker line[m]:

$$H_{sbr} = h_{br} * \gamma \tag{D.21}$$

Wave angle at breaker line (degrees relative to shore-normal):

$$\theta_{br} = \sin^{-1}\frac{c_{br}/c_0}{\sin\theta_0} \tag{D.22}$$

D.6 Transport quantities

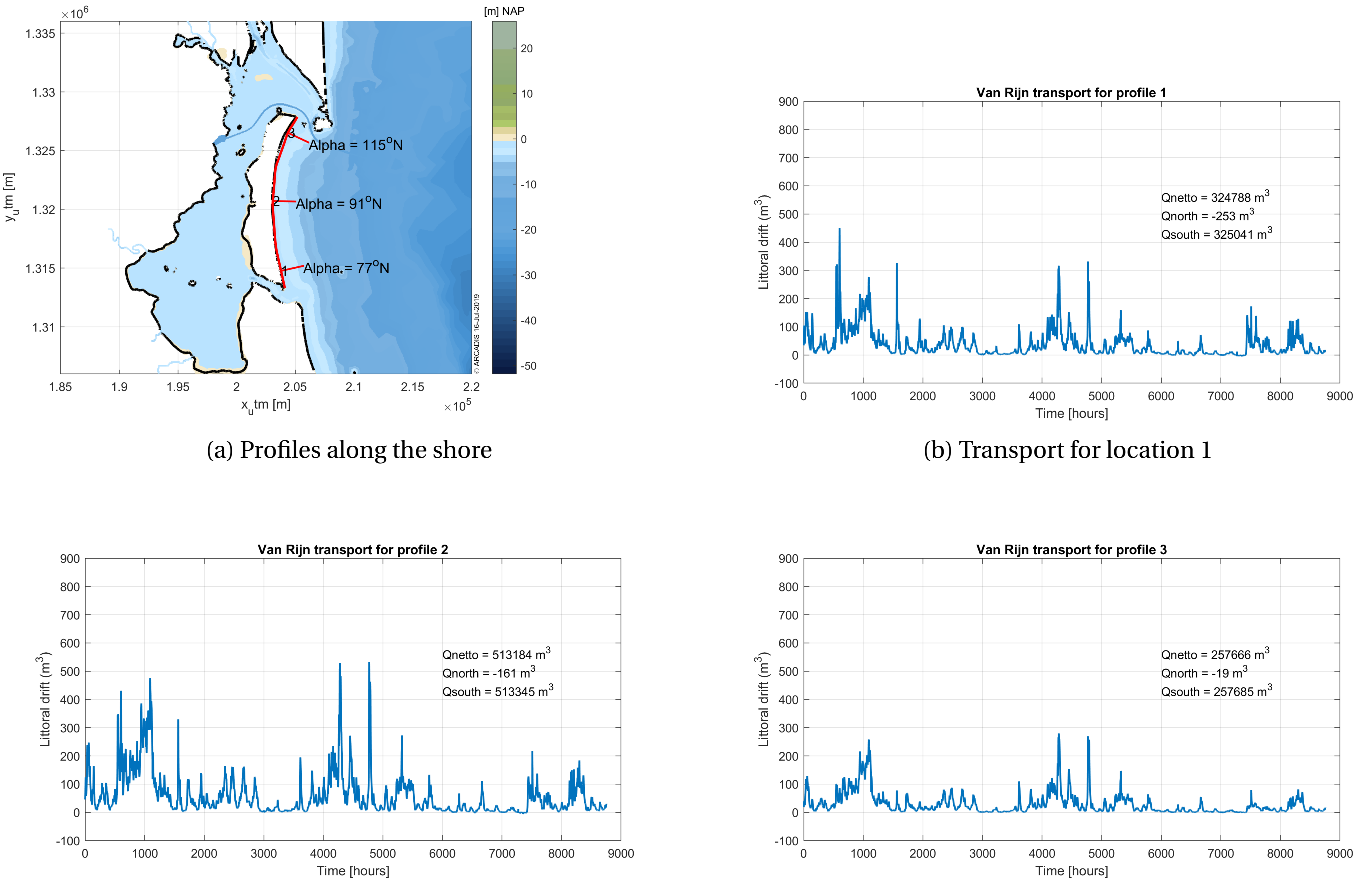

(a) Profiles along the shore

(b) Transport for location 1

(c) Transport for location 2

(d) Transport for location 3

Figure D.6: Transport for D200 for the different locations

E Results Hydrodynamics

E.1 Flow velocities and directions

Figure E.1 shows the mean flow velocities and directions in March and July. During the dry period, the mean depth-averaged velocity is almost zero. As the river discharge is around the $150m^3/s$, the flow field is predominated by the tide. During the wet period, the flow velocity field increases a lot in the northern part of the lagoon of the area, due to the river discharges resulting in an estuary type of behaviour of this area. With increasing discharge, more sediment is transported by the river, as shown in Equation 3.1. The flow to the south increases a little, meaning there is a chance an amount of sediment is transported to the south. In the southern part of the lagoon, the average velocity field is close to zero for both cases. No large discharges of rivers are found in this area, as no channels are in this area. Sediment transport will be mainly dependent on the residual currents. Because the residual currents are not directed to the north, sediment transport going from south to north is not likely. The study area is concentrated on the northern part of the basin from now on. Reason for this area is that the port, and its structures are planned to be constructed in this area.

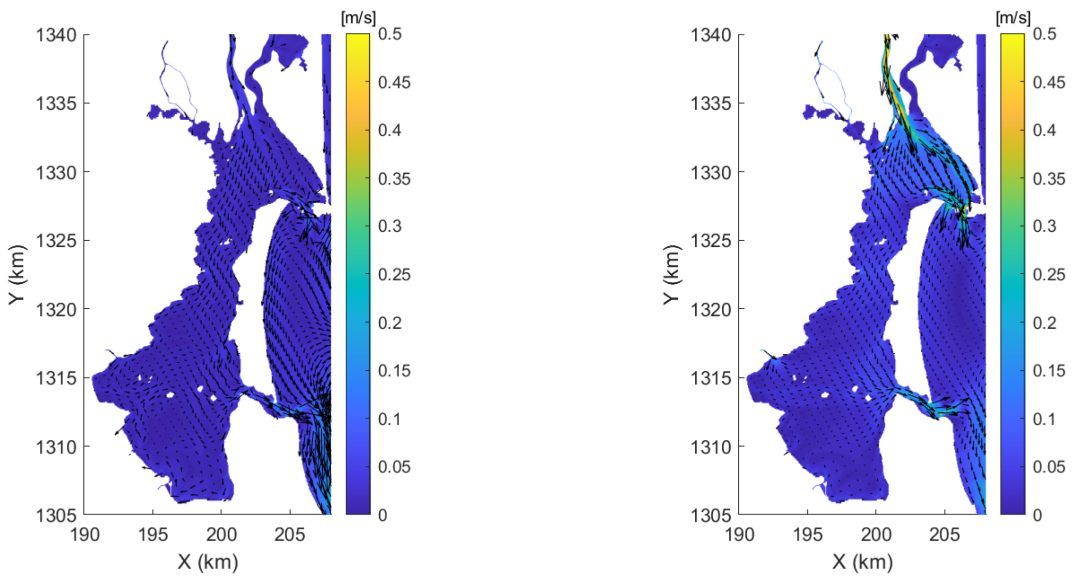

(a) Dry period

(b) Wet period

Figure E.1: Average flow velocities over a month

To get more insight into the reach of flood and ebb Figures E.2 and E.3 show the directions of the flow during flood and ebb of the spring tide in the dry and wet season. The tidal currents reach to around the $1321km$ line of the y-axis. This range of flow means that if the flow velocity and concentration of sediment are high enough, the sediment transportation reaches far in the basin. In the dry season, it is seen that during flood and ebb, the current field is dominated by the tide. The influence of only the tide is in this way better understood. It seems that the influence of tide reaches further during this period.

E.2 Current during flood and ebb

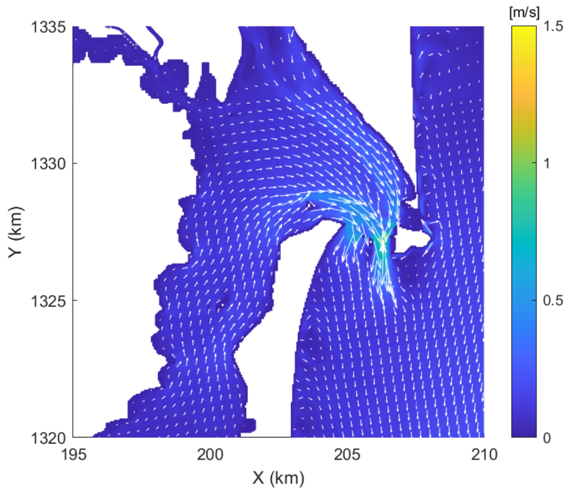

(a) Ebb

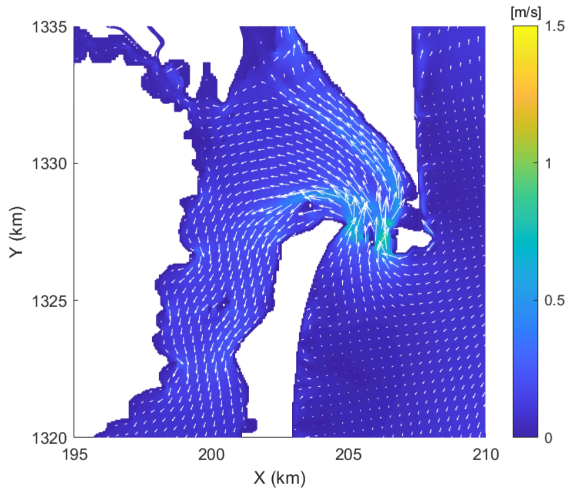

(b) Flood

Figure E.2: Flow velocities during the dry season

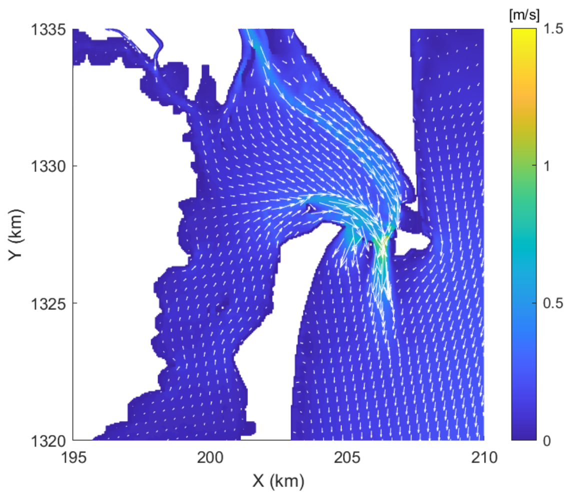

(a) Ebb

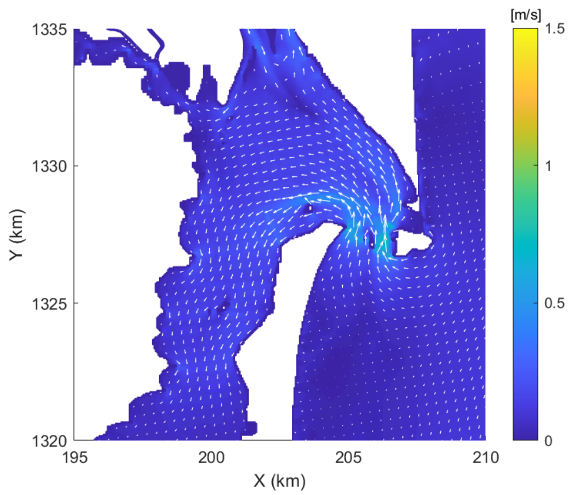

(b) Flood

Figure E.3: Flow velocities during the wet season

E.3 Residual currents at the southern inlet

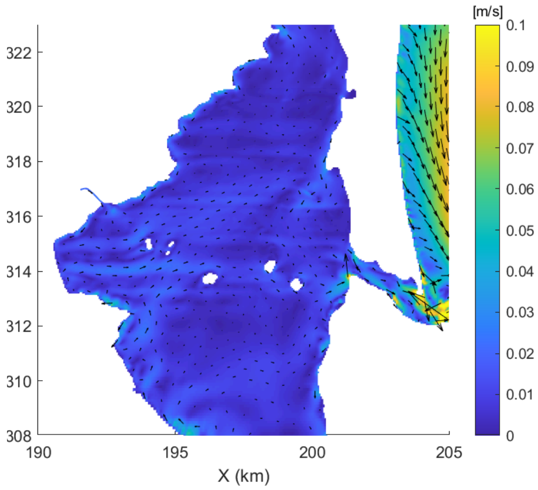

(a) Dry period

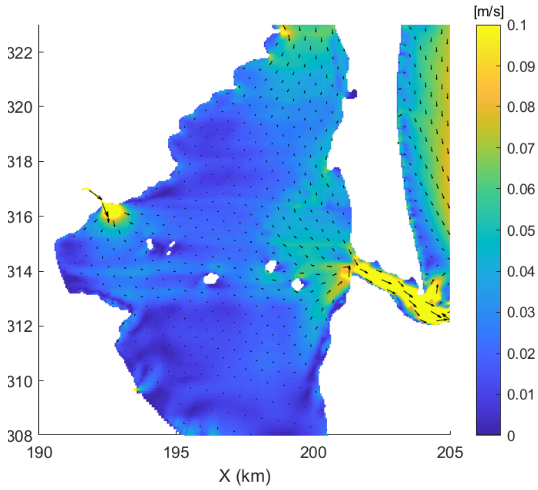

(b) Wet period

Figure E.4: Residual currents at the southern inlet

E.4 Water level and velocity at the southern inlet

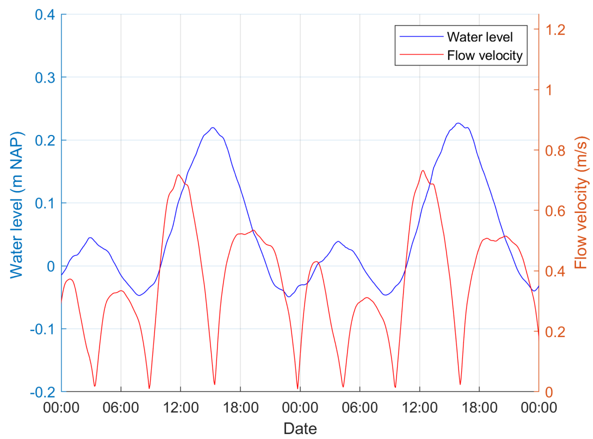

(a) Dry period

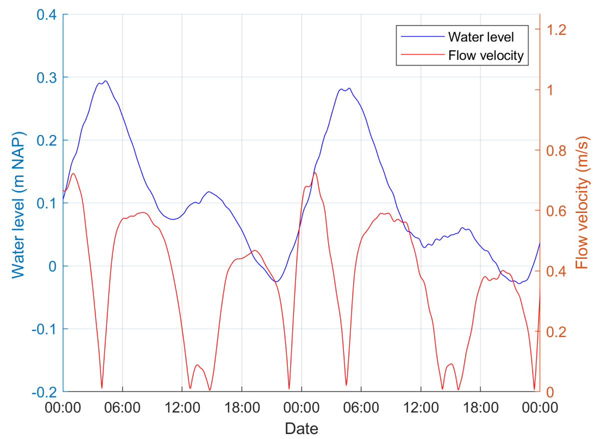

(b) Wet period

Figure E.5: Water level and velocity at the southern tidal inlet during a spring tide

F Results Morphodynamics

F.1 Sediment balance

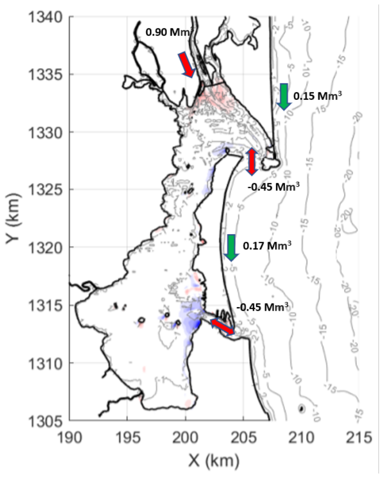

Figure F.1: Sediment balance of the existing situaiton for an annual period

G Results Alternatives

G.1 Water level and discharge for the alternatives

Figure G.2 shows the water levels for stations in the basin. The water levels are nearly the same for each time step, and it can be concluded that the network acts as a storage basin where the water level varies in time but not in space. The tidal basin and the northern inlet are a discrete system. The system has a conveying area, the inlet, and a storage area, the basin. The dimensionless parameter Γ can therefore be calculated through Equation G.1. The equation expresses the dimensionless parameter as a function of the discrete system (Battjes and Labeur, 2017). When an inlet is enlarged, the dimensionless parameter factor (Γ) is assumed constant. The only variable that is changed is the cross-sectional area (A_c). For Γ to remain constant, the water elevation at the seaside of the basin ($\hat{\zeta}_s$) increases.

$$\Gamma = \frac{8}{3\pi}\chi(\frac{A_b}{A_c})^2\frac{\omega^2\hat{\zeta}_s}{g} \tag{G.1}$$

Γ	$=$	Dimensionless parameter	$[-]$
χ	$=$	Resistance parameter	$[-]$
A_b	$=$	Basin area	$[m^2]$
A_c	$=$	Cross-sectional channel area	$[m^2]$
ω	$=$	Radial frequency in harmonic motion	$[rad/s]$
$\hat{\zeta}_s$	$=$	Elevation sea	$[m]$
g	$=$	gravity	$[kgm/s^2]$

Figure G.1 in Appendix G.2 shows that the elevation indeed increases for a larger cross-sectional area. For Alternative 1B the elevation shows about the same changes as for Alternative 1A. The newly created gap is relatively not far away compared to the tidal wavelength. The newly created opening is therefore seen as a cross-sectional expansion of the northern tidal inlet. The changes in the discharge in the northern tidal inlet is compensated with the discharge through the new opening.
The discharge amplitude at the entrance is computed with Equation G.2. The elevation in the basin is the only variable that changes, by changing the cross-sectional area in Equation G.1. By an increase of elevation at the seaside, the elevation in the basin also increases as it remains a discrete system. Figure G.3 in Appendix G.3 shows that the elevation is the same over the tidal basin. With an increase in water elevation, the discharge also increases according to Equation G.2.
An extra reinforcing effect of an enlargement of the elevation and discharge is that resistance decreases when there is a deepening in the bathymetry (Battjes and Labeur, 2017). As the deepening is large here, the resistance decreases substantial, and thus the water level elevation and discharge due to the tidal wave increases.

$$\hat{Q} = A_b\omega\hat{\zeta}_b \tag{G.2}$$

$\hat{Q}$	$=$	Amplitude discharge	$[m^3]$
A_b	$=$	Basin area	$[m^2]$
ω	$=$	Radial frequency in harmonic motion	$[rad/s]$
$\hat{\zeta}_b$	$=$	Elevation basin	$[m]$

G.2 Water level at entrance

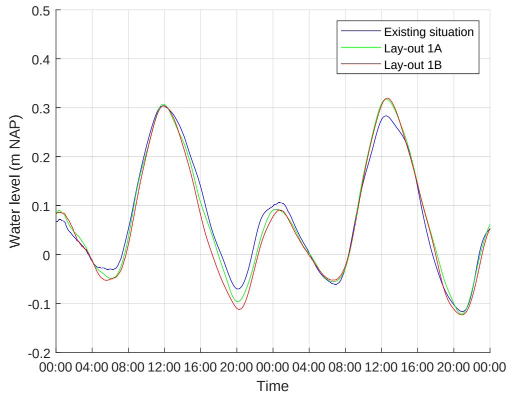

Figure G.1: Water level at the northern inlet for the alternatives

G.3 Water level throughout basin

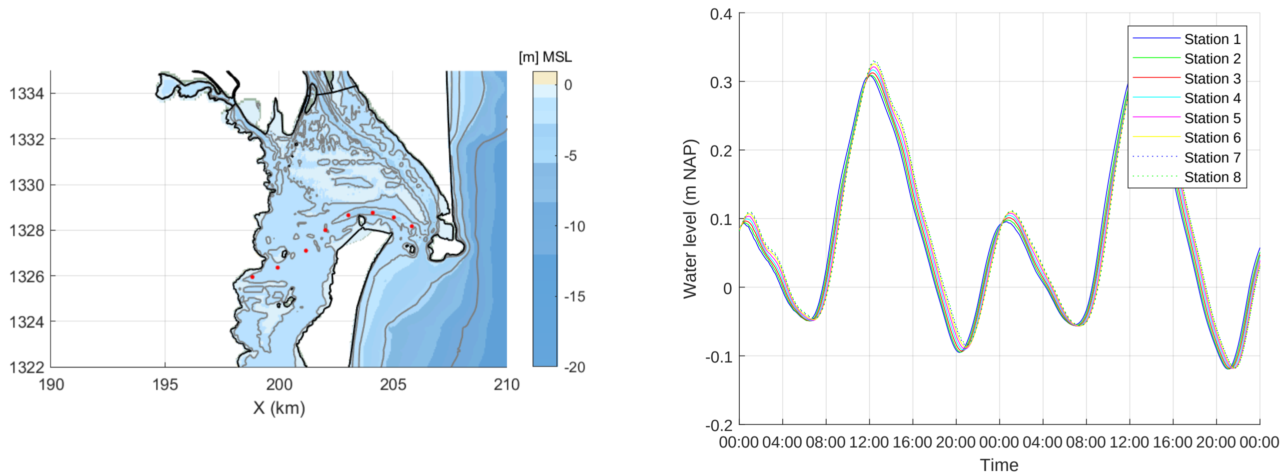

(a) Measuring points

(b) Water level

Figure G.2: Water level at different stations in the basin

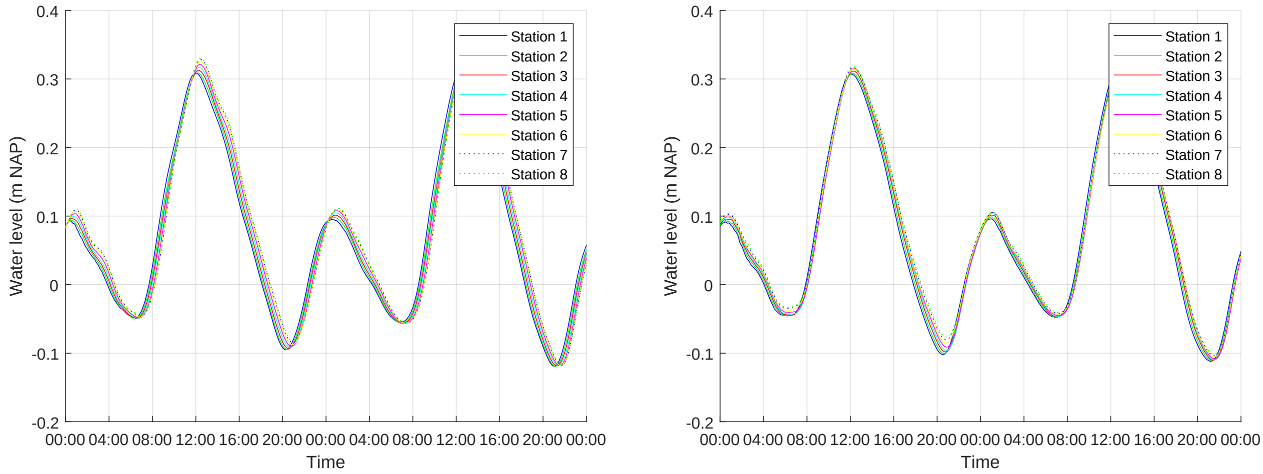

(a) Alternative 1A

(b) Alternative 1B

Figure G.3: Water level at different stations in the basin for the alternatives

G.4 Discharges southern tidal inlets

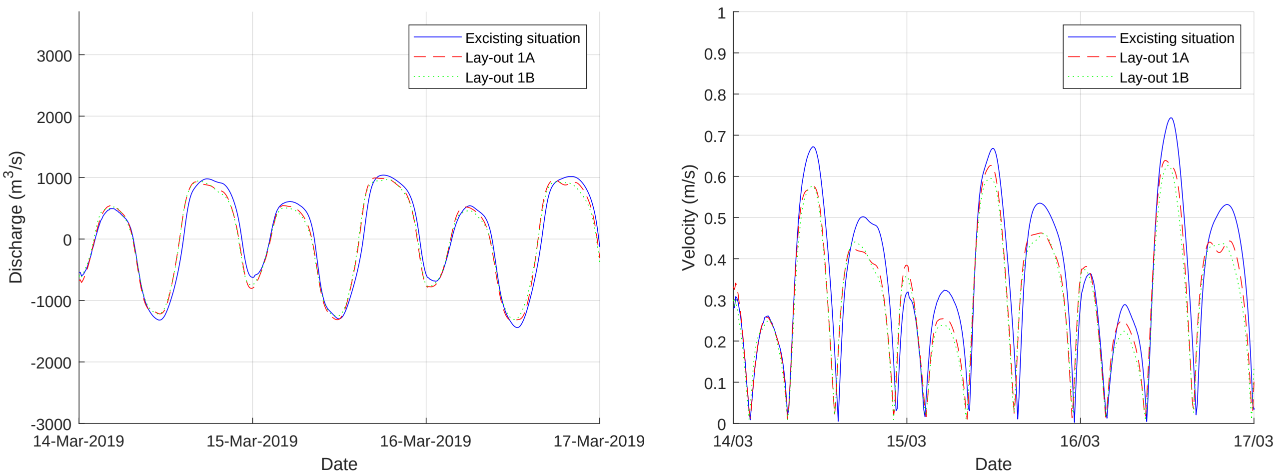

(a) Discharges

(b) Flow velocities

Figure G.4: Discharges and flow velocities at the southern tidal inlet for the existing figure and the alternatives

G.5 Current during flood and ebb for Alternative 1A

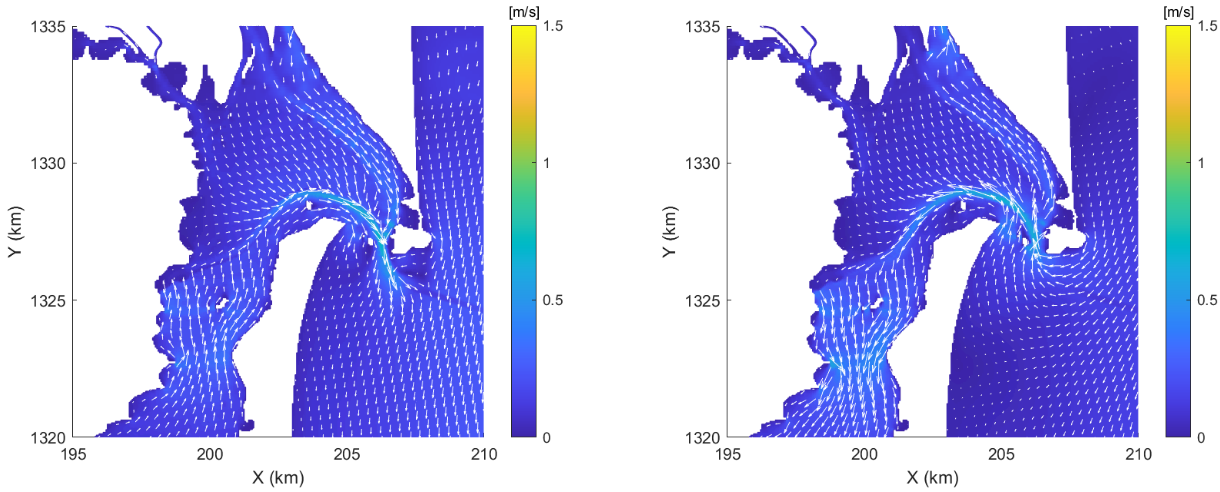

(a) Ebb

(b) Flood

Figure G.5: Flow velocities for Alternative 1A during the dry season

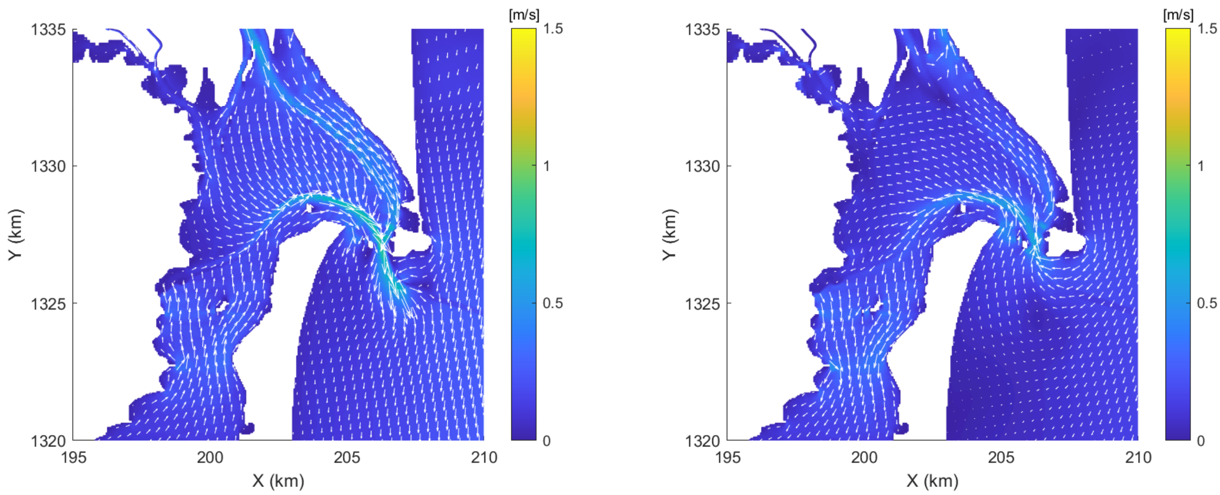

(a) Ebb

(b) Flood

Figure G.6: Currents for Alternative 1A during the wet season

G.6 Current during flood and ebb for Alternative 1B

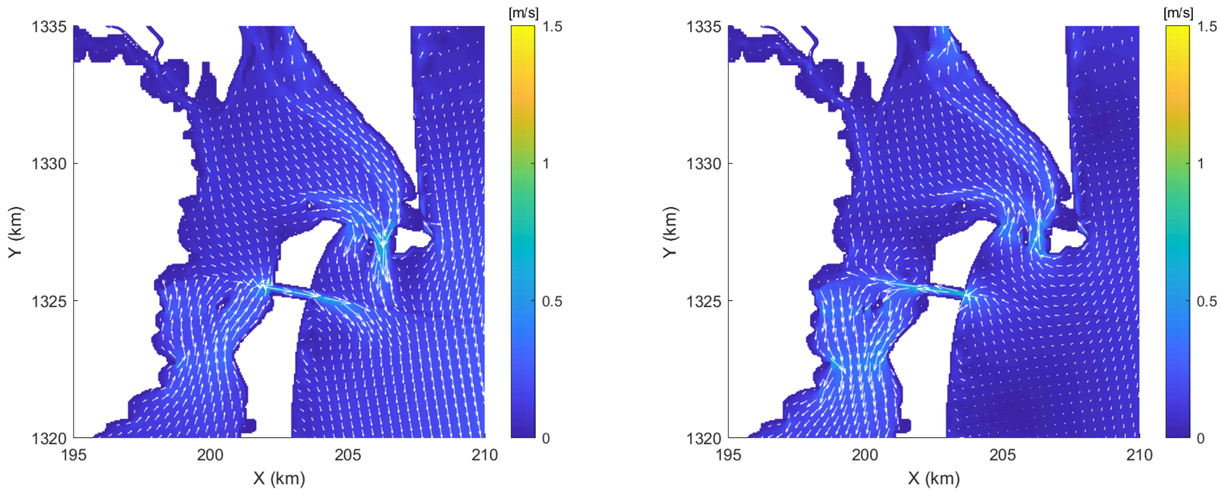

(a) Ebb (b) Flood

Figure G.7: Currents for Alternative 1B during the dry season

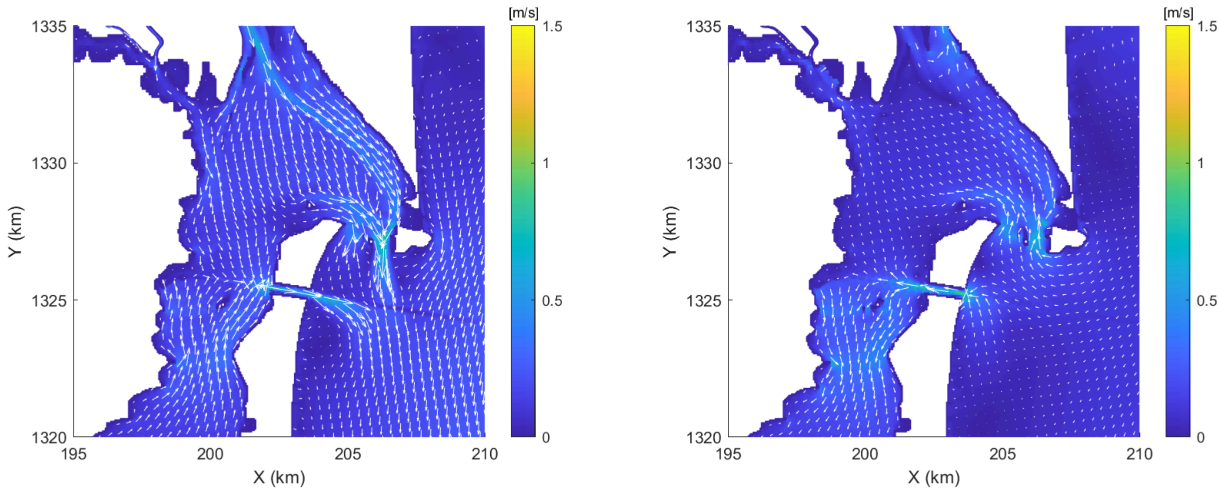

(a) Ebb (b) Flood

Figure G.8: Currents for Alternative 1B during the wet season

G.7 Residual currents at the southern inlet for Alternatives 1A and 1B

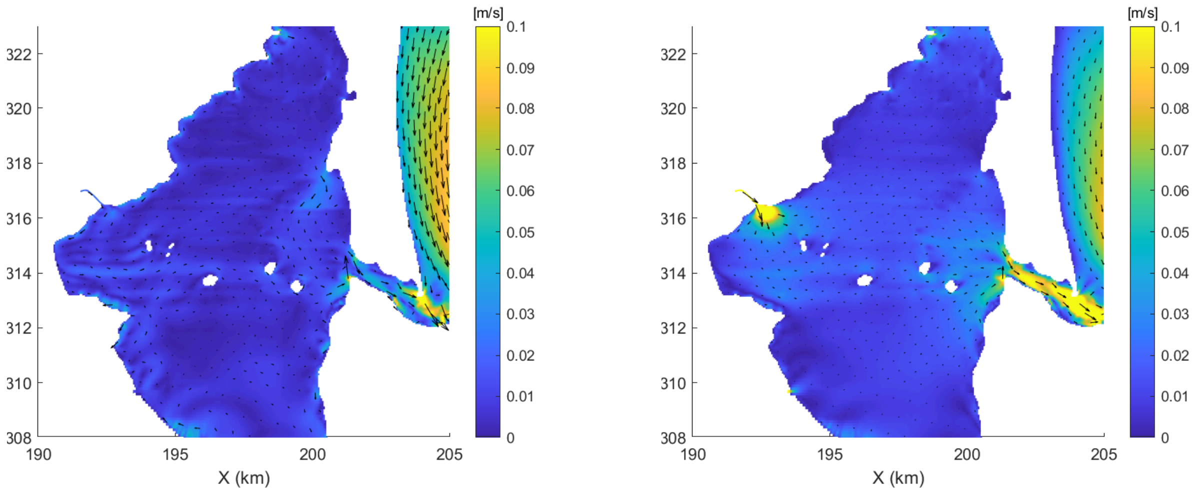

(a) Dry period (b) Wet period

Figure G.9: Residual currents for Alternative 1A at the southern inlet

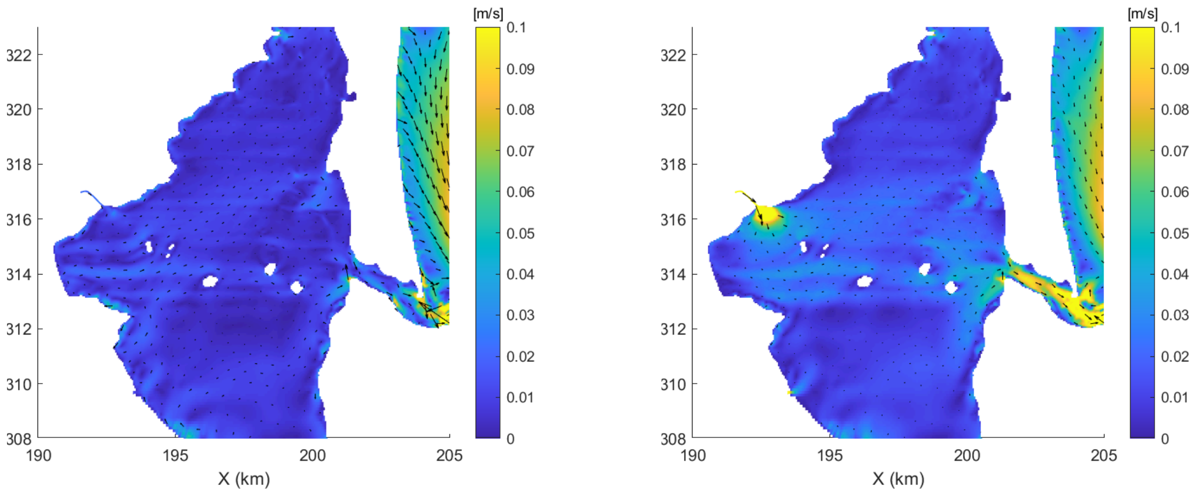

(a) Dry period (b) Wet period

Figure G.10: Residual currents for Alternative 1B at the southern inlet

H Results Sedimentation

H.1 Sedimentation Alternative 1A

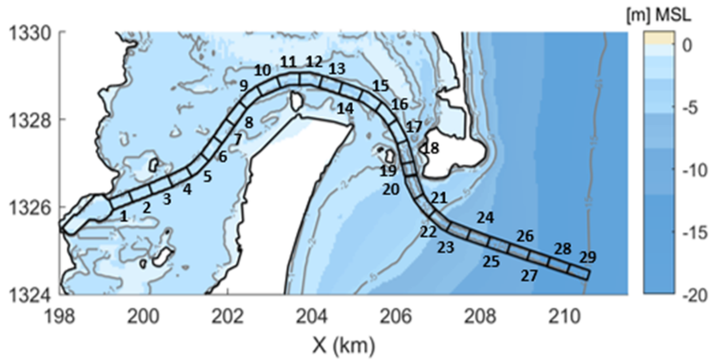

Figure H.1: Numbering of the sections for Alternative 1A

	Dry season				Wet season				Total year
	Density (kg/m^3)	Volume (m^3)	Height (m)	Weight (ton)	Density (kg/m^3)	Volume (m^3)	Height (m)	Weight (ton)	Height (m/yr)
Port	500	324.076	0,77	162.038	500	183.950	0,44	91.975	1,20
Inner channel									
Section 1	500	80.909	1,32	40.454	500	48.246	0,78	24.123	2,10
Section 2	500	82.240	1,34	41.120	500	51.298	0,83	25.649	2,17
Section 3	500	93.201	1,52	46.601	500	61.654	1,00	30.827	2,52
Section 4	500	86.785	1,41	43.392	500	61.448	1,00	30.724	2,41
Section 5	500	87.759	1,43	43.880	500	63.610	1,03	31.805	2,46
Section 6	500	90.676	1,47	45.338	500	60.748	0,99	30.374	2,46
Section 7	500	88.047	1,43	44.024	500	50.820	0,83	25.410	2,26
Section 8	500	71.683	1,17	35.841	500	26.433	0,43	13.217	1,60
Section 9	500	52.250	0,85	26.125	500	3.552	0,06	1.776	0,91
Section 10	500	33.126	0,54	16.563	500	-16.017	-0,26	-8.009	0,28
Section 11	500	31.789	0,52	15.894	501	-12.258	-0,20	-6.136	0,32
Section 12	500	28.009	0,46	14.004	505	-9.017	-0,15	-4.550	0,31
Section 13	500	16.805	0,27	8.406	500	-15.571	-0,25	-7.790	0,02
Section 14	507	5.721	0,09	2.903	506	-17.957	-0,29	-9.079	-0,20
Section 15	500	4.645	0,08	2.322	501	-11.667	-0,19	-5.849	-0,11
Section 16	501	8.722	0,14	4.370	521	-5.957	-0,10	-3.103	0,04
Section 17	500	12.139	0,20	6.070	689	-7.789	-0,13	-5.367	0,07
Section 18	555	21.390	0,35	11.871	1511	-5.440	-0,09	-8.221	0,26
Section 19	867	14.569	0,24	12.631	1232	6.796	0,11	8.376	0,35
Total		910.462		461.809		332.932		164.179	
Outer channel									
Section 20	1296	295.242	4,31	382.776	1563	79.852	1,17	124.774	5,48
Section 21	621	77.455	1,13	48.097	739	17.874	0,26	13.216	1,39
Section 22	551	148.626	2,17	81.919	569	31.385	0,46	17.870	2,63
Section 23	562	132.410	1,93	74.418	593	27.095	0,40	16.076	2,33
Section 24	576	100.796	1,47	58.059	606	17.201	0,25	10.431	1,72
Section 25	576	62.930	0,92	36.269	587	9.991	0,15	5.868	1,06
Section 26	596	35.260	0,51	21.009	623	4.870	0,07	3.033	0,59
Section 27	717	19.164	0,28	13.747	841	2.109	0,03	1.773	0,31
Section 28	812	11.802	0,17	9.580	1260	811	0,01	1.022	0,18
Section 29	860	9.126	0,13	7.849	2681	189	0,00	506	0,14
Section 30	10756	-166	0,00	-1.780	1254	-2.466	-0,04	-3.093	-0,04
Total		892.844		731.942		188.910		191.476	
Total		2.127.182		1.355.789		705.792		447.630	
Total rounded		**2.127.000**		**1.356.000**		**706.000**		**448.000**	

Table H.1: Sedimentation in the channel and port of Alternative 1A

H.2 Sedimentation Alternative 1B

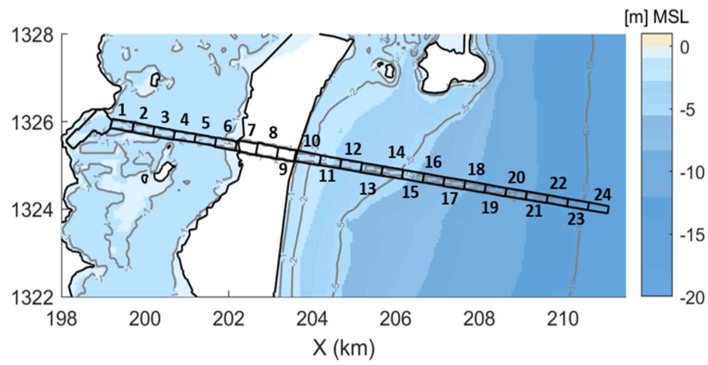

Figure H.2: Numbering of the sections for Alternative 1B

	Dry season				Wet season				Total year
	Density (kg/m^3)	Volume (m^3)	Height (m)	Weight (ton)	Density (kg/m^3)	Volume (m^3)	Height (m)	Weight (ton)	Height (m/yr)
Port	500	271.692	0,64	135.846	500	196.454	0,47	98.227	1,11
Inner channel									
Section 1	500	92.448	1,50	46.224	500	60.474	0,98	30.237	2,49
Section 2	500	98.522	1,60	49.261	500	63.508	1,03	31.754	2,63
Section 3	500	101.655	1,65	50.828	500	66.516	1,08	33.258	2,73
Section 4	500	105.328	1,71	52.664	500	67.432	1,10	33.716	2,81
Section 5	500	77.750	1,26	38.876	500	21.219	0,35	10.610	1,61
Section 6	825	62.254	1,01	51.389	3955	2.553	0,04	10.096	1,05
Section 7	527	70.968	1,15	37.403	1478	-320	-0,01	-473	1,15
Section 8	503	75.928	1,23	38.161	1209500	-0	0,00	-94	1,23
Section 9	34219	-175	0,00	-5.995	1413	-5.148	-0,08	-7.272	-0,09
Total		276.234		141.831		276.234		141.831	
Outer channel									
Section 10	918	277.146	4,05	254.429	2615	14.349	0,21	37.527	4,26
Section 11	527	206.598	3,02	108.834	30234	-50	0,00	-1.504	3,02
Section 12	599	244.801	3,57	146.597	704	52.394	0,76	36.860	4,34
Section 13	589	232.329	3,39	136.855	624	67.651	0,99	42.207	4,38
Section 14	586	208.738	3,05	122.383	596	61.895	0,90	36.915	3,95
Section 15	581	170.256	2,49	98.843	592	47.034	0,69	27.826	3,17
Section 16	548	128.022	1,87	70.179	555	29.263	0,43	16.251	2,30
Section 17	543	95.461	1,39	51.830	551	18.390	0,27	10.131	1,66
Section 18	587	71.148	1,04	41.735	563	12.520	0,18	7.044	1,22
Section 19	598	43.762	0,64	26.162	559	7.114	0,10	3.977	0,74
Section 20	620	27.366	0,40	16.971	576	3.792	0,06	2.186	0,45
Section 21	710	13.193	0,19	9.362	700	1.230	0,02	861	0,21
Section 22	891	9.619	0,14	8.570	2116	186	0,00	394	0,14
Section 23	937	8.018	0,12	7.514	9416	17	0,00	157	0,12
Section 24	740	4.972	0,07	3.679	2382	-49	0,00	-116	0,07
Total		1.741.428		1.103.945		315.737		220.717	
Total		2.697.799		1.598.601		788.424		460.775	
Total rounded		**2.698.000**		**1.599.000**		**788.000**		**461.000**	

Table H.2: Sedimentation in the channel and port of Alternative 1B

H.3 Coastal regression

$$Regression = \frac{\frac{S}{A}}{\alpha} \tag{H.1}$$

S	=	Total sedimentation in the channel	$[m^3]$
A	=	Area of erosion	$[m^2]$
α	=	Slope of the shore	$[-]$